AN AUTOMATED MICROFLUIDIC NUCLEIC ACID EXTRACTION SYSTEM FOR SAMPLE PREPARATION WITH AN INTEGRATED POLYMERASE CHAIN REACTION MODULE

by

Michael Aaron Johnson

A dissertation submitted to the faculty of
The University of Utah
in partial fulfillment of the requirements for the degree of

Doctor of Philosophy

Department of Mechanical Engineering

The University of Utah

May 2018

Copyright © Michael Aaron Johnson 2018

All Rights Reserved

The University of Utah Graduate School

STATEMENT OF DISSERTATION APPROVAL

The dissertation of **Michael Aaron Johnson**

has been approved by the following supervisory committee members:

Bruce Gale	, Chair	**6/6/2015** Date Approved
Tim Ameel	, Member	**6/19/2015** Date Approved
Kuan Chen	, Member	Date Approved
Debra Mascaro	, Member	**6/18/2015** Date Approved
Hanseup Kim	, Member	Date Approved

and by **Tim Ameel** , Chair/Dean of

the Department/College/School of **Mechanical Engineering**

and by David B. Kieda, Dean of The Graduate School.

ABSTRACT

This project will produce an automated microfluidic system capable of extracting and purifying nucleic acids from raw samples for detection and analysis. The first step will be the development and characterization of microfluidic components and fabrication methods that will be implemented into the final device. The gas permeability properties of PDMS will be utilized to demonstrate integrated components for pumping, gas bubble trapping and removal, and enhanced mixing.

Next, a three-layer PDMS with silicone membrane microfluidic platform will be developed to control fluid flow for nucleic acid purification processes. This microfluidic chip will be capable of taking a raw biological sample through the steps of cell lysis and solid phase nucleic acid extraction to deliver purified DNA or RNA for testing and analysis. The microfluidic chip will be mounted on a portable, desktop control system to allow automated device operation in clinics, laboratories, or the field.

Finally, a disposable oscillatory flow PCR chip will be made from polycarbonate to amplify low concentrations of nucleic acid. The PCR module will also be controlled by the same instrument used for nucleic acid extraction. Temperature control will be provided by external heating blocks, and internal chip fluid temperature will be determined by numerical simulations. This device will be a step towards having a universal nucleic acid purification device to fill the much-needed niche in sample preparation for lab-on-a-chip applications.

TABLE OF CONTENTS

LIST OF TABLES

Tables

CHAPTER 1

INTRODUCTION

1.1 Motivation

Biological assays based on nucleic acid (DNA and RNA) analysis have been explored for a wide range of applications: pathogen detection,[1-8] genetic analysis,[9-12] environmental monitoring,[13-18] terrorism or biowarfare agent detection,[19, 20] foodborn illness prevention,[21-24] and others. In each of these cases rapid on-site detection is desired, but current laboratory-based nucleic acid detection methods are generally not compatible with this goal. Such methods require highly trained laboratory staff, specialized equipment, and clean environments to reduce the risk of contaminating samples. As an alternative to lab-based methods, microfluidic lab-on-a-chip devices may be able to deliver rapid, on-site detection and are appealing for their ability to consolidate the steps needed for nucleic acid analysis onto a single, compact device.

Since its inception over two decades ago, the field of microfluidics has surged as people have seen the potential benefits of miniaturized systems capable of performing rapid biological assays. Microfluidic systems progressing towards the goal of reducing complex laboratory analysis processes onto a single lab-on-a-chip device often rely on nucleic acids as the main analysis target because of their ubiquity, stability, and specificity. Many different sensing systems have been developed using techniques such as melting analysis after polymerase chain reaction (PCR),[25] surface plasmon resonance (SPR),[26, 27] microarrays,[28-31] and other technologies.[32-36] While work in microfluidics has been ongoing for many years, there have been few significant advances towards widespread commercialization of microfluidic systems in recent years and some have expressed doubt about whether microfluidic devices will be able to reach this potential. George Whitesides, one of the leading microfluidic authorities, illustrates this issue and

provides potential reasons for this lack of progress in the following statement:

> [Microfluidics] offers so many advantages and so few disadvantages. . . . But it has not yet become widely used. Why not? . . .
> Revolutions in technology require both a broad range of different types of components and subsystems, and their integration into complete, functional systems. . . that can be used by non-experts. . . .
> The original hope for microfluidics, and that which still motivates many of us working in the field, is that it will be a practical technology. . . Above all, it must become successful commercially, rather than remain a field based on proof-of-concept demonstrations and academic papers.[37]

This statement aptly summarizes the motivation behind the research presented in this work. As supported by the above statement, the first requirement for a microfluidic technological revolution is an increase in the number and variety of microfluidic components and subsystems. Work on new components, and their application to lab-on-a-chip fluid handling, increases the number of tools available to researchers. These components form the basic units which can be used to assemble more complex systems capable of performing the fluid handling tasks for on-chip assays.

Once sufficient components and subsystems have been identified, there remains the task of integrating these components into functional systems. Primary research on improved microscale pumps, valves and mixers does little to expand the use of microfluidics if they cannot be integrated into operative systems. Such integration needs to consider the compatibility of these components with each other as well as to the samples, chemical reagents, and control architecture.

The last requirement is that the integrated microfluidic system must be usable by nonexperts. This need highlights a problem faced by a large number of microfluidic devices where the expertise and equipment required to operate the microfluidic device prohibit its widespread use. Such systems have come to be known as “chip-in-a-lab”

devices, a critical term derived from the "lab-on-a-chip" designation, drawing attention to the failure of microfluidic systems to simplify laboratory processes.

Even with some of these unsolved challenges in microfluidics, there are several specific application areas that have benefited from microfluidic technologies. An example of one such application is single cell analysis,[38, 39] where the economies of scale available with microfluidics permit higher throughput with lower cost, while simultaneously simplifying the automation of analysis. In this manner single cells have been the target for protein analysis[40] and gene expression.[41] Microfluidic devices have also been successfully used to synthesize carriers for drug delivery systems.[42, 43] But perhaps the largest field of success in current microfluidic research and technology is biomolecule detection. Microfluidic devices have the ability to isolate, amplify, or detect target molecules, most often DNA and RNA.

While such techniques show great promise in expanding the role of microfluidic systems in reducing human intervention in performing bioassays, there is still a problem. These sensing platforms demand purified nucleic acids, which typically require manual genetic extraction and purification methods to remove unwanted background material from the sample. Incomplete integrated sample preparation has thus limited the use of lab-on-a-chip devices to specialized laboratories with the capability to perform the sample preparation steps. To achieve the widespread development of bench-top and portable microfluidic analysis systems with true sample-in, answer-out capabilities, development of highly integrated and efficient nucleic acid purification sample preparation devices will be needed.

The need for sample preparation devices is especially evident in cases where

analysis chips neglect the important sample preparation step. Instead, off-chip laboratory-based nucleic acid sample preparation methods are used as preliminary steps to provide purified nucleic acid as the sample. Current bench-top nucleic acid sample preparation techniques are highly labor intensive, requiring skilled human interaction at multiple junctions to perform steps such as: filtration, cell lysis, centrifugation, nucleic acid separation, etc.[44] The incorporation of these steps into a single lab-on-a-chip device would yield many benefits including the elimination of the need to have highly skilled laboratory personnel perform the operations, a reduction in the chance of sample cross contamination, and the minimization of the amounts of costly reagents.

A wide variety of researchers have been working to achieve these goals. The current state of microfluidic nucleic acid sample preparation systems is summarized in Table 1.1, with further discussion in section 1.3. Table 1.1 demonstrates a current lack of microfluidic sample preparation systems capable of starting with multiple sample types to

Table 1.1 Current state of reported microfluidic nucleic acid sample preparation systems. Only the Utah system reports successful integration of the features listed.

References	Extract DNA	Extract RNA	Integrated PCR or Module	Automated	Multiple Sample Types
15, 47-61	✓				
12, 14, 62-65	✓		✓		
66-71	✓			✓	
9, 13, 72-79	✓		✓	✓	
80-82	✓				✓
29, 83, 84		✓			
85, 86		✓	✓		
87, 88		✓		✓	
89-91	✓	✓			
92	✓	✓		✓	
93-95	✓	✓			✓
96-98	✓	✓	✓	✓	
99	✓	✓		✓	✓
Utah System	✓	✓	✓	✓	✓

extract the target molecule (DNA or RNA) in an automated fashion with an optional PCR module for amplification. There are a large number of devices capable of extracting DNA or RNA, but targeting both types of nucleic acid is less common. Of those that can extract both DNA and RNA, there are even fewer that report automation, the capability of handling multiple sample times, or integrated PCR capability. However, all of these processes are needed in a generic nucleic acid sample preparation to be fully successful and enable further development and commercialization of microfluidic nucleic acid analysis systems. Accordingly, this work introduces a system capable of filling this need and is a step towards solving the problems which have labeled nucleic acid sample preparation the weak link in microfluidic biodetection,[45] and the most important obstacle to a revolution in biomolecule analysis.[46]

1.2 PDMS-Based Microfluidic Components and Fabrication Background

The adaptation of the multiple fluid handling steps of sample preparation to a lab-on-a-chip system requires on-chip components such as pumps, microchannels, valves, and mixers. There have been many reports in the literature on component improvements and fabrication methods for these components in substrates of glass,[100-102] silicon,[47, 103] and polymers.[104-106]

One method for fabricating microfluidic chips evolved from integrated circuit (IC) silicon micromachining. This technique creates microchannels and functional microfluidic components using microfabrication processes such as photolithography, wet or reactive ion etching, chemical vapor deposition, and others. Devices created in this manner exhibit complexity and versatility in performing microfluidic fluid handling

operations. Another benefit derives from the ability to seamlessly integrate control circuitry on the same chip using IC fabrication protocols. However, production complexity and cost are deterrents for silicon microfluidic chips to find widespread use as disposable medical diagnostic devices. In addition, microfluidic devices tend to be relatively large, compared to typical silicon structures, so silicon processing technologies tend to be expensive and over-capable when considered for microfluidic technologies.

Polymers have emerged as alternative substrates to silicon-based microfluidics with the promise of providing inexpensive disposable chips. Fabrication of these devices is accomplished using injection molding, hot embossing, layered stacks and casting. Active components are difficult to achieve with polymers, so these chips usually rely on external actuators and pumps to perform on-chip operations.

One polymer of note that finds extensive use in the microfluidic community is polydimethyl siloxane (PDMS), a silicone-based flexible elastomer that has desirable chemical properties and can be rapidly molded around structures to create sub-micrometer features. Publications reporting the use of replica molding of PDMS as a substrate for microfluidic applications began to appear in the late 1990s.[107-109] An increase in the popularity of PDMS was precipitated by several landmark papers: PDMS as a microfluidic substrate and a rapid prototyping process introduced by the George Whitesides group,[110, 111] and monolithic valves and large scale integration by the Stephen Quake group.[106, 112] Advancements in PDMS-based components and integration have continued with new valve designs[101, 113] and pumping schemes,[114] allowing other researchers to create more complex microfluidic platforms.[115] Further study of the capabilities of PDMS as a microfluidic substrate will help in the development of devices

with the capabilities to handle the complex fluid handling for nucleic acid extraction.

1.3 Microchip-Based Nucleic Acid Extraction

1.3.1 Solid Phase Extraction Introduction and Background

In order to use nucleic acids as target molecules for bioanalysis, the nucleic acid first needs to be released from the cells, isolated, and purified by purging unwanted cellular debris. While there are other means (e.g., phenol-chloroform based precipitation, isotachophoresis) for completing this extraction process, a large portion of the recent methods for both bench-top and microfluidic extraction have relied on the principle of solid phase extraction. Solid phase extraction relies on three main steps: binding, washing, and elution. In the binding step, nucleic acid is bound to the surface of a solid phase under certain buffer conditions. For washing, cellular debris and unwanted contaminants are rinsed off of the solid phase while the nucleic acid remains attached. Finally, the nucleic acid is eluted from the solid phase with a low ionic strength elution buffer.

One of the first demonstrations of solid phase extraction was performed in 1979 by Vogelstein and Gillespie and used a glass surface as the solid phase to extract DNA. Vogelstein and Gillespie used a chaotropic salt solution to selectively bind DNA to glass surfaces (in powdered form) to elute the DNA molecules from the surrounding agarose separation medium.[116] Under the conditions reported, they found that 1 μg of DNA would bind to a glass surface of about 750 mm^2. To increase the surface area, they employed a glass that had been ground to powder. Glass fiber filters were also used, but they found that recovery was too small to quantify. In their experiment, over 99% of the DNA was bound to the glass, with a recovery of about 90%. It should be noted that they

were using prepurified DNA that had previously been separated in agarose gel, and their DNA extraction was simply a separation from agarose, not from original cellular material.

This method was expanded upon in 1990 by Boom et al.[117] They demonstrated that a similar procedure could be used to purify nucleic acids (both DNA and RNA) from cell-rich samples similar to clinical samples. In their process, they introduced the use of two new chaotropic salt solutions to act as the binding buffer. Guanadinium thiocyanate (GuSCN) and guanadinium hydrochloride (GuCHl) proved to be powerful tools for the purification of nucleic acids because they have the ability to lyse target cells and subsequently bind the released nucleic acid to the solid particles. GuSCN also has the beneficial property of deactivating nucleases, making it especially useful in purifying more fragile RNA molecules. Nucleic acid extraction from human urine and serum was shown to have over 50% efficiency using their method, despite evidence that nucleic acid was being lost at each major step of the extraction process.

Baker et al. used glass fiber filters to extract pure DNA from whole blood, but their process does not depend on chemical buffers to promote reversible DNA adhesion to the glass solid phase.[118] Instead, white blood cells are trapped in the filter matrix and lysed using a detergent solution. The DNA is then also physically trapped in the filter until released in a special incubation vessel and eluted. This process demonstrates the ability of glass filters to be used to purify DNA, but does not explore using the filters as the binding surface using solid phase extraction techniques with chaotropic salts.

1.3.2 Current State of Microfluidic Nucleic Acid Sample Preparation

The NA purification processes described thus far involve several steps requiring manual manipulation by personnel. Commercial systems often used in laboratories today use variations on this process. These and other similar methods require pipetting, mixing, centrifuging, vortexing, transferring containers, incubation and other time consuming and labor intensive steps. Labor reduction has been achieved by the implementation of robotics to complete the fluid handling steps, but such systems are too expensive to see much use outside of centralized laboratories. Microfluidic chip analysis methods lend themselves well to such situations by reducing the required human involvement by integrating the essential steps onto small benchtop platforms. The literature shows that nucleic acid extraction is a process that has been adapted in several variations to microfluidic chips.

Performing nucleic acid extraction on-chip has been the focus of much attention in the literature. Appendix A is a published literature review of microfluidic advancements in on-chip cell lysis and nucleic acid purification. An updated review including emphasis on devices related to the system presented in this work is discussed in the remainder of this chapter.

The stability and specificity of DNA, as compared to RNA, has made it an attractive option as the target for microfluidic based bioassays, leading to a large number of on-chip DNA extraction devices.[15, 47-61] A few of the most recent and most powerful will be discussed.

The research group of James P. Landers has published extensively on methods of performing solid phase based nucleic acid extraction on microchips. In 2003 Wolfe et

al.[61] introduced the idea of using a sol-gel to immobilize silica beads inside microfluidic channels to form a porous, high-surface area solid phase on which nucleic acids can bind. This method eliminated the difficulties of including a weir to hold the beads in place. A guanidine-based binding solution with DNA was passed through the porous matrix, washed with ethanol, and eluted with TE buffer. This process generated extraction efficiencies ranging from 8.7% to 70.6%.

Breadmore et al. expanded on this work by using biological samples, including whole blood and bacteria.[95] Extraction efficiency data were not presented, but the effectiveness of extraction was qualitatively demonstrated by amplifying the extraction product by PCR and performing gel electrophoresis. As with their previous work, no mention was made on how pumping and interfacing with samples and reagents were done. Similar results were later obtained by the same group[80, 81] with the distinction that the solid phase was fabricated as a porous monolith instead of immobilized beads. Other research groups have reported similar results using an amino silica monolith.[55]

One final method of note introduced by the Landers group deviates from their common practice of using guanidine-based buffers to bind nucleic acid to silica surfaces. Instead, Hagan et al.[91] coat the silica surface of glass microchannels with chitosan. The nucleic acid can then be bound to and eluted from the chitosan using buffers at different pH that create induced-charge electrostatic means. Using this method, a slight improvement in extraction efficiency was observed (65% vs 40% for chitosan vs plain silica, respectively), and reagents that can inhibit later PCR amplification reactions were avoided.

Other efforts to perform nucleic acid purification on the microscale include using

optimized microfabricated silica pillar structures as the solid phase to extract DNA from *E. Coli* bacteria.[47] Mesoporous silica was used to demonstrate that pore sizes of 2-5nm were effective at binding duplex DNA without needing high ionic strength chaotropic salt solutions.[119] Similarly, DNA was extracted on a nanoporous aluminum oxide membrane with NaCl acting as the binding promoter.[53, 120] Xing et al. fabricated a porous silicon dioxide matrix on a silicon chip to serve as the solid phase.[121]

In a step towards more disposable chips, Bhattacharyya and Klapperich presented a thermoplastic microfluidic chip for nucleic acid purification fabricated by hot embossing.[3, 49] To create the solid phase, a porous plastic monolith was impregnated with silica particles. Successful purification of RNA and DNA was demonstrated. Another plastic-based chip used layered double hydroxides (LDH) on the surface of polycarbonate chips to bind DNA, which was released in a slight acid etch of the LDH.[52]

Yet another approach to solid phase extraction employs a lab-on-valve system with a renewable silica microcolumn packed inside a channel.[51] A finding of note from this setup is that longer residence times of the target in proximity with the silica surface increase the elution efficiency. Nanassy et al. also avoided microchip extraction by extracting DNA directly onto glass microscope slides.[50]

A highly parallel system was shown by Park et al. where a polycarbonate 96-well microfabricated titration plate was used to extract DNA from bacteria using a NaCl immobilization buffer, ethanol wash and DI water elution.[122]

The works discussed above are very valuable at exploring the methods and effectiveness of microchip-based solid phase extraction of nucleic acids. However, little effort has been made in the publications discussed to address the interface between the

microchip and the outside world. Expensive and complicated fluid pumping and analysis apparati are required to run such microchips, demanding the same kind of technical expertise required with current benchtop protocols. To make a practical difference, microfluidic extraction systems need to be highly integrated and automated, as well as effective.

One more integrated system was reported in 2007, which used a silicon/glass microfabricated chip as the heart of the extraction process.[69, 123, 124] The chip included a size-based exclusion filter to remove red blood cells in order to extract DNA and viral RNA from blood samples. The integrated system was shown to be effective by performing PCR and RT-PCR on DNA and RNA samples, respectively, but separate, portable systems had to be made for the DNA and RNA protocols.

Beier et al. devised a sample preparation chip with integrated components such as inlet, filter, solid phase extraction chamber, reagent storage, valves, etc.[87] The chip is operated by an instrument, eliminating the need for other external equipment. While this device demonstrates hands-free automation of sample preparation, the target application is very specific: extracting viral RNA from cervical liquid for the detection of HPV infections.

Another popular method of performing solid phase extraction is to use silica superparamagnetic particles, which allows the mobile solid phase to be manipulated using magnetic fields. One device uses these particles, immobilized by permanent magnets, to purify DNA from blood and perform PCR.[12, 125] Commercial extraction magnetic bead systems have also been used in conjunction with microfluidic systems to combine sample preparation and hybridization for microarrays.[28]

Chen et al. presented a disposable polycarbonate cassette that contains reagents, a silica membrane modified from a commercial extraction kit, and a PCR chamber.[97] The temperature of the stationary PCR reaction chamber is controlled using thermoelectric units at a rate of approximately 5˚C/sec. While their work is impressive in providing a self-contained chip that performs extraction, PCR, and RT-PCR for RNA and DNA detection, the types of samples used were limited to spiked saliva samples. No efforts were reported to extract nucleic acids from blood or other more complex matrices.

Another fully integrated sample preparation chip was demonstrated by Ritzi-Lehnert et al. with application towards analysis of respiratory viruses from nasal swabs.[96] They present a lab-on-a-chip nucleic acid purification and amplification system focused on viral RNA detection based on the one-tube RT-PCR QIAplex method. The on-chip RT-PCR and PCR thermal cycling is achieved using rotating constant temperature clamps on the top and bottom of the PCR reaction chamber with ramp rates of approximately 5˚C/sec for large volume (120 μl) PCR reactions. While this device demonstrates the ability to extract both RNA (target) and DNA (control), the sample preparation method is explicitly assay specific for RNA respiratory viral detection and no effort was reported to expand the types of sample inputs to create a more universal sample preparation device.

Previously reported work from Bruce Gale's lab at the University of Utah has produced a microfluidic chip for extraction of RNA and DNA from blood and bacteria samples as a step towards universal sample preparation.[99] However, this device required several off-chip lysis steps that are specific to the target cell prior to loading in the chip. Also, no attempt has been made to integrate PCR control into the automated extraction

process. The current system is an improvement in that it integrates cell lysis on-chip and a PCR module for nucleic acid amplification.

1.4 Nucleic Acid Amplification

Using microfluidics to perform nucleic acid extraction and analysis presents a barrier in that only small amounts of sample are used, which makes the detection of scarce target molecules especially difficult because there can be very low concentrations of the target available. Using polymerase chain reaction (PCR) to amplify the number of molecules available for analysis shows great promise in overcoming this difficulty. PCR makes copies of targeted DNA strands by using enzymatic primers to locate and replicate specific nucleotide sequences. The process depends on having the primers go through a temperature cycle where the DNA molecule denatures (unzips the double-strand into two single strands) at a high temperature, anneals (the primers attach to the specific sequence of interest) at a low temperature, and extends (the primer moves along the strand, inserting complementary base pairs to again create a double-stranded DNA molecule) at a moderate temperature. Thus, the amount of target DNA can be doubled simply by putting the prepared sample through a single temperature cycle.

1.4.1 Microchip Based PCR

Adapting PCR to the microchip has seen much attention because of the rapid thermal cycling possibilities when using small liquid volumes, the reduced reagent usage, and the ability to reduce contamination between processing steps. There are several substrates that have been used in the manufacture of microfluidic PCR systems. The most prolific substrates are silicon,[2, 126-137] glass[11, 138-150] or a silicon/glass hybrid.[83, 151-156] These substrates are attractive as they take advantage of well-established micromachining

practices and allow easy integration with optical and electrical components. Polymers have seen accelerated interest as substrates for PCR chips as the less expensive manufacturing processes enhance the possibility of making the chips disposable. Polymer substrates used include PDMS,[73, 157-163] polycarbonate,[75, 98, 164-168] or other plastics.[169-173]

1.4.2 Oscillatory Flow PCR

While there are a wide range of techniques that can be applied to performing PCR, oscillatory-flow PCR is of particular interest and will be used extensively in this dissertation. Oscillatory flow PCR operates on the principle of pumping the sample fluid through distinct zones held at the required cycle temperature. With this system architecture, the plug of fluid moving to the new temperature zones is the only component in the device that undergoes temperature transitions, thus eliminating the need to unnecessarily heat and cool the chip itself. Oscillatory flow PCR has the added advantage over continuous flow PCR devices due to its flexibility in cycle times and temperatures. Specifically, many PCR protocols require a long incubation period at a set temperature for initialization or finalization of the PCR process. This incubation period is especially evident when dealing with RNA, which requires an initial reverse transcription step to convert the RNA strand to a more stable complementary DNA strand before PCR operation. These advantages make an oscillatory flow PCR chip advantageous as a module for a sample preparation device that deals with both DNA and RNA.

Such an oscillatory PCR device was presented by Bu et al. to provide the flexibility in thermal cycling control with the thermal advantages of flow based PCR.[174] They presented a microfabricated silicon chip with integrated heaters, a peristaltic pump, and optical sensors to detect fluid droplet position. However, the expensive, complex

fabrication methods make this chip a poor candidate for widespread use as a disposable chip.

Hardt et al. and Muchow et al. presented polymer chips (PMMA and cyclo olefin copolymer) that rest on three heater blocks with embedded heater cartridges.[175, 176] A pneumatically coupled ferrofluid pump was used as the actuation chamber for droplet pumping. Fluid droplet temperatures were predicted by CFD simulations based on temperature settings and infrared measurements. Evaporation was observed, but no attempt at evaporation control was reported.

Auroux et al. presented the first results obtained by oscillatory flow PCR.[177] Previous to their efforts, oscillatory flow PCR as a technology was theoretical or computational in nature. Channels were formed using patterned SU-8 on PMMA substrates. Pumping was done by an external syringe pump. The flexibility of the oscillatory flow PCR concepts was demonstrated by running several PCR programs with modifications to the fluid residence times. The nonoptimized system demonstrated amplification, although at a significantly reduced efficiency (25%) compared to commercial systems.

A radial temperature gradient oscillatory PCR geometry was presented by Cheng et al. where a PMMA fluid chip was placed in contact with a circular ITO/glass heater substrate.[178] They also attempted to mitigate evaporation loss by increasing the pressure in the channel as the fluid was pumped over the high temperature zone, which was accomplished by having the high temperature zone near the termination of a dead-end channel causing the air in the channel to be pressurized as the fluid approaches, thus raising the vapor pressure. Using this method, they reported 30% evaporation after 30

cycles. However, the high pressures produced by this method require pumping by an external syringe pump.

Another silicon-based microfluidic chip reported by Wang et al. demonstrated amplification of a human papilloma virus target sequence after 35 cycles in 15 minutes.[179] While this chip demonstrated good amplification, faster than conventional instruments, it suffered from a high degree of fabrication complexity that will make it difficult to be integrated as a disposable component.

Ohashi et al. performed PCR in a droplet-in-oil system where sliding permanent magnets were used to move magnetic particles containing PCR droplets across a temperature gradient.[166]

Another paradigm for oscillatory PCR is based in digital microfluidics as presented by Sista et al.[1] In this system, fluid droplets are moved by electrowetting manipulation. Their device performs PCR on a printed circuit board substrate by shuttling a droplet back and forth between two temperature zones heated by aluminum heater bars. While providing flexibility, this chip requires high voltages for electrowetting and laborious glass drilling and bonding processes.

Sciancalepore et al. cast a capillary tube in PDMS and positioned the tube over three patterned microheaters.[180] A droplet of PCR reagents was suspended in an oil phase and pumped by syringe pumps over the temperature zones. A nested PCR cycle is achieved four times faster (50 min) than with conventional systems. A later report showed the capability of this design to greatly reduce evaporation of the fluid droplet during the PCR process.[181] Drawbacks to this design include a 4 ˚C temperature variation in the temperature zones and a slightly slower thermal response time due to

interference from layers of glass and PDMS.

Sugumar et al. developed a glass chip with serpentine channels that pass over three temperature zones for the amplification of salmonella DNA.[182] While their use of oil, a sealed channel and elevated pressure kept evaporation to about 10% (lower than the rate seen in other polymer chips up to this point in this discussion), the difficulty in fabricating glass channels and bonding glass substrates makes polymers a more attractive option for disposable chips.

Zhang et al. presented a multichannel oscillatory flow PCR device with applications in detecting food-borne pathogens. PCR was carried out in PTFE capillary tubes which were set into small channels cut into copper blocks. A glass cover was then bound over the top of the channels.[183] Temperature zones were heated by cartridge heaters set into the copper blocks; pumping was done by an external syringe pump; and the temperature was controlled by a computer interface and monitored by a thermocouple embedded in the copper. Successful multiplexed amplification of food-borne pathogens from bacteria was demonstrated. Evaporation control was achieved using oil plugs on either side of the sample plug.

Mechanical pumping of a PCR fluid droplet between temperature zones on a PDMS/glass hybrid chip was demonstrated by Chia et al.[184] The electromagnetic coil actuator depresses a plastic flake into the PDMS chamber, forcing the fluid out into a different temperature zone. While they reported the time it takes heat up the temperature zones, there was no discussion of the time required for the fluid to heat and cool when pumped to different zones. Also, no discussion of evaporation rates was included.

The above discussion of the state of the art in microfluidic sample preparation

systems shows the need for a device like the Utah system, capable of performing automated extraction of both DNA and RNA. PDMS has proven a viable substrate for microfluidic devices, but further expansion of component capabilities will lead to more complex devices. Solid phase extraction has been successfully applied to microfluidic devices, but further work is needed to demonstrate automated systems with enough protocol adaptability to handle different sample types and target molecules. Microfluidic PCR devices are effective at rapidly amplifying nucleic acids. The oscillatory flow PCR chips provide flexibility in temperature, cycle number, and residence times with accompanying rapid cycles. An oscillatory flow PCR device on a plastic substrate that can control evaporation will be a step forward in disposable PCR chips integrated with extraction systems.

1.5 Project Overview

1.5.1 Summary

The research presented here is a step towards the realization of the goal to have functional microfluidic systems that can be operated by nonexperts by implementing practical solutions to problems that have hindered widespread adoption of microfluidic systems. Specifically, this work focuses on the generation of a nucleic acid sample preparation system for the purification of nucleic acid from biological samples of blood, bacteria cells, and cultured virus samples. This system incorporates on-chip chemical lysis of blood and bacteria cells and extracts purified DNA or RNA using solid phase extraction techniques. The system incorporates automated control of all process steps, so users need only load the sample. A polymerase chain reaction (PCR) module is also incorporated to allow amplification of target nucleic acids to increase assay sensitivity.

1.5.2 Chapter Overviews

Chapter 2 of this work presents findings on how PDMS membranes can be incorporated into microfluidic devices to perform essential fluid handling tasks. Specifically, the chapter outlines how the gas permeability of PDMS membranes is turned from a weakness to a strength to perform controlled pumping at low flow rates, reduce air bubble interference, and enhance mixing. These component advancements were instrumental in proving the versatility of three-layer PDMS chips at fluid handling tasks. Consequently, a three-layer PDMS chip platform was chosen for development of the main fluid control chip for the nucleic acid sample preparation platform.

Fabrication methods and microfluidic components are explored that will aid in reducing the complexity of device fabrication, making a final microfluidic system feasible. A thin PDMS membrane will be included into microfluidic devices to perform pumping, valving, bubble removal, and mixing tasks. All of these components will be fabricated using a simple three-layer technique, where a thin membrane is bonded between two thicker substrates (PDMS or glass) that house the fluid channels and packaging/control mechanisms. Having such a simple fabrication method with the ability to control many fluid-handling tasks can help reduce the complexity of manufacturing microfluidic platforms and minimize the number of external controls required for a lab-on-a-chip device.

In Chapter 3 a masked corona discharge bonding method[185] will be explored to improve pumping and valving for the more complex fluid handling applications that will be required based on the choice of cell lysis and extraction methods. Chemical cell lysis and subsequent solid phase extraction of nucleic acids require a complex sequence of

reagent mixing to efficiently recover the nucleic acid.

A major focus of Chapter 3 is on the generation of a single PDMS microfluidic chip with the capacity to control all needed fluid handling tasks for nucleic acid extraction. A range of possible extraction protocols will be considered in the design in order to make the device applicable to multiple situations. The chip will be able to draw from a bank of reagents to perform different extraction protocols. The system will be automated, controlled by a programmable LabView interface. Different extraction sequence programs will be run to selectively purify DNA or RNA from different samples. Following extraction, the purified nucleic acid samples will be delivered to several different detection platforms to verify that the device adequately interfaces between raw sample and genetic analysis. Specifically, DNA will be extracted and quantified using fluorescence, spectroscopic absorption, and PCR. RNA will similarly be extracted and analyzed with fluorescence and RT-PCR with applications for viral detection.

Advances in this field will facilitate an increase in the spread and scope of nucleic acid analysis, leading to more insight and discovery of underlying biological phenomena. The proposed work intends to generate these insights by increasing the ability of next generation analysis systems to rapidly process multiple samples using microfludic-based extraction systems.

The work presented in Chapter 4 demonstrates a chip that couples the flexibility of oscillatory flow PCR in a disposable polymer chip with good temperature uniformity and low evaporation. A thin multilayer polycarbonate chip will be fabricated from laminates. The chip will contact an external heater block module with PID temperature controllers to create fixed temperature zones on the PCR chip. Extra chip layers that

surround the fluid channel with pressurized water will provide evaporation control at the high temperatures experienced during PCR. Numerical simulations will be used to determine internal chip temperatures and required residence times of the fluid droplet at the temperature zones. Rapid on-chip PCR will be demonstrated controlled by a pumping module controlled by the same instrument that performs the nucleic acid extraction discussed in Chapter 3.

In total, these advancements in microfluidic sample preparation technology combine to demonstrate a system that improves on current reported devices by performing the complex fluid handling required to extract DNA and RNA from different sample types with an integrated PCR module for amplification.

1.6 References

1. R. Sista, Z. Hua, P. Thwar, A. Sudarsan, V. Srinivasan, A. Eckhardt, M. Pollack and V. Pamula, Lab on a Chip **8** (12), 2091-2104 (2008).

2. P. Belgrader, W. Benett, D. Hadley, G. Long, R. Mariella, F. Milanovich, S. Nasarabadi, W. Nelson, J. Richards and P. Stratton, Clinical Chemistry **44** (10), 2191-2194 (1998).

3. A. Bhattacharyya and C. M. Klapperich, Sensors & Actuators: B. Chemical **129** (2), 693-698 (2008).

4. E. M. Elnifro, A. M. Ashshi, R. J. Cooper and P. E. Klapper, Clinical Microbiology Reviews **13** (4), 559-570 (2000).

5. D. N. Fredricks and D. A. Relman, Clinical Infectious Diseases **29** (3), 475-486 (1999).

6. V. Srinivasan, V. K. Pamula and R. B. Fair, Lab on a Chip **4** (4), 310-315 (2004).

7. S. Yang, S. Lin, G. D. Kelen, T. C. Quinn, J. D. Dick, C. A. Gaydos and R. E. Rothman, Journal of Clinical Microbiology **40** (9), 3449-3454 (2002).

8. S. Yang, P. Ramachandran, A. Hardick, Y.-H. Hsieh, C. Quianzon, M. Kuroki, J. Hardick, A. Kecojevic, A. Abeygunawardena and J. Zenilman, Journal of Clinical

Microbiology **46** (4), 1386-1390 (2008).

9. L. A. Legendre, C. J. Morris, J. M. Bienvenue, A. Barron, R. McClure and J. P. Landers, JALA - Journal of the Association for Laboratory Automation **13** (6), 351-360 (2008).

10. P. Liu and R. A. Mathies, Trends in Biotechnology **27** (10), 572 (2009).

11. C. J. Easley, J. M. Karlinsey, J. M. Bienvenue, L. A. Legendre, M. G. Roper, S. H. Feldman, M. A. Hughes, E. L. Hewlett, T. J. Merkel and J. P. Ferrance, Proceedings of the National Academy of Sciences **103** (51), 19272-19277 (2006).

12. Y. Zhang, S. Park, S. Yang and T.-H. Wang, Biomedical Microdevices **12** (6), 1043-1049 (2010).

13. C. J. Bruckner-Lea, N. C. Anheier Jr, D. A. Holman, T. Tsukuda, M. T. Kingsley, F. J. Brockman, J. M. Price, J. W. Grate and D. P. Chandler, presented at the Environmental and Industrial Sensing, 2000 (unpublished).

14. C. Delattre, C. P. Allier, Y. Fouillet, D. Jary, F. Bottausci, D. Bouvier, G. Delapierre, M. Quinaud, A. Rival and L. Davoust, Biosensors and Bioelectronics **36** (1) (2012).

15. S. Isabel, M. Boissinot, I. Charlebois, C. M. Fauvel, L.-E. Shi, J.-C. Lévesque, A. T. Paquin, M. Bastien, G. Stewart and É. Leblanc, Applied and Environmental Microbiology **78** (5), 1505-1512 (2012).

16. J. C. Jokerst, J. M. Emory and C. S. Henry, Analyst **137** (1), 24-34 (2012).

17. E. A. Ottesen, J. W. Hong, S. R. Quake and J. R. Leadbetter, Science **314** (5804), 1464-1467 (2006).

18. Y. Li, C. Zhang and D. Xing, Analytical Biochemistry **415** (2), 87-96 (2011).

19. D. Ivnitski, D. J. O Neil, A. Gattuso, R. Schlicht, M. Calidonna and R. Fisher, Biotechniques **35** (4), 862-869 (2003).

20. S. Yang, R. E. Rothman, J. Hardick, M. Kuroki, A. Hardick, V. Doshi, P. Ramachandran and C. A. Gaydos, Academic Emergency Medicine **15** (4), 388-392 (2008).

21. A. Cifuentes, ISRN Analytical Chemistry **2012** (2012).

22. P.-G. Lantz, B. Hahn-Hägerdal and P. Rådström, Trends in Food Science & Technology **5** (12), 384-389 (1994).

23. A. G. Sciancalepore, E. Mele, V. Arcadio, F. Reddavide, F. Grieco, G. Spano, P. Lucas, G. Mita and D. Pisignano, Food Microbiology **35** (1) (2013).

24. V. Velusamy, K. Arshak, O. Korostynska, K. Oliwa and C. Adley, Biotechnology Advances **28** (2), 232-254 (2010).

25. N. Crews, C. T. Wittwer, J. Montgomery, R. Pryor and B. Gale, Analytical Chemistry **81** (6), 2053-2058 (2009).

26. P. Englebienne, A. Van Hoonacker and M. Verhas, Spectroscopy: An International Journal **17** (2), 255-273 (2003).

27. L. Malic, T. Veres and M. Tabrizian, Biosensors and Bioelectronics **24** (7), 2218-2224 (2009).

28. T. Chien-Hsuan, S. Jyh-Wei, C. Tsuey-Yu, H. Suz-Kai, L. Chun-Che and L. Gwo-Bin, Microfluidics and Nanofluidics **10** (5), 999-1009 (2011).

29. C.-H. Tai, J.-W. Shin, T.-Y. Chang, S.-K. Hsiung, C.-C. Lin and G.-B. Lee, Microfluidics and Nanofluidics **10** (5), 999-1009 (2011).

30. D. Rose, Microarray Biochip Technology, (M. Shena. Ed.), Eaton Publishing, Natick, MA, 19-38 (2000).

31. C. Situma, M. Hashimoto and S. A. Soper, Biomolecular Engineering **23** (5), 213-231 (2006).

32. C. Ziegler, Analytical and Bioanalytical Chemistry **379** (7-8), 946-959 (2004).

33. J. Li, H. T. Ng, A. Cassell, W. Fan, H. Chen, Q. Ye, J. Koehne, J. Han and M. Meyyappan, Nano Letters **3** (5), 597-602 (2003).

34. D. Branton, D. W. Deamer, A. Marziali, H. Bayley, S. A. Benner, T. Butler, M. Di Ventra, S. Garaj, A. Hibbs and X. Huang, Nature Biotechnology **26** (10), 1146-1153 (2008).

35. Z. Xu, T. Esumi, N. Ikuta and T. Hirokawa, Journal of Chromatography A **1216** (17), 3602-3605 (2009).

36. K. M. Ririe, R. P. Rasmussen and C. T. Wittwer, Analytical Biochemistry **245** (2), 154-160 (1997).

37. G. M. Whitesides, Nature **442** (7101), 368-373 (2006).

38. A. R. Wheeler, W. R. Throndset, R. J. Whelan, A. M. Leach, R. N. Zare, Y. H. Liao, K. Farrell, I. D. Manger and A. Daridon, Analytical Chemistry **75** (14), 3581-3586

(2003).

39. V. Lecault, A. K. White, A. Singhal and C. L. Hansen, Current Opinion in Chemical Biology **16** (3), 381-390 (2012).

40. M. Wu and A. K. Singh, Current Opinion in Biotechnology **23** (1), 83-88 (2012).

41. V. Sanchez-Freire, A. D. Ebert, T. Kalisky, S. R. Quake and J. C. Wu, Nature Protocols **7** (5), 829-838 (2012).

42. F. S. Majedi, M. M. Hasani-Sadrabadi, S. H. Emami, M. A. Shokrgozar, J. J. VanDersarl, E. Dashtimoghadam, A. Bertsch and P. Renaud, Lab on a Chip **13** (2), 204-207 (2013).

43. R. R. Hood, E. L. Kendall, D. L. DeVoe, Z. Quezado, M. Junqueira, J. C. Finkel and W. N. Vreeland, presented at the Microsystems for Measurement and Instrumentation (MAMNA), 2013, 2013 (unpublished).

44. C. W. Price, D. C. Leslie and J. P. Landers, Lab on a Chip **9** (17), 2484-2494 (2009).

45. R. Mariella, Jr., Biomedical Microdevices **10** (6), 777-784 (2008).

46. D. Xia, J. Yan and S. Hou, Small **8** (18), 2787-2801 (2012).

47. N. C. Cady, S. Stelick and C. A. Batt, Biosensors & Bioelectronics **19** (1), 59-66 (2003).

48. C. Xing, D.-F. Cui and L. Chang-Chun, presented at the Nano/Micro Engineered and Molecular Systems, 2006. NEMS '06. 1st IEEE International Conference on, 2006 (unpublished).

49. A. Bhattacharyya and C. M. Klapperich, Analytical Chemistry **78** (3), 788-792 (2006).

50. O. Z. Nanassy, P. V. Haydock and M. W. Reed, Analytical Biochemistry **365** (2), 240-245 (2007).

51. X.-W. Chen, Z.-R. Xu, B.-Y. Qu, Y.-F. Wu, J. Zhou, H.-D. Zhang, J. Fang and J.-H. Wang, Analytical and Bioanalytical Chemistry **388** (1), 157-163 (2007).

52. C.-H. Chan, J.-K. Chen and F.-C. Chang, Sensors and Actuators, B: Chemical **133** (1), 327-332 (2008).

53. J. Kim and B. K. Gale, Lab on a Chip **8** (9), 1516-1523 (2008).

54. D.-W. Park, M. Hupert, M. Witek, B. You, P. Datta, J. Guy, J.-B. Lee, S. Soper, D. Nikitopoulos and M. Murphy, Biomedical Microdevices **10** (1), 21-33 (2008).

55. L. Liu, S. Yu, S. Yang, P. Zhou, J. Hu and Y. Zhang, Journal of Separation Science **32** (15-16, Sp. Iss. SI), 2752-2758 (2009).

56. J. Kim, H. Kido, J. V. Zoval, D. Gagné, R. Peytavi, F. J. Picard, M. Bastien, M. Boissinot, M. G. Bergeron and M. J. Madou, presented at the MOEMS-MEMS 2006 Micro and Nanofabrication, 2006 (unpublished).

57. E. Hoppmann and I. White, presented at the 26th Southern Biomedical Engineering Conference SBEC 2010, April 30-May 2, 2010, College Park, Maryland, USA, 2010 (unpublished).

58. A. Govindarajan, S. Ramachandran, G. Vigil, P. Yager and K. Böhringer, Lab on a Chip **12** (1), 174-181 (2012).

59. M. M. Packard, M. Shusteff and E. C. Alocilja, Biosensors **2** (4), 405-416 (2012).

60. K.-Y. Hwang, S. H. Kwon, S.-O. Jung, H.-K. Lim, W.-J. Jung, C.-S. Park, J.-H. Kim, K.-Y. Suh and N. Huh, Lab on a Chip **11** (21), 3649-3655 (2011).

61. K. A. Wolfe, M. C. Breadmore, J. P. Ferrance, M. E. Power, J. F. Conroy, P. M. Norris and J. P. Landers, Electrophoresis **23** (5), 727-733 (2002).

62. E. A. Oblath, W. H. Henley, J. P. Alarie and J. M. Ramsey, Lab on a Chip **13** (7) 1325-1332 (2013).

63. J. A. Lounsbury, A. Karlsson, D. C. Miranian, S. M. Cronk, D. A. Nelson, J. Li, D. M. Haverstick, P. Kinnon, D. J. Saul and J. P. Landers, Lab on a Chip **13** (7), 1384-1393 (2013).

64. M. Mahalanabis, J. Do, H. ALMuayad, J. Y. Zhang and C. M. Klapperich, Biomedical Microdevices **12** (2), 353-359 (2010).

65. H. Becker, N. Hlawatsch, R. Klemm and C. Gärtner, presented at the SPIE MOEMS-MEMS, 2011 (unpublished).

66. L. Xie, C. Premachandran, M. Chew and S. C. Chong, Advanced Packaging, IEEE Transactions on **32** (2), 528-535 (2009).

67. L. Xie, C. Premachandran, M. Chew, S. C. Chong, L. C. Wai and J. Lau, presented at the Electronic Components and Technology Conference, 2008. ECTC 2008. 58th, 2008 (unpublished).

68. C.-H. Weng, K.-Y. Lien, S.-Y. Yang and G.-B. Lee, Microfluidics and

Nanofluidics **10** (2), 301-310 (2011).

69. W. C. Hui, L. Yobas, V. D. Samper, H. Chew-Kiat, S. Liw, J. Hongmiao, C. Yu, C. Lin, L. Jing and L. Tit Meng, Sensors and Actuators A (Physical) **133** (2), 335-339 (2007).

70. H. M. Ji, V. Samper, Y. Chen, W. C. Hui, H. J. Lye, F. B. Mustafa, A. C. Lee, L. Cong, C. K. Heng and T. M. Lim, Sensors and Actuators A: Physical **139** (1), 139-144 (2007).

71. L. A. Marshall, L. L. Wu, S. Babikian, M. Bachman and J. G. Santiago, Analytical Chemistry **84** (21), 9640-9645 (2012).

72. J.-H. Wang, L. Cheng, C.-H. Wang, W.-S. Ling, S.-W. Wang and G.-B. Lee, Biosensors & Bioelectronics **41**, 484-491 (2013).

73. C. Chiou, D. Shin, S. Hosmane, Y. Zhang and T. Wang, presented at the Micro Electro Mechanical Systems (MEMS), 2013 IEEE 26th International Conference on, 2013 (unpublished).

74. S. Petralia, R. Verardo, E. Klaric, S. Cavallaro, E. Alessi and C. Schneider, Sensors and Actuators B: Chemical **187,** 99-105 (2013).

75. N. Hlawatsch, R. Klemm, C. Carstens, T. Brandstëtter, H. Becker, R. Elbracht and C. Gärtner, presented at the SPIE MOEMS-MEMS, 2012 (unpublished).

76. R. Klemm, N. Hlawatsch, T. E. Hansen-Hagge, H. Becker and C. Gärtner, presented at the Proceedings of SPIE, 2012 (unpublished).

77. A. J. Hopwood, C. Hurth, J. Yang, Z. Cai, N. Moran, J. G. Lee-Edghill, A. Nordquist, R. Lenigk, M. D. Estes and J. P. Haley, Analytical Chemistry **82** (16), 6991-6999 (2010).

78. M. D. Estes, J. Yang, B. Duane, S. Smith, C. Brooks, A. Nordquist and F. Zenhausern, The Analyst **137** (23), 5510-5519 (2012).

79. Y. Sun, J. Høgberg, T. Christine, L. Florian, L. G. Monsalve, S. Rodriguez, C. Cao, A. Wolff, J. M. Ruano-Lopez and D. D. Bang, Lab on a Chip **13**, 1509-1514 (2013).

80. Q. Wu, J. M. Bienvenue, B. J. Hassan, Y. C. Kwok, B. C. Giordano, P. M. Norris, J. P. Landers and J. P. Ferrance, Analytical Chemistry **78** (16), 5704-5710 (2006).

81. J. Wen, C. Guillo, J. P. Ferrance and J. P. Landers, Analytical Chemistry **78** (5), 1673-1681 (2006).

82. J. Siegrist, R. Gorkin, M. Bastien, G. Stewart, R. Peytavi, H. Kido, M. Bergeron

and M. Madou, Lab on a Chip **10** (3), 363-371 (2010).

83. S. Bhattacharya, S. Salamat, D. Morisette, P. Banada, D. Akin, Y.-S. Liu, A. K. Bhunia, M. Ladisch and R. Bashir, Lab on a Chip **8** (7), 1130-1136 (2008).

84. C. N. Hughes-Chinkhota, M. Banda, J. M. Smolinski, R. A. Thomas, D. M. Petibone, J. D. Tucker and G. W. Auner, Sensors and Actuators B: Chemical **155** (2), 437-445 (2011).

85. K. A. Hagan, C. R. Reedy, M. L. Uchimoto, D. Basu, D. A. Engel and J. P. Landers, Lab on a Chip **11** (5), 957-961 (2011).

86. Q. Cao, M. Mahalanabis, J. Chang, B. Carey, C. Hsieh, A. Stanley, C. A. Odell, P. Mitchell, J. Feldman and N. R. Pollock, PLoS One **7** (3), e33176 (2012).

87. T. Baier, T. E. Hansen-Hagge, R. Gransee, A. Crombe, S. Schmahl, C. Paulus, K. S. Drese, H. Keegan, C. Martin, J. J. O'Leary, L. Furuberg, L. Solli, P. Gronn, I. M. Falang, A. Karlgard, A. Gulliksen and F. Karlsen, Lab on a Chip **9** (23), 3399-3405 (2009).

88. J. Kim, J. Elsnab, M. Johnson and B. K. Gale, presented at the MOEMS-MEMS, 2010 (unpublished).

89. R. Zhang, H.-Q. Gong, X. Zeng, C. Lou and C. Sze, Analytical Chemistry **85** (3), 1484-1491 (2012).

90. S. M. Berry, E. T. Alarid and D. J. Beebe, Lab on a Chip **11** (10), 1747-1753 (2011).

91. K. A. Hagan, W. L. Meier, J. P. Ferrance and J. P. Landers, Analytical Chemistry **81** (13), 5249-5256 (2009).

92. G. Xu, D. Y. San Lee, H. Xie, D. Chiew, T.-M. Hsieh, E. M. Ali, X. L. Looi, M.-H. Li and J. Y. Ying, Biomicrofluidics **5**, 034107 (2011).

93. X. Zhao and T. Dong, Analytical Chemistry **84** (20), 8541-8548 (2012).

94. T. Poeckh, S. Lopez, A. O. Fuller, M. J. Solomon and R. G. Larson, Analytical Biochemistry **373** (2), 253-262 (2008).

95. M. C. Breadmore, K. A. Wolfe, I. G. Arcibal, W. K. Leung, D. Dickson, B. C. Giordano, M. E. Power, J. P. Ferrance, S. H. Feldman, P. M. Norris and J. P. Landers, Analytical Chemistry **75** (8), 1880-1886 (2003).

96. M. Ritzi-Lehnert, R. Himmelreich, H. Attig, J. Claußen, R. Dahlke, G. Großhauser, E. Holzer, M. Jeziorski, E. Schaeffer and A. Wende, Biomedical

Microdevices **13** (5), 819-827 (2011).

97. D. Chen, M. Mauk, X. Qiu, C. Liu, J. Kim, S. Ramprasad, S. Ongagna, W. R. Abrams, D. Malamud, P. L. A. M. Corstjens and H. H. Bau, Biomedical Microdevices **12** (4), 705-719 (2010).

98. X. Qiu, D. Chen, C. Liu, M. G. Mauk, T. Kientz and H. H. Bau, Biomedical Microdevices **13** (5), 809-817 (2011).

99. J. Kim, M. Johnson, P. Hill, R. S. Sonkul, J. Kim and B. K. Gale, Journal of Micromechanics and Microengineering **22** (1), 015007 (2012).

100. L.-M. Fu, W.-J. Ju, R.-J. Yang and Y.-N. Wang, Microfluidics and Nanofluidics, 1-9 (2013).

101. W. H. Grover, A. M. Skelley, C. N. Liu, E. T. Lagally and R. A. Mathies, Sensors and Actuators B (Chemical) **B89** (3), 317-325 (2003).

102. C. Yamahata, F. Lacharme, Y. Burri and M. A. Gijs, Sensors and Actuators B: Chemical **110** (1), 1-7 (2005).

103. T. Lemke, G. Biancuzzi, H. Feth, J. Huber, F. Goldschmidtböing and P. Woias, Sensors and Actuators A: Physical **168** (1), 213-222 (2011).

104. K. Li, C. Miville-Godin, F. Normandin, E. Roy and T. Veres, presented at the Proceedings of the 2nd European Conference on Microfluidics, 2010 (unpublished).

105. D. Snakenborg, H. Klank and J. P. Kutter, Microfluidics and Nanofluidics **10** (2), 381-388 (2011).

106. M. A. Unger, H. P. Chou, T. Thorsen, A. Scherer and S. R. Quake, Science (New York, N.Y.) **288** (5463), 113-116 (2000).

107. C. S. Effenhauser, G. J. Bruin, A. Paulus and M. Ehrat, Analytical Chemistry **69** (17), 3451-3457 (1997).

108. E. Delamarche, A. Bernard, H. Schmid, B. Michel and H. Biebuyck, Science **276** (5313), 779-781 (1997).

109. K. Hosokawa, T. Fujii and I. Endo, Analytical Chemistry **71** (20), 4781-4785 (1999).

110. D. C. Duffy, J. C. McDonald, O. J. Schueller and G. M. Whitesides, Analytical Chemistry **70** (23), 4974-4984 (1998).

111. J. C. McDonald and G. M. Whitesides, Accounts of Chemical Research **35** (7),

491-499 (2002).

112. T. Thorsen, S. J. Maerkl and S. R. Quake, Science **298** (5593), 580-584 (2002).

113. N. L. Jeon, D. T. Chiu, C. J. Wargo, H. Wu, I. S. Choi, J. R. Anderson and G. M. Whitesides, Biomedical Microdevices **4** (2), 117-121 (2002).

114. M. A. Eddings and B. K. Gale, Journal of Micromechanics and Microengineering **16** (11), 2396 (2006).

115. Y. Li, W. Jones, F. Rasti, I. Blaga, G. Bogdan, D. Eberhart, B. Kobrin, D. Lee, B. Nielsen and E. van Gelder, Lab on a Chip **11** (15), 2541-2550 (2011).

116. B. Vogelstein and D. Gillespie, Proceedings of the National Academy of Sciences of the United States of America **76** (2), 615-619 (1979).

117. R. Boom, C. J. A. Sol, M. M. M. Salimans, C. L. Jansen, P. M. E. Wertheim-Van Dillen and J. Van Der Noordaa, Journal of Clinical Microbiology **28** (3), 495-503 (1990).

118. M. P. Baker, A. Mitchell, C. Bridge, S. Martin, F. Holder, N. D. Pathirana, A. Jarvis and N. Butt, Biotechniques **31** (1), 142-145 (2001).

119. M. Fujiwara, F. Yamamoto, K. Okamoto, K. Shiokawa and R. Nomura, Analytical Chemistry **77** (24), 8138-8145 (2005).

120. M. G. Elgort, M. G. Herrmann, M. Erali, J. D. Durtschi, K. V. Voelkerding and R. E. Smith, Clinical Chemistry **50** (10), 1817-1819 (2004).

121. C. Xing, C. Da-Fu and L. Chang-Chun, presented at the 2006 1st IEEE International Conference on Nano/Micro Engineered and Molecular Systems, 18-21 Jan. 2006, Piscataway, NJ, USA, 2006 (unpublished).

122. D. S. W. Park, M. Hupert, M. Witek, B. You, P. Datta, J. Guy, J. B. Lee, S. Soper, D. Nikitopoulos and M. Murphy, Biomedical Microdevices **10** (1), 21-33 (2008).

123. L. Yobas, J. Hongmiao, H. Wing-Cheong, C. Yu, L. Tit-Meng, H. Chew-Kiat and K. Dim-Lee, IEEE Journal of Solid-State Circuits **42** (8), 1803-1813 (2007).

124. J. Hong Miao, V. Samper, C. Yu, H. Wing Cheong, L. Hui Jen, F. B. Mustafa, L. Ai Cheng, C. Lin, H. Chew Kiat and L. Tit Meng, Sensors & Actuators: A. Physical **139** (1-2), 139-144 (2007).

125. Z. Yi and W. Tza-Huei, presented at the 23rd IEEE International Conference on Micro Electro Mechanical Systems (MEMS 2010), 24-28 Jan. 2010, Piscataway, NJ, USA, 2010 (unpublished).

126. M. A. Burns, B. N. Johnson, S. N. Brahmasandra, K. Handique, J. R. Webster, M. Krishnan, T. S. Sammarco, P. M. Man, D. Jones and D. Heldsinger, Science **282** (5388), 484-487 (1998).

127. P. Neuzil, C. Zhang, J. Pipper, S. Oh and L. Zhuo, Nucleic Acids Research **34** (11), e77-e77 (2006).

128. M. A. Northrup, B. Benett, D. Hadley, P. Landre, S. Lehew, J. Richards and P. Stratton, Analytical Chemistry **70** (5), 918-922 (1998).

129. D. Trau, T. M. Lee, A. I. Lao, R. Lenigk, I.-M. Hsing, N. Y. Ip, M. C. Carles and N. J. Sucher, Analytical Chemistry **74** (13), 3168-3173 (2002).

130. P. Wilding, L. J. Kricka, J. Cheng, G. Hvichia, M. A. Shoffner and P. Fortina, Analytical Biochemistry **257** (2), 95-100 (1998).

131. J. Wu, R. Kodzius, K. Xiao, J. Qin and W. Wen, Biomedical Microdevices **14** (1), 179-186 (2012).

132. N. R. Beer, B. J. Hindson, E. K. Wheeler, S. B. Hall, K. A. Rose, I. M. Kennedy and B. W. Colston, Analytical Chemistry **79** (22), 8471-8475 (2007).

133. N. R. Beer, E. K. Wheeler, L. Lee-Houghton, N. Watkins, S. Nasarabadi, N. Hebert, P. Leung, D. W. Arnold, C. G. Bailey and B. W. Colston, Analytical Chemistry **80** (6), 1854-1858 (2008).

134. Z. Guttenberg, H. Müller, H. Habermüller, A. Geisbauer, J. Pipper, J. Felbel, M. Kielpinski, J. Scriba and A. Wixforth, Lab on a Chip **5** (3), 308-317 (2005).

135. D. Verdoy, Z. Barrenetxea, J. Berganzo, M. Agirregabiria, J. M. Ruano-López, J. M. Marimón and G. Olabarría, Biosensors and Bioelectronics **32** (1), 259-265 (2012).

136. D.-S. Lee, S. H. Park, H. Yang, K.-H. Chung, T. H. Yoon, S.-J. Kim, K. Kim and Y. T. Kim, Lab on a Chip **4** (4), 401-407 (2004).

137. E. T. Lagally, C. A. Emrich and R. A. Mathies, Lab on a Chip **1** (2), 102-107 (2001).

138. H. Lee, N. Han, I.-H. Choi and K.-H. Han, Biomedical Microdevices **15** (1), 9-15 (2013).

139. Y. Yu, B. Li, C. A. Baker, X. Zhang and M. G. Roper, Analytical Chemistry **84** (6), 2825-2829 (2012).

140. C. J. Easley, J. M. Karlinsey and J. P. Landers, Lab on a Chip **6** (5), 601-610 (2006).

141. M. U. Kopp, A. J. De Mello and A. Manz, Science **280** (5366), 1046-1048 (1998).

142. E. Lagally, J. Scherer, R. Blazej, N. Toriello, B. Diep, M. Ramchandani, G. Sensabaugh, L. Riley and R. Mathies, Analytical Chemistry **76** (11), 3162-3170 (2004).

143. L. A. Legendre, J. M. Bienvenue, M. G. Roper, J. P. Ferrance and J. P. Landers, Analytical Chemistry **78** (5), 1444-1451 (2006).

144. M. N. Slyadnev, Y. Tanaka, M. Tokeshi and T. Kitamori, Analytical Chemistry **73** (16), 4037-4044 (2001).

145. P. Vulto, C. Hermann, P. Zahn, U. Maier, G. Dame and G. Urban, presented at the Solid-State Sensors, Actuators and Microsystems Conference, 2009. TRANSDUCERS 2009. International, 2009 (unpublished).

146. J. Pipper, Y. Zhang, P. Neuzil and T. M. Hsieh, Angewandte Chemie **120** (21), 3964-3968 (2008).

147. S. K. Jha, G.-S. Joo, G.-S. Ra, H. H. Lee and Y.-S. Kim, Sensors Journal, IEEE **11** (9), 2065-2070 (2011).

148. J. J. Chen, C. M. Shen and S. J. Chen, Applied Mechanics and Materials **284**, 883-887 (2013).

149. J. Y. Choi, Y. T. Kim, J. Ahn, K. S. Kim, D.-G. Gweon and T. S. Seo, Biosensors and Bioelectronics (2012).

150. S. Li, D. Y. Fozdar, M. F. Ali, H. Li, D. Shao, D. M. Vykoukal, J. Vykoukal, P. N. Floriano, M. Olsen and J. T. McDevitt, Microelectromechanical Systems, Journal of **15** (1), 223-236 (2006).

151. Y.-F. Lee, K.-Y. Lien, H.-Y. Lei and G.-B. Lee, Biosensors and Bioelectronics **25** (4), 745-752 (2009).

152. R. Pal, M. Yang, R. Lin, B. Johnson, N. Srivastava, S. Razzacki, K. Chomistek, D. Heldsinger, R. Haque and V. Ugaz, Lab on a Chip **5** (10), 1024-1032 (2005).

153. N. J. Panaro, X. J. Lou, P. Fortina, L. J. Kricka and P. Wilding, Biomolecular Engineering **21** (6), 157-162 (2005).

154. S. S. Yeung, T. M. Lee and I.-M. Hsing, Analytical Chemistry **80** (2), 363-368 (2008).

155. P. K. Yuen, L. J. Kricka, P. Fortina, N. J. Panaro, T. Sakazume and P. Wilding, Genome Research **11** (3), 405-412 (2001).

156. T. G. Kang, H. M. Ji, S. P. M. Tan, G. K. I. Tay, M. Y. D. Ang, S. Rafei, K. C. Tang, L. Zhang, X. Zhang and Y. Chen, presented at the Electronics Packaging Technology Conference (EPTC), 2010 12th, 2010 (unpublished).

157. W. Wan and J. T. Yeow, Biomedical Microdevices **14** (2), 337-346 (2012).

158. S. Quake, Electrophoresis **23**, 1531-1536 (2002).

159. M. M. Kiss, L. Ortoleva-Donnelly, N. R. Beer, J. Warner, C. G. Bailey, B. W. Colston, J. M. Rothberg, D. R. Link and J. H. Leamon, Analytical Chemistry **80** (23), 8975-8981 (2008).

160. L. Mazutis, A. F. Araghi, O. J. Miller, J.-C. Baret, L. Frenz, A. Janoshazi, V. Taly, B. J. Miller, J. B. Hutchison and D. Link, Analytical Chemistry **81** (12), 4813-4821 (2009).

161. S. Kumar, M. A. Cartas-Ayala and T. Thorsen, International Journal of Thermal Sciences **67**, 72-86 (2013).

162. J. M. Karlsson, T. Haraldsson, S. Laakso, A. Virtanen, M. Maki, G. Ronan and W. van der Wijngaart, presented at the Solid-State Sensors, Actuators and Microsystems Conference (TRANSDUCERS), 2011 16th International, 2011 (unpublished).

163. G. Kokkoris, D. Moschou, E. Mavraki, S. Chatzandroulis and A. Tserepi, presented at the 3rd Micro and Nano Flows Conference, Thessaloniki, Greece, 22-24 August 2011, 2011 (unpublished).

164. M. Hashimoto, F. Barany and S. A. Soper, Biosensors and Bioelectronics **21** (10), 1915-1923 (2006).

165. Y. Liu, C. B. Rauch, R. L. Stevens, R. Lenigk, J. Yang, D. B. Rhine and P. Grodzinski, Analytical Chemistry **74** (13), 3063-3070 (2002).

166. T. Ohashi, H. Kuyama, N. Hanafusa and Y. Togawa, Biomedical Microdevices **9** (5), 695-702 (2007).

167. M. Hashimoto, P.-C. Chen, M. W. Mitchell, D. E. Nikitopoulos, S. A. Soper and M. C. Murphy, Lab on a Chip **4** (6), 638-645 (2004).

168. R. H. Liu, J. Yang, R. Lenigk, J. Bonanno and P. Grodzinski, Analytical Chemistry **76** (7), 1824-1831 (2004).

169. Y.-K. Cho, J.-G. Lee, J.-M. Park, B.-S. Lee, Y. Lee and C. Ko, Lab on a Chip **7** (5), 565-573 (2007).

170. S. R. Jangam, A. K. Agarwal, K. Sur and D. M. Kelso, Biosensors and

Bioelectronics **42**, 69-75 (2013).

171. J.D. Kim, C.Y. Park, S.Y. Kim, O.D. Gwak, D.J. Lee, Y.S. Kim and H.J. Song, International Journal of Multimedia and Ubiquitous Engineering, **7** (2), 395-402 (2012)

172. N. Pak, D. C. Saunders, C. R. Phaneuf and C. R. Forest, Biomedical Microdevices **14** (2), 427-433 (2012).

173. Q. Cao, M. C. Kim and C. Klapperich, Biotechnology Journal **6** (2), 177-184 (2011).

174. M. Bu, T. Melvin, G. Ensell, J. S. Wilkinson and A. G. Evans, Journal of Micromechanics and Microengineering **13** (4), S125 (2003).

175. S. Hardt, D. Dadic, F. Doffing, K. Drese, G. Münchow and O. Sörensen, Nanotechnology **1**, 55-58 (2004).

176. G. Münchow, D. Dadic, F. Doffing, S. Hardt and K.-S. Drese, Expert Review of Molecular Diagnostics **5** (4), 613-620 (2005).

177. P. Auroux, P. Day and A. Manz, NSTI-Nanotechnol **1**, 67-69 (2004).

178. J.-Y. Cheng, C.-J. Hsieh, Y.-C. Chuang and J.-R. Hsieh, Analyst **130** (6), 931-940 (2005).

179. W. Wang, Z.-X. Li, R. Luo, S.-H. Lü, A.-D. Xu and Y.-J. Yang, Journal of Micromechanics and Microengineering **15** (8), 1369 (2005).

180. A. G. Sciancalepore, A. Polini, E. Mele, S. Girardo, R. Cingolani and D. Pisignano, Biosensors and Bioelectronics **26** (5), 2711-2715 (2011).

181. A. Polini, E. Mele, A. G. Sciancalepore, S. Girardo, A. Biasco, A. Camposeo, R. Cingolani, D. A. Weitz and D. Pisignano, Biomicrofluidics **4**, 036502 (2010).

182. D. Sugumar, A. Ismail, M. Ravichandran, I. Aziah and L. X. Kong, Biomicrofluidics **4** (2), 024103 (2010).

183. C. Zhang, H. Wang and D. Xing, Biomedical Microdevices **13** (5), 885-897 (2011).

184. B. Chia, S.-A. Yang, M.-Y. Cheng, C.-W. Lin and Y.-J. Yang, Journal of Mechanics **27** (03), 357-364 (2011).

185. Y. Chenying, W. Wei and L. Zhihong, presented at the 2009 4th IEEE International Conference on Nano/Micro Engineered and Molecular Systems (IEEE-NEMS 2009), 5-8 Jan. 2009, Piscataway, NJ, USA, 2009 (unpublished).

CHAPTER 2

BUBBLE INCLUSION AND REMOVAL USING PDMS MEMBRANE-BASED GAS PERMEATION FOR APPLICATIONS IN PUMPING, VALVING AND MIXING IN MICROFLUIDIC DEVICES

Journal of Micromechanics and Microengineering, (2009) **19**, Bubble inclusion and removal using PDMS membrane-based gas permeation for applications in pumping, valving and mixing in microfluidic devices. M. Johnson, G. Liddiard, M. Eddings, B. Gale. © Owned by IOP, published by IOP, 2009. Reprinted with kind permission of IOP Publishing.

IOP PUBLISHING JOURNAL OF MICROMECHANICS AND MICROENGINEERING

J. Micromech. Microeng. **19** (2009) 095011 (9pp) doi:10.1088/0960-1317/19/9/095011

Bubble inclusion and removal using PDMS membrane-based gas permeation for applications in pumping, valving and mixing in microfluidic devices

Michael Johnson[1], **Greg Liddiard**[2], **Mark Eddings**[3,4] **and Bruce Gale**[1,3]

[1] Department of Mechanical Engineering, University of Utah, Salt Lake City, UT 84112, USA
[2] Department of Electrical and Computer Engineering, University of Utah, Salt Lake City, UT 84112, USA
[3] Department of Bioengineering, University of Utah, Salt Lake City, UT 84112, USA

E-mail: mike.johnson@utah.edu

Received 10 March 2009, in final form 27 May 2009
Published 26 August 2009
Online at stacks.iop.org/JMM/19/095011

Abstract

Several advancements in fluid handling applications of a gas-permeable polydimethylsiloxane (PDMS) membrane are demonstrated. Devices for controlled pumping, bubble injection, bubble removal and mixing are demonstrated using a three-layered fabrication method. The ability of a gas-permeable membrane to control flow in glass channels is determined. Consistent flow rates ranging from approximately 1 to 14 μl min^{-1} were observed using control pressures from 100 to 700 mbar. Bubble injection and removal from microfluidic channels was performed in monolithic PDMS devices using several bubble trap geometries at fluid flow rates over 100 μl min^{-1}. The rate of removal of the air in the bubble trap was determined as a function of the area of membrane exposed and the applied vacuum. The PDMS membrane was shown to be an effective tool for the injection and removal of air bubbles in a method of enhancing mixing using bubbles and branched microchannels. The amount of mixing was optically determined before and after bubbles entered the fluid channel. The ability to produce all of these compatible components using a single fabrication process is a step toward inexpensive, parallel, highly integrated microfluidic systems with minimal external controls.

(Some figures in this article are in colour only in the electronic version)

1. Introduction

Microfluidic devices—particularly for lab-on-a-chip applications—can require a high degree of complexity to manipulate, mix and analyze fluids. Unfortunately, increasing the complexity of operations performed on-chip usually increases the number of off-chip controls, pumps, valves and imaging equipment. This increase in complexity presents difficulties for the development of more portable, potentially hand-held devices for use in military, environmental or clinical settings where ease of use and/or limited resources is of concern. Another problem with complex microfluidic devices is that integrating multiple components and materials can lead to costly manufacturing, which hinders the production of inexpensive, disposable testing chips.

A production method that combines complexity in the allowable operations and simplicity of fabrication is desirable. Polydimethylsiloxane (PDMS) has been a leading material in the development of microfluidic devices because of its many desirable qualities, including optical transparency, three-dimensional structure capability, ease of molding and rapid prototyping, and low cost [1]. Unger *et al* [2] have

[4] Present address: Department of Molecular and Medical Pharmacology, University of California, Los Angeles, Los Angeles, CA 90066, USA.

 © 2009 IOP Publishing Ltd Printed in the UK

demonstrated a multi-layer PDMS fabrication technique for the creation of valves and on-chip peristaltic pumps. A pneumatic control layer is separated from the fluid channel layer by a PDMS membrane that deflects to either block the channel or pump the fluid.

Gas permeability is a PDMS property that is desirable for biological applications. Recently, the amount of gas diffusion through a PDMS membrane was explored as it relates to feeding aqueous solution by pressure difference, and presents an analysis model for cell cultures [3]. Other applications, including the pumping of fluid, take advantage of the gas permeability of PDMS. Eddings *et al* [4] used a similar three-layer PDMS device with a membrane to explore the gas permeability of PDMS as a means for removing and injecting air into a channel, and thus pushing or pulling fluid through complex structures, or into dead-end channels. Pumping fluid in this manner shows considerable promise for the development of highly parallel and complex microfluidic systems on a single chip with minimal external controls.

This work is focused on possible applications for a gas permeable PDMS membrane as it relates to the production of microfluidic systems. We will show that a thin PDMS membrane can be included in microfluidic devices to perform pumping, valving, bubble removal and mixing tasks. All of these devices can be fabricated in a PDMS substrate using a simple three-layer technique, where a thin membrane is bonded between two thicker PDMS slabs that house the fluid channels and packaging mechanism. Having such a simple fabrication method with the ability to control many fluid-handling tasks can help reduce the complexity of manufacturing and the number of external controls required for a lab-on-a-chip device. We will also demonstrate the ability of the PDMS membrane to control flow in channels in glass substrates, showing that the gas-permeable membrane can be a valuable tool for a wide range of microfluidic applications.

2. Background

2.1. Pumping

The permeability of PDMS to various gases has been explored by Merkel *et al* [5], and the gas flux through a membrane is described as

$$N = P \cdot (p2 - p1)/l, \tag{1}$$

where N is the gas flux through the membrane, P is the permeability coefficient, $p2$ and $p1$ are the pressures on opposite sides of the membrane, and l is the membrane thickness. Hence, the flow rate of the gas through the membrane is increased by having a larger pressure difference, a thinner membrane and a larger area through which the gas can diffuse. It is of note that the permeability coefficient is dependent on the material properties of the fluid permeating through the PDMS. Air is used for all experiments throughout this work and results will thus need to be adjusted if another permeate is used.

The permeability of PDMS can be exploited by using a thin PDMS membrane to operate as a pump when a pressure difference is applied between a pneumatic control channel and a fluid channel on opposite sides of the membrane. If the pressure is lower in the control channel, air leaves the fluid channel and enters the control channel, drawing fluid toward the diffusion area of the membrane. If the pressure is higher in the control channel, air enters the fluid channel and pushes fluid away from the diffusion area. It has been shown that such a method can produce flow rates in PDMS channels on the order of several microliters per minute [4]. The flow rate of the fluid depends on rate at which the air in the channel can be removed through the membrane.

Another advantage to the PDMS membrane diffusion pump is that it allows for a straightforward integration with on-chip valves for complex fluid handling. Using a PDMS membrane as an on-chip pneumatic valve has already been demonstrated [2] and is in widespread use as a simple and effective fluid control mechanism. The PDMS membrane acts as a valve when a control channel is pressurized, causing the membrane to expand and block a fluid channel. The three-layered design (control channel, membrane and fluid channel) for the valves is fabricated using the same process to facilitate use of the membrane as a pump. Consequently, the valves and the pump can be fabricated simultaneously in the same layers and can be controlled by the same pneumatics.

As pumping in this manner has proven effective in a monolithic PDMS device, it would be instructive to see if the same membrane permeation mechanism would be effective using other fluid channel substrates, such as glass. There are several reasons for testing this pump in a glass substrate. To begin with, the surface chemistry of glass is well understood and easily altered, which makes it the substrate of choice for numerous applications. Also, PDMS is a hydrophobic material, and treatments such as oxygen plasma or corona discharge that activate the surface and render it slightly hydrophilic have a limited duration, usually on the order of several hours depending on environmental conditions. PDMS is unlikely to be the material of choice when a hydrophilic channel is required, as hydrophilic surface conditions can typically only be maintained for a few hours or days. Since glass is hydrophilic, aqueous solution from an open well will wick down the glass channels by capillary forces without outside pumping. This wicking is undesirable when precise flow rates or more fluid handling control are required. Having one side of the channel closed by a gas permeable membrane allows operators control of fluid flow in the hydrophilic glass channel.

To demonstrate the versatility of using gas diffusion through a PDMS membrane as a microfluidic pump, we desire to show that it can be integrated with glass substrates. The fabrication method for creating a membrane pump in glass is similar to creating a PDMS device, except the focus is on bonding the PDMS membrane to the glass using a corona discharge method.

2.2. Bubble injection and removal

Gas bubbles are a major concern in microfluidic systems because they can have devastating effects when blocking reactor sites and inhibiting fluid flow. At the same time, they

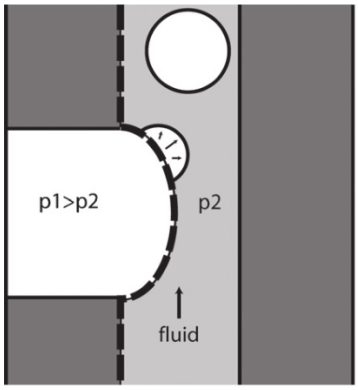

Figure 1. Bubble injection. Air will diffuse through the membrane when the pressure in the control channel ($p1$) is greater than the pressure in the fluid channel ($p2$).

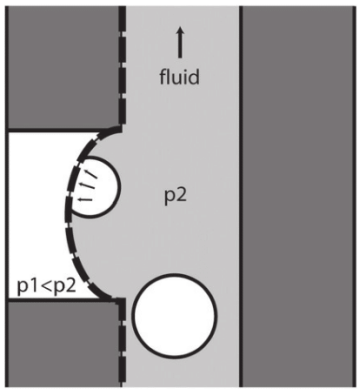

Figure 2. Bubble removal. Air bubbles in the fluid channel will diffuse into the control channel when the pressure in the control channel ($p1$) is less than the pressure in the fluid channel ($p2$).

can be a powerful tool for tasks such as separating plugs of different fluids, enhancing mixing and introducing reagents. The problem in purposefully using bubbles in microfluidic systems is that they are often difficult to remove when they are unwanted further downstream. The gas-permeable membrane proves to be effective at both injecting and removing bubbles while leaving the essential aspects of the system unchanged.

Gas can be inserted into a fluid channel by forcing it through the gas-permeable PDMS membrane. Positive pressure in a control channel will push the gas through the membrane into the fluid channel (see figure 1). Having the control channel directly under the line of fluid flow tends to deflect the membrane to obstruct the fluid channel and is ineffective at consistent bubble inclusion. An alternative method involves the control channel injecting air or another gas into an empty side-channel that meets the fluid channel at a T-junction [6]. Altering the pressure and diffusion area of this side-channel can effectively adjust the rate of bubble inclusion. As the bubble exits the side channel, it fills the fluid channel and is tugged downstream until it is pinched off and creates a plug of the gas and divides the fluid into plugs. Smaller channel sizes will cause the bubble to be pinched off earlier, so changing the channel widths can allow adjustment of plug sizes.

Whether a bubble is purposefully injected into the fluid channel, is accidentally introduced, or nucleates during a heating process, it is often imperative to have a way to remove the bubble at some point to avoid impeding the function of the device. Several methods have been proposed to remove unwanted gases from microfluidic devices. One method is described by Meng *et al* [7] in which a degassing plate is used to capture and remove gas bubbles in microfluidic devices. The plate is fabricated so that hydrophobic areas (flat or concave) surround venting holes. The hydrophobic areas attract and trap the bubbles, which can then be vented through the hydrophobic capillaries under a certain pressure. The fluid is kept from leaking out of the capillaries by surface tension forces, or by a hydrophobic porous membrane that covers the holes. Other methods for removing gaseous plugs from the fluid of interest involve using capillary pressure to separate the gas and the liquid [8, 9]. Initially wetted capillary tubes are kept at a pressure less than the capillary pressure and intersect the flow channel at right angles. Fluid is drawn into the capillaries while the gas continues down the flow channel.

We propose using a gas-permeable PDMS membrane to remove gas bubbles in the reverse operation described for bubble inclusion. An advantage of using a PDMS membrane to remove unwanted gas bubbles is that it eliminates the need of costly microfabrication techniques. Drawing the bubbles through a PDMS membrane prevents the difficulties relating to manufacturing small capillaries, and has the benefit of being minimally intrusive to the fluid in the main flow channel. To remove the bubbles, a negative pressure difference is applied to the control channel on one side of the membrane (see figure 2). Gas bubbles in the fluid stream on the other side of the membrane are driven by the pressure difference to diffuse through the thin membrane. There is difficulty when a bubble in flowing fluid would generally move across the membrane too quickly for all of the air to be extracted in the short time it is in contact with the membrane. A solution is to trap and hold the bubble in contact with the membrane long enough so that it can be removed.

Being hydrophobic, PDMS proves to be a good material for trapping gas bubbles in aqueous fluid flow, so all experiments in this work use water or a water/dye solution. Use of different liquids and gases with other properties may alter the surface energy balance to the extent that the gas bubbles are not held in contact with the membrane, thus compromising bubble removal. It is energetically favorable to have air in contact with the PDMS channel walls, so PDMS, air and water systems will spontaneously adjust to maximize the contact surface area between air (or other gases) and the PDMS. Several designs have arisen to take advantage of this inherent property to create areas in fluid channels where gas bubbles will be held in place. One method is to place the membrane between the fluid channel and a similarly sized control channel perpendicular to the flow channel as in figure 3(*a*). When negative pressure is applied to the control

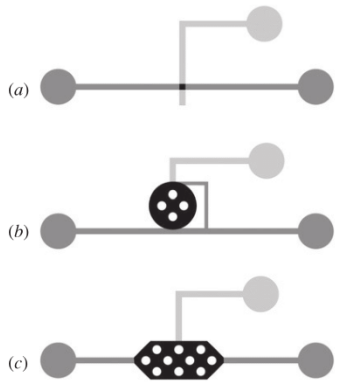

Figure 3. Three different geometries for fabrication of a bubble trap. Fluid channels are 100 μm tall and 500 μm wide. Light gray indicates pneumatic control channels, dark gray indicates fluid channels and black indicates the membrane diffusion area where they overlap. In (*a*), bubbles are trapped in depressions formed at the overlaps of the fluid and control channels. In (*b*), a reservoir to the side of the channel traps the bubbles. In (*c*), the bubbles are trapped on the posts where the fluid channel widens.

channel, the membrane deflects downward, causing a small depression in the fluid channel. The air bubble stays in the small depression because it minimizes the surface area of the fluid in contact with the hydrophobic surface, which is the thermodynamically desirable state for the system. The bubble stays in the depression until it is removed through the membrane. One advantage of this method is that when the bubble drops down to fill the depression, it no longer obstructs the fluid stream—even before it is completely removed through the membrane.

The depression method does well to remove small, intermittent bubbles, but is quickly overloaded when there are large bubbles or bubbles that come rapidly. There are several other methods that overcome this problem. One method involves creating an opening in the side of the fluid channel that leads to a small reservoir with the control channel directly under the reservoir as in figure 3(*b*). When a bubble comes down the channel, it is drawn into the reservoir to minimize the surface free energy, as in the small depression explanation above. The bubble is thus removed from the fluid stream and held over the membrane until it is totally diffused into the control channel. Larger volumes of gas can thus be stored in the reservoirs and removed. Because the gas diffusion rate is proportional to the area of gas-membrane contact, this method also allows for a higher rate of bubble removal as the reservoirs fill with gas.

Another method involves making the fluid channel wider over the membrane diffusion area as in figure 3(*c*). Small posts are also spaced throughout the widened fluid channel to support the membrane and provide more hydrophobic surface area for the bubbles to adhere to. The widened channel reduces the fluid's speed, and the posts stop the bubbles until they are dissipated. The width of the bubble trap area and the number and sizes of support posts can be optimized to create enough area to trap and remove the gas at the desired rate.

2.3. Bubble enhanced mixing

An application based on bubble injection and removal is bubble-enhanced mixing. Liquids in microfluidic systems generally operate in the laminar flow regime, making the mixing of fluids difficult because the absence of turbulence makes diffusion by random molecular motion the main mixing mechanism. Current microfluidic mixers cause the fluid to go through sharp turns or other restricted areas that aid the mixing of the fluid but also cause a relatively high-pressure drop. Injecting air bubbles into the fluid stream causes the fluid to be separated into plugs. The velocity profile in the fluid plug sets up currents that enhance mixing. The bubble can then be removed further downstream by one of the methods described above.

It has been demonstrated that injecting bubbles into a branched channel system further enhances mixing by folding the fluid across laminar boundaries [10, 11]. A bubble will enter one branch of the channel and increase the fluid resistance there, causing the fluid to divert and go down the other branch. A second bubble will then lodge in the open branch forcing the first bubble out, and the fluid folds back and forth. The fluid is mixed by this action, but the first bubble that enhanced the mixing must be removed. A thin PDMS membrane can act as the mechanism to both inject and remove the bubbles used to help mix the fluid.

3. Materials and methods

3.1. Pumping

Testing the effectiveness of the gas permeable PDMS membrane as a pump for glass channels was done using a rapid prototyping method. We used double-sided tape to form the walls of channels between two glass substrates using a method known as xurography [12]. Figure 4 shows the layers used in fabricating the test devices. A thin tape is used to create relatively low aspect ratio channels so that the glass dominates the surface properties of the channels. The double-sided tape was approximately 35 μm thick and was cut using a knife plotter to produce channels of various widths (250, 500 and 750 μm). The tape channels were sandwiched between two glass slides with through-holes drilled using a diamond-coated bit. One through-hole was the interface with the PDMS membrane pump, while the other served as a well into which the fluid was deposited. The PDMS membrane to cover the through-hole and act as the pump was bonded to the outside of the glass plate using a corona discharge surface treatment method. The channels were designed to be long and serpentine to allow for the determination of a wide range of flow rates.

The well was filled with water that was dyed to enhance visibility and contrast for optical determination of the flow rates. A negative pressure difference was applied to the membrane to pull the fluid through the glass/tape channels. The volumetric flow rate was determined by taking pictures of the fluid in the channels at intervals and measuring the distance traveled by the fluid in a given time (see figure 5). The pictures were taken using a CCD camera connected to

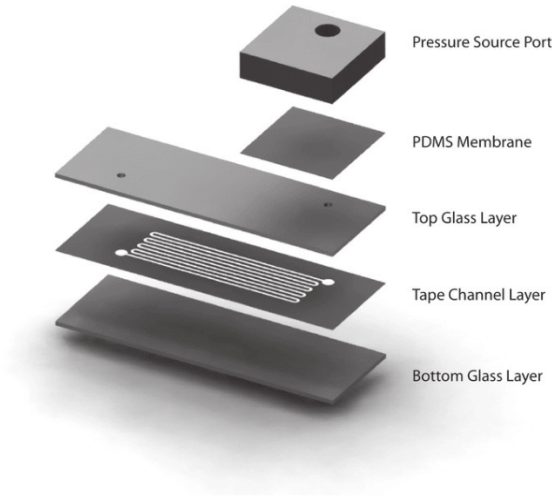

Figure 4. Fabrication of glass channels. Channels of different widths are cut into double-sided tape using a knife plotter. The tape channels are sandwiched between two glass slides into which access holes have been drilled. One hole is covered by a thin PDMS membrane acting as the pump. The other hole is used as a fluid well.

a microscope, and the images were evaluated using Image J software to accurately determine the distance traveled. After the fluid had filled the glass/tape channels, the pressure on the membrane was reversed so that a positive pressure forced air through the membrane and pushed the fluid back out of the channel into the well. Pictures were then taken again at intervals and flow rates were calculated. The experiments were repeated with different pressures ranging from 50 to 700 mbar. Due to the fixed size of the through holes in the glass, the diffusion area for the pump was constant for each individual chip tested.

3.2. Bubble injection and removal

A bubble injection device was fabricated using three layers of PDMS (Sylgard 184, Dow Corning). The control layer and the fluid layer were fabricated using soft lithography and a mold manufacturing technique known as xurography. The membrane layer is fabricated by spinning uncured PDMS onto a polystyrene substrate at 3000 rpm for 30 s. Following a 60 min partial cure at 60 °C, the control layer is bonded to the membrane which can then be peeled of the substrate. The fluid channel is then aligned and bonded to the open side of the membrane. The area of overlap between the control channel and the fluid channel was a circle with a 3 mm diameter. This diffusion area was connected to the main fluid channel at a T-junction. Injection of an air bubble into the fluid channel was demonstrated by applying a positive pressure to the control channel, forcing air through the membrane and into the flowing fluid channel. The air bubble extruded into the fluid channel until it was pinched off and carried down the channel by fluid flow.

In a similar manner, a PDMS membrane was used to extract bubbles from a moving fluid by using negative pressure in the control channel further downstream. Several generations of designs for trapping and removing the bubbles were fabricated. The first involved having a small control channel perpendicularly intersect the fluid channel with a small rectangular area of PDMS membrane separating the two channels. While this method proved to work for small amounts of air bubbles, a larger membrane diffusion area was needed to remove larger, more continuous bubble streams. To accomplish this, the fluid channel was designed with a break in the sidewall that opened into a reservoir for holding the gas bubbles. The reservoir floor was a thin PDMS membrane suspended over a control channel that would remove the trapped bubbles. The reservoir and control channel were dotted with posts to help support the membrane. When the reservoir was filled with fluid, bubbles from the fluid stream would often not enter the reservoir; likely because doing so would require a displacement of the fluid already in the reservoir. Consequently, a small exit channel was made at the rear of the reservoir to allow displaced fluid to re-enter the fluid stream when a bubble entered the reservoir. This method proved effective. Having the fluid stream widen to create an in-stream reservoir for the gas bubbles was the final design for a bubble removal device.

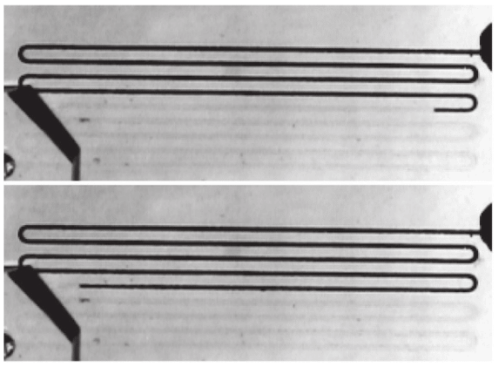

Figure 5. Determining volumetric flow rate in glass channels. Pictures of the chip are taken at different times to show the change of position of the fluid in the channel.

Rates of bubble removal were determined in an optical manner similar to previous examples in order to determine flow rates in glass channels. A CCD camera took video of the bubble trap as a single large bubble was injected into a bubble trap and removed through the membrane. Frames from the video at known time intervals were analyzed using Image J software to determine the volume of air in the bubble trap. A series of these frames were used to determine changes in bubble volume per unit time to calculate the rate of air removal.

3.3. Mixing

A mixing device that employs bubble injection and removal was fabricated using the three-layered PDMS membrane method described above. Fluid was pumped into the device using a dual syringe pump, which injected clear water and heavily dyed water into two openings at flow rates of

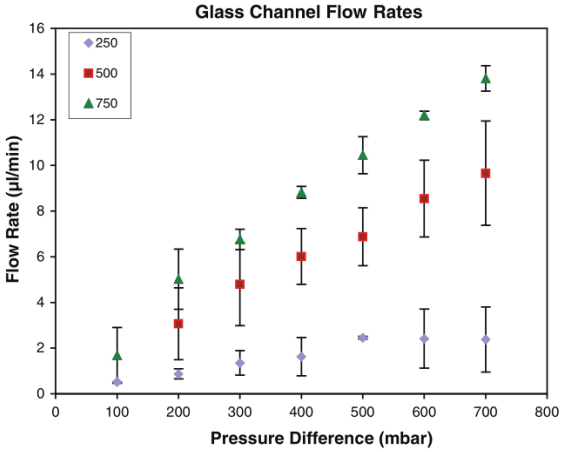

Figure 6. Volumetric flow rates in glass channels. The flow rates were determined for different channel widths at a range of pressures applied to the pneumatic control channel.

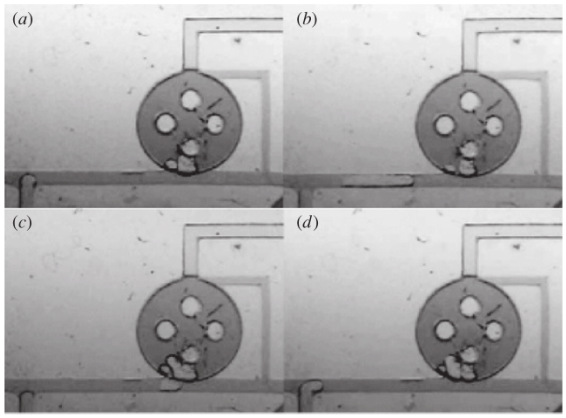

Figure 7. Bubble removal from a channel with a circular bubble trap reservoir. (*a*) A previously trapped bubble (lighter color) is seen in the bubble trap and another bubble prepares to enter the fluid channel. (*b*) The new bubble moves down the fluid channel toward the bubble trap. Bubbles already in the bubble trap are seen to reduce in size as time progresses. (*c*) The moving bubble is stopped by the bubble trap and drawn into the reservoir. (*d*) The bubble is fully trapped and is being removed through the membrane while another bubble prepares to enter the fluid stream. The circular reservoir has a 4 mm diameter. The support posts are 750 μm in diameter with a 1.3 mm spacing.

50 μl min^{-1} each for a total system flow rate of 100 μl min^{-1}. The two fluids met at a Y-junction, but remained relatively unmixed through the rest of the system. Bubbles were injected into the fluid channel at a T-junction using the membrane diffusion method explained previously. The fluid channel passed through a set of two branches that served as locations for the bubbles to get trapped and fold the fluid in on itself to enhance mixing. The fluid channel then widened into a bubble trap area where the air could be removed through a PDMS membrane.

A microscope connected to a CCD camera was positioned to take pictures of the fluid downstream of the mixing apparatus. The amount of mixing was determined by analyzing the pictures using Image J software. The distribution of the dark fluid was measured by plotting the relative amount of dye in the fluid channel from one wall to the other.

4. Results and discussions

4.1. Glass channels

Flow rates measured for various pressures and channel widths in the glass-tape channels with a PDMS pumping membrane are presented in figure 6. These flow rates were determined for the specific fluid (dyed water) and channel geometry described above. Flow rates would be different for pumping fluids with different viscosities or for different pump and channel geometries. The main observation is to note the low flow rates and good control capabilities associated with this pumping method.

An important aspect of flow in glass microfluidic structures is how the hydrophilic nature of the glass causes fluid to flow through the glass channels by capillary action, if both ends of the channel are open to the atmosphere. Using a PDMS membrane as a pump, however, holds in enough pressure to prevent the fluid from wicking down the channel until a pressure is applied at the membrane. This property could be useful in applications where small glass channels are desired, but fluids need to be kept from entering certain branches for a limited period during chip operation.

4.2. Bubble removal

Figures 7 and 8 show two series of photographs taken as air bubbles are removed from fluid channels using two different designs of a bubble trap and removal system. In figure 7, the bubble injected at the T-junction travels down the fluid channel until it passes the bubble trap. At that point, surface tension forces draw the bubble into the bubble trap reservoir where it is held in place while the air is removed through the membrane. In figure 8, an injected bubble similarly travels down the fluid channel until it is trapped and removed in the widened bubble trap section.

Both of these bubble trap designs proved effective at trapping bubbles to prevent them from traveling further downstream and removing the air through the permeable membrane. The circular reservoir bubble trap design was beneficial in that the bubble was removed completely out of the moving fluid stream. The widened channel design takes up slightly less real estate and could be used when it is desirable to hold the bubble in the fluid stream, such as in mixing applications.

The rate of air removal through the membrane is proportional to the area through which the bubble can diffuse, which is proportional to the volume of air inside the bubble trap. Consequently, the rate of air removal increases when there is a higher rate of bubble injection until an equilibrium state is reached where the removal rate equals the injection rate. Figure 9 shows the volume of two air bubbles in the channel

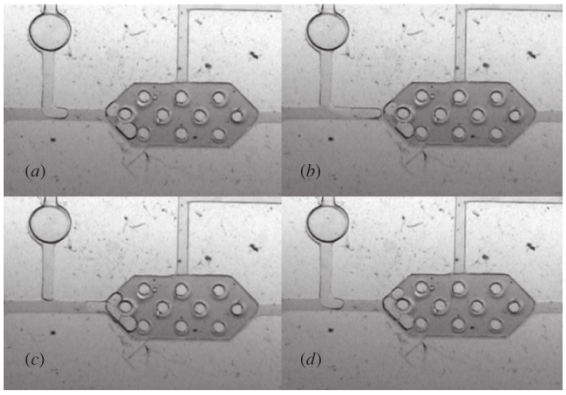

Figure 8. Bubble removal using a widening channel. The channel widens from a width of 500 μm to 3.2 mm into a large area with support posts (same dimensions as above) to hold a membrane between the fluid and control channels. (*a*) A bubble enters the fluid stream at a T-junction while two previously injected bubbles are already trapped by the support posts. (*b*) The bubble approaches the widened-channel bubble trap region. (*c*) The bubble enters the bubble trap region and is stopped by the support posts. (*d*) The bubble is fully trapped and is being removed through the membrane while another bubble prepares to enter the fluid stream. It is important to note that the trapped bubbles do not completely block the fluid channel. The bubbles remain immobile and attached to the PDMS support posts in the widened channels while the fluid flow rate is held steady at 100 μl min^{-1}.

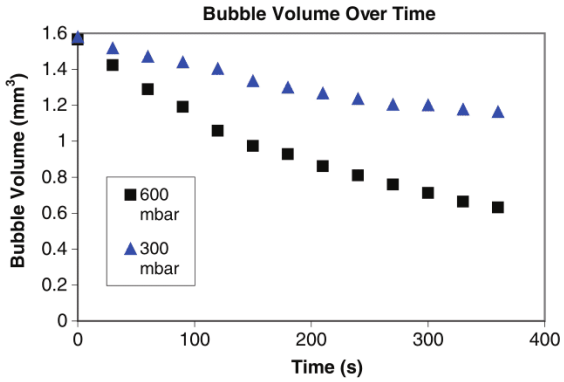

Figure 9. Bubble volume. The volume of an air bubble in a bubble trap is reduces over time as the air diffuses through the PDMS membrane into the control channel.

expansion bubble trap as time progresses and they are removed through the membrane with different pressure differences in the control channel. Both tests started with a bubble of similar size, and it is apparent that the control channel with the larger pressure difference removes the air at a much higher rate. It is also evident in both cases that the rate of air removal decreases as time progresses because the diffusion area decreases.

Figure 10 is a summary of the air removal rates taken at several different pressures. In order to compare the air removal rates for bubbles of different sizes, we looked at the rate of air removal per membrane diffusion area.

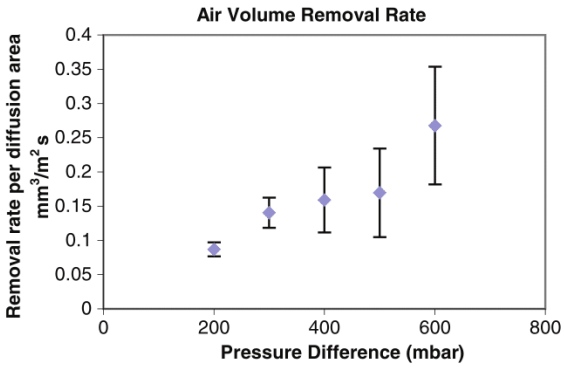

Figure 10. Bubble volume removal rate. The rate of air bubble removal per diffusion area for several different pressures is examined and follows the expected pattern of having a higher removal rate for a higher pressure difference.

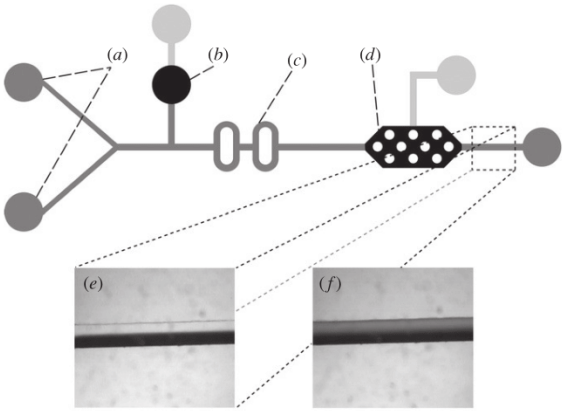

Figure 11. Bubble enhanced mixing apparatus schematic. (*a*) Fluid injection ports. A dyed water solution is pumped into one side of the channel and clear water into the other. (*b*) Bubble injection device. Applied pressure forces air through a membrane and into the fluid channel. (*c*) Mixing section. Bubbles enter the branched channels and force the fluid to fold over and cross streamlines to enhance mixing. (*d*) Bubble trap. Bubbles are trapped and removed in this section. (*e*) Photograph of fluid channel after the bubble trap with no bubble injection. The clear and dyed fluids are clearly discernable. (*f*) Photograph of fluid channel after the bubble trap with bubble injection. The clear and dyed fluids are markedly better mixed indicating the increased mixing efficiency from bubble inclusion.

4.3. Mixing

The ability of the bubble injection/removal system to aid in the mixing of fluids was determined by examining photographs of a mixing channel before and after a bubble is injected (see figure 11). The channel section examined is located downstream from the bubble injection, mixing, and bubble trap regions of the device. Before the bubble is injected, the channel is clearly divided into dark and clear regions indicating the lack of mixing between the two fluids. After a bubble is injected, a significantly higher amount of the dyed fluid is found in the previously clear half of the channel. The increase in mixing

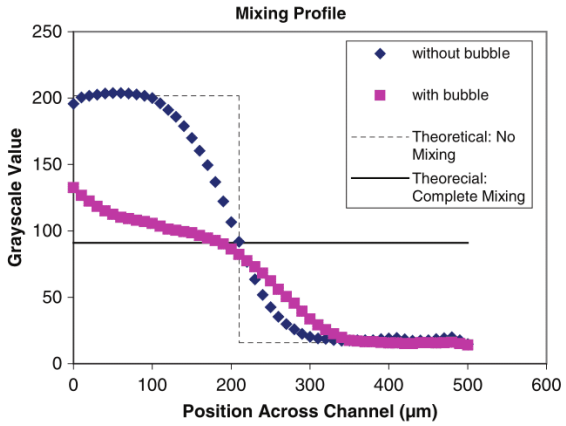

Figure 12. Cross-channel mixing profile. The amount of dye in the solution on a line across the channel is indicated by optically determining the grayscale values in the picture on a 0–255 scale. Lower grayscale values indicate the presence of more dye.

is readily apparent and is more qualitatively described in figure 12. Image J software was used to determine the grayscale value of the image on a line across the channel perpendicular to the flow direction to indicate the amount of mixing produced. The mixing profile in the channel without bubble injection shows a wide disparity in grayscale values that approaches the theoretical step function expected when no mixing is taking place. When a bubble is injected, the profile approaches the more uniform straight line expected from total mixing, indicating the increased mixing produced. The standard deviation of the normalized grayscale values across the channel shows a reduction from 0.45 to 0.20 when a bubble is used to enhance mixing, where a standard deviation of 0.5 would indicate total fluid separation and 0.0 would indicate total mixing. This result indicates the tightening of the grayscale value distribution which represents increased mixing. These results indicate that there was a significant increase in mixing when a bubble was introduced. While complete mixing was not achieved with this device, the desired result was produced in demonstrating that membrane permeation could be used as the source and sink for bubbles used to enhance mixing while leaving the downstream systems unaffected.

An external syringe pump was used as the fluid pumping mechanism for the mixing experiments. The mixing technology could be integrated with the gas-permeation fluid pumping technology detailed above to create a system that only requires a pneumatic pressure source instead of an entire external pumping system. Such a system, however, would be more limited in that the gas-permeation pump would require the fluids to be mixed to be located in dead-end channels.

5. Conclusion

Using the three-layered fabrication technique to create a PDMS device with a fluid channel, a thin membrane and a pneumatic control channel has proven a relatively simple way to integrate several microfluidic control components onto a single chip. This technique facilitates a unique fluid pumping method in microfluidic systems that uses gas permeation through the membrane to push or pull fluids away from or toward a dead-end channel. This pumping system was demonstrated to be capable of controlling flow rates in glass channels. This pumping method shows promise in its ability to precisely control flow rates using pneumatic pressure sources which are commonly used in microfluidic systems to control valves, etc. This eliminates the need for another external control system for pumping purposes.

The gas permeability of the membrane was also proven effective for injection of gas bubbles into the fluid channel and their later removal. Injecting bubbles into a microfluidic system can be of benefit when reagent gasses need to be combined with liquids in a microfluidic system. Varying the gas pressure, PDMS membrane thickness and diffusion area will allow precise control of gas injection rates. Bubble removal by diffusion of the gas through the membrane was demonstrated using several geometries of bubble traps. Such components can perform an essential function in microfluidic systems by removing unwanted bubbles that can interfere with fluid flow or detection and analysis components.

Finally, the ability to add and remove bubbles from a fluid channel was used to enhance the mixing of two fluids flowing through a series of branched channels. While bubble enhanced mixing through branched channels is not novel, the use of a gas-permeable membrane to be the source and sink of the bubbles shows an advance in providing a simple control system to ensure that the injected bubbles do not affect downstream microfluidic components. All of these applications of a thin PDMS membrane advance the microfluidic industry toward versatile microfluidic systems with limited external controls. Multiple components with diverse uses can be simultaneously fabricated using the same three-layer soft lithography approach. Implementation of these advances will lead toward inexpensive (perhaps even disposable) microfluidic systems capable of operating in resource-limited environments.

References

[1] McDonald J C and Whitesides G M 2002 Poly(dimethylsiloxane) as a material for fabricating microfluidic devices *Acc. Chem. Res.* **35** 491–9

[2] Unger M A, Chou H, Thorsen T, Scherer A and Quake S R 2000 Monlithic microfabricated valves and pumps by multiplayer soft lithography *Science* **288** 113–6

[3] Kang J, Kim Y and Park J 2008 Analysis of pressure-driven air bubble elimination in a microfluidic device *Lab Chip* **8** 176–8

[4] Eddings M and Gale B 2006 A PDMS-based gas permeation pump for on-chip handling in microfluidic devices *J. Micromech. Microeng.* **16** 2396–402

[5] Merkel T C, Bondar V I, Nagai K, Freeman B D and Pinnau I 2000 Gas sorption, diffusion, and permeation in poly(dimethylsiloxane) *J. Polym. Sci.* B **38** 415–34

[6] Garstecki P, Fuerstman M J, Stone H A and Whitesides G M 2006 Formation of droplets and bubbles in a microfluidic T-junction—scaling and mechanisms of break-up *Lab Chip* **6** 437–46

[7] Meng D D, Kim J and Kim C 2006 A degassing plate with hydrophobic bubble capture and distributed venting for microfluidic devices *J. Micromech. Microeng.* **16** 419–24

[8] Gunther A, Jhunjhunwala M, Thalmann M, Schmidt M and Jensen K F 2005 Micromixing of miscible liquids in segmented gas-liquid flow *Langmuir* **21** 1547–55

[9] Gunther A, Khan S A, Thalmann M, Trachsel F and Jensen K F 2004 Transport and reaction in microscale segmented gas-liquid flow *Lab Chip* **4** 278–86

[10] Garstecki P, Fischbach M A and Whitesides G M 2005 Design for mixing using bubbles in branched microfluidic channels *Appl. Phys. Lett.* **86** 244108

[11] Garstecki P, Fuerstman M J, Fischbach M A, Sia S K and Whitesides G M 2006 Mixing with bubbles: a practical technology for use with portable microfluidic devices *Lab Chip* **6** 207–12

[12] Bartholomeusz D A, Boutte R W and Andrade J D 2005 Xurography: rapid prototyping of micro-structures using a cutting plotter *J. Microelectromech. Syst.* **14** 1364–74

CHAPTER 3

NUCLEIC ACID EXTRACTION SYSTEM

3.1 Introduction

Bioassays for detection or quantification of organisms often rely on nucleic acid detection. The varied conditions of the sources of target genetic material (i.e., prokaryotic or eukaryotic cells in blood, water, stool, soil, and others) and the stringent purity requirements of analysis techniques most often force system-specific sample preparation operations, which often require time consuming and expensive manual handling.[1] Self-contained lab-on-a-chip systems capable of preparing genetic material out of raw biological samples have been achieved with varying levels of success as presented in Chapter 1. The benefits envisioned by making nucleic acid analysis more readily available will be closer to realization when steps are taken towards universal sample preparation with the ability to take samples from various sources (blood, bacteria cultures, and virus samples) and selectively extract and purify nucleic acids (DNA or RNA).

3.1.1 Extraction System Overview

In the work described in this chapter, efforts to build and test a system for automated NA purification from a variety of biological samples are described. The nucleic acid is purified using an integrated microfluidic fluid handling chip and a solid-phase extraction chip. The overall extraction process operates by pumping the sample and various reagents using integrated metering/mixing reservoirs through an extraction filter on the extraction chip where the nucleic acid is selectively bound and released depending on buffer conditions. Altering the amounts, types, and sequences of reagents allows selective adjustment of the protocol to handle different sample types and control the output as DNA or RNA. These adjustments are easily accomplished by modifying a

control program and input reagents.

This chapter is composed of several sections that report on the development of the microfluidic NA extraction system. First, the design and fabrication of the individual components are discussed. Details are provided of the fabrication of a three-layer polydimethylsiloxane (PDMS) microfluidic chip designed to perform the main fluid handling tasks. A multilayer mold and rapid prototyping technique is employed in the fabrication of integrated microchannels, valves, and metering diaphragm pumps. Second, a separate module is fabricated to incorporate the silica membrane used as the disposable solid phase for nucleic acid extraction. Calculations and experiments are performed to develop the filter chip architecture. The nucleic acid extraction efficiency of the solid phase filters are characterized with respect to parameters such as flow rate and filter material. Third, the ability of the system to handle different sample inputs is demonstrated by extracting DNA from both a stock DNA solution and whole blood, and by recovering RNA form known RNA solution standard, living *E. Coli* cells, and FMDV virus cultures. Following extraction, the purified genetic material can be mixed with other reagents required for analysis techniques such as electrochemical detection or transfer to a PCR module as will be discussed in Chapter 4.

3.2 Materials and Methods

3.2.1 Chip Design and Fabrication

3.2.1.1. PDMS chip overview

The heart of the NA extraction system is a microfluidic fluid handling chip fabricated using a three-layer approach with a fluid layer, a flexible membrane, and a pneumatic control layer see Figure 3.1. The pneumatic layer forces membrane actuation

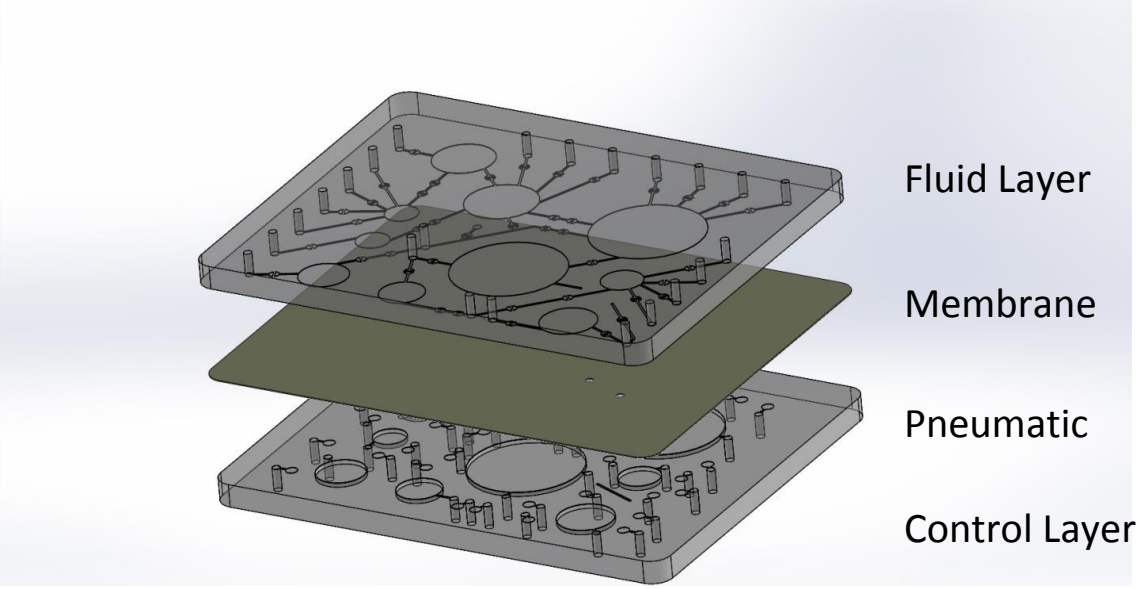

Figure 3.1: Diagram of 3-layer microfluidic chip.

to operate the embedded pumps and valves. The chip design incorporates eight fixed-volume, on-chip metering diaphragm pumps similar to those reported by Grover et al.[2] These pumps interface with 17 fluid inlet ports and two module access ports to facilitate adaptable protocols for nucleic acid extraction. Different pump volumes allow a range of input volumes to accommodate the mixing ratios of extraction protocols.

Figure 3.2 is a schematic of where the valves and pumps are located on the chip layout. Locations of other features important to chip function are also indicated.

3.2.1.2 Valve design and operation

On-chip valves operate by applying pressure to the control layer which pushes the membrane against the valve seat, sealing the channel. Vacuum applied to the control channel pulls the membrane away from the valve seat, and fluid is then free to flow through the open channel. Valve function is described by the schematic in Figure 3.3.

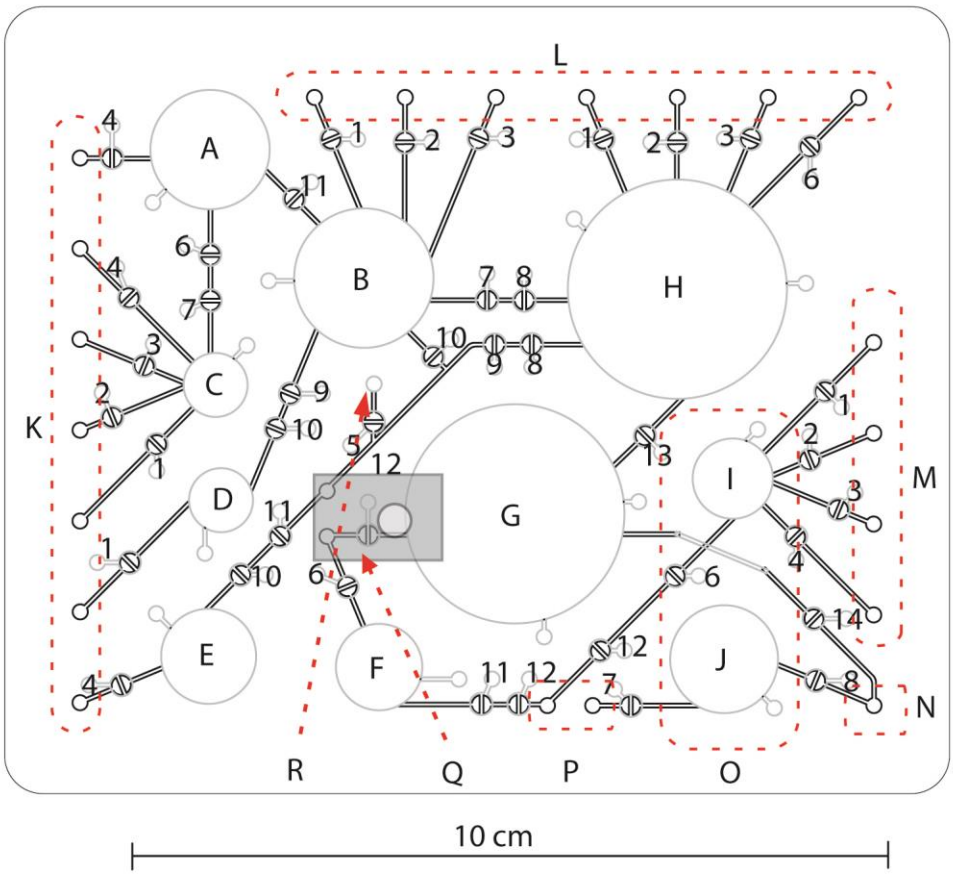

Figure 3.2. Diagram of functional features incorporated onto PDMS extraction chip. Numerically labeled features are on-chip valves, with numbers indicating the associated off-chip solenoid valve. Features A-J are the metering pumps and mixing chambers, K-M are sample and reagent input ports, N is the waste output, O highlights postextraction processing section, P indicates extraction process output and external module connection, Q is the location of the solid phase chip, and P is the direct pressure line for drying and channel clearing steps.

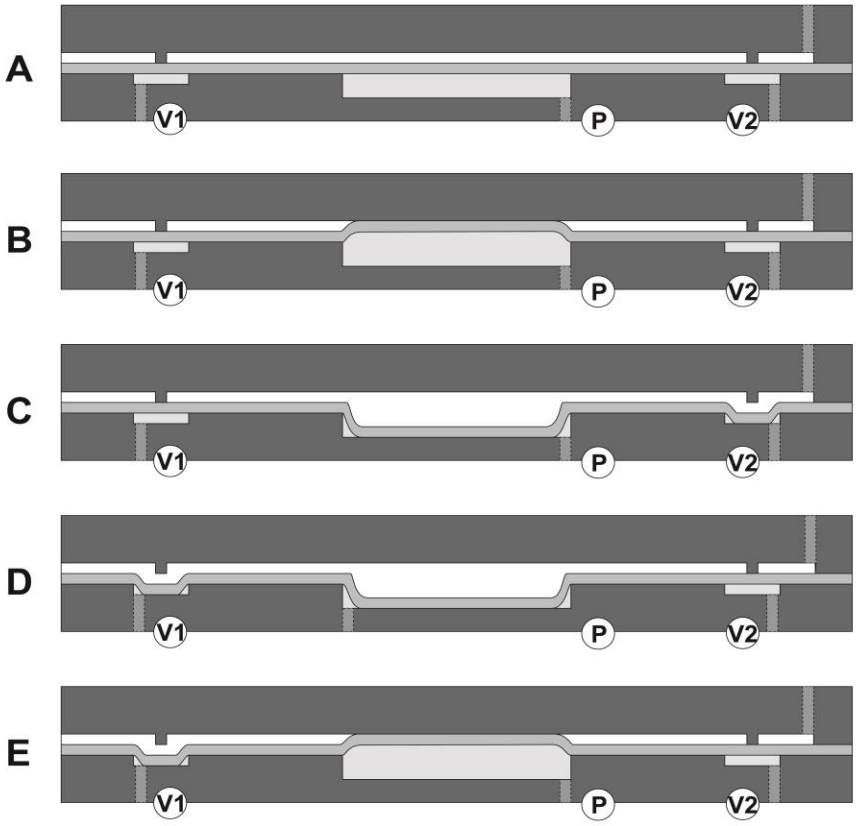

Figure 3.3: Diagram of on-chip valve and metering pump operation. A) chip with membrane at equilibrium. B) Pressure applied to the Pump, P and valves V1 and V2. C) Vacuum applied to V2 and P2 opens a channel for fluid to enter the inlet port and fill the pump reservoir. D) V2 is closed with pressure, and V1 is opened with Vacuum. E) Fluid in the reservoir is forced out through the channel passing V1.

On-chip valves are actuated by switching the control layer portion of the valve between pressure and vacuum using an off-chip electrically actuated three-way solenoid valve.

The valve design has the channel opening into a circular area with a gap in the middle. The widened circle increases the area exposed to the pressure difference and reduces the pressure required to overcome the innate stiction of the membrane to the valve seat. The control channel side of the valve is made a slightly larger circle than in the fluid channel side to reduce alignment tolerance requirements to produce a high yield

of operational valves over the large are of the PDMS chip.

3.2.1.3 Pumps

Metering diaphragm pumps pull fluid into the chip through the access ports. In the default state of the pump, control pressure pushes the flexible membrane against the top of the fluid reservoir, reducing the volume in the fluid side of the reservoir to the space around the sharp corners where the membrane cannot extend. When vacuum is then applied to the control layer, the membrane is pulled to the bottom of the reservoir, and fluid is drawn in to fill the evacuated space. The fluid is forced out of the reservoir pump by again applying pressure to the control layer, forcing the membrane up and displacing the fluid which exits through an open channel. The fluid layer and the pneumatic control layer are created by casting PDMS (Slygard 184, Dow Corning). Molds are made using a xurographic technique[3] with features being cut from a vinyl tape (Instachange, 3M, St. Paul, MN) on a knife-plotter (Graphtec, Irvine CA). After the features were cut in the vinyl tape, they were transferred to a PMMA substrate. This rapid prototyping fabrication technique allows the formation of molds with fluid channel widths as low as 200 μm, without the need for conventional microfabrication or micromachining methods, in as little as 10 minutes.

This fabrication method was also improved for the fabrication of the fluid handling chip by including larger mesoscale 3D structures to interface with a range of larger fluid volumes (50-1000 μl) required for the extraction process. The pneumatic control layer mold was designed with features of different heights to increase diaphragm pump volumes and improve valve performance. Different mold heights for valve controls were achieved by stacking cut tape layers. Large reservoirs for the on-chip fixed

volume diaphragm pumps were made by bonding laser-cut PMMA features to the corresponding tape features using a cyanoacrylate adhesive (421, Loctite, Westlake, OH).

Following mold fabrication, PDMS was mixed at a ratio of 10:1 with curing agent, degassed in a vacuum chamber for 15 minutes, and poured into the molds. The filled molds were cured in a 60 ˚C oven until fully cured (more than 2 hours). The cured fluid and pneumatic control layers were removed from the molds, and pneumatic and fluid connection ports were cored using a 1.5 mm diameter biopsy punch (Uni-Punch, Clear Lake, WI). The fluid and control layer were aligned optically under the microscope prior to any bonding operations and four alignment holes were cored through the PDMS to allow alignment of the two layers through the opaque membrane.

A thin silicone sheet (Bisco HT-6135, Stockwell Elastomerics, Philadelphia, PA) was used for the membrane layer. The membrane was first bonded to the pneumatic control layer using plasma treatment bonding which operates by creating hydrophilic, chemically active functional groups on the PDMS surface that bind to other activated groups on the mating surface.[4] The areas to be bonded on the membrane and control layer were exposed to the discharge from an air plasma surface treater (Enercon Industries, Menomonee Falls, WI) so that all surfaces were exposed for approximately 1 minute with the treater head approximately 0.5 inches above the surface. The treated surfaces were then brought into contact and pressed together with a rubber roller. The control layer/membrane assembly was then incubated for 20 minutes at 60 ˚C.

Following the first bonding step, holes were cored through the membrane to open the alignment holes and to produce three cross-membrane vias. One provides the port through which pressurized air can directly enter the chip for drying steps or to aid in

emptying channels. The other two vias route the waste channel to the other side of the membrane in order to cross another channel without interference.

When bonding the fluid layer to the membrane/pneumatic control layer assembly, steps were taken to prevent unwanted bonding at the valve seat and over the large surface areas of the metering diaphragm pumps. Covering the PDMS layer to be bonded with a masking material during corona discharge treatment blocks areas from exposure to the corona plasma so that only desired surfaces are activated, as shown in Figure 3.4. Several masking materials were shown to be effective: rubylith electrostatic film, 3M Instachange tape, mineral oil, and liquid spin-on glass. Subsequent removal of the mask and contact with another activated PDMS surface is shown to produce selective bonding, with the masked areas remaining unbound. 3M Instachange tape was used as the mask for this device with the mask shapes cut on the knife plotter. Masks were manually placed over the areas that were not to be bonded. Again the surfaces were treated with air plasma for approximately 1 minute. Following treatment, the mask material is removed and alignment pins are placed through the alignment holes. The two layers to be bonded are then brought into contact, compressed, and incubated as described above.

3.2.2 Solid Phase Extraction Chip Fabrication

The purification of target nucleic acid from background compounds that would impede analysis is performed using solid phase extraction techniques with a silicate substrate acting as the solid phase. For nucleic acid purification on a microfluidic chip, the solid phase needs to be easy to integrate into the flow control structure of the chip and be disposable to avoid cross-contamination between extraction assays.

The first generation of the integrated solid phase module (SPE chips) consists of a

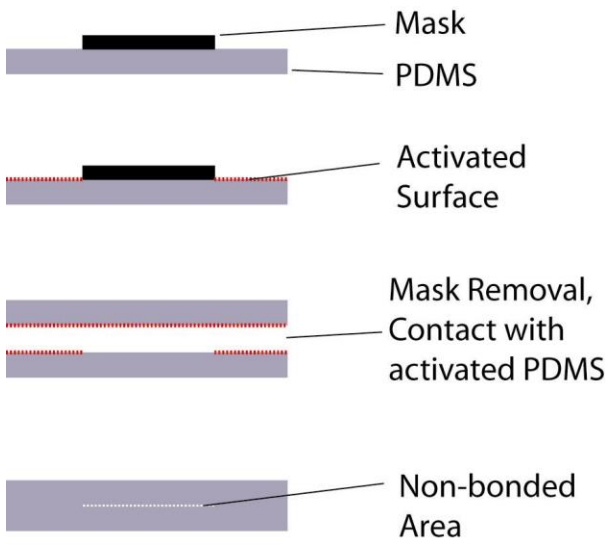

Figure 3.4. Masked plasma bonding process. The PDMS face is covered with a mask that exposes the surfaces to be bonded. The surface is then activated by exposing it to corona discharge. The mask is removed and the surface is brought into contact with another activated PDMS surface. Areas where two activated surfaces contact are irreversibly bonded, while other areas remain nonbonded, even if they are in direct contact.

PDMS casing enclosing a stack of silica beads (Sigma-Aldrich Corp. St. Louis, MO).

The PDMS casing is molded in four layers, each layer bonded to the others using a plasma surface treatment activation method. The beads are held in the solid phase chamber between two glass microfiber filters (GF/D, Whatman, Maidstone, Kent, UK) at the inlet and outlet of the solid phase module.

The next generation of silica chips omitted the beads in favor of silicate filter membranes only because of fabrication difficulty and the calculation that the microfiber filter material had approximately an order of magnitude more surface area per volume than the beads (5.6×10^4 vs 8.8×10^3 $m^{2/}m^3$).

Disposable filter chips shown in Figure 3.5 were fabricated by sandwiching the

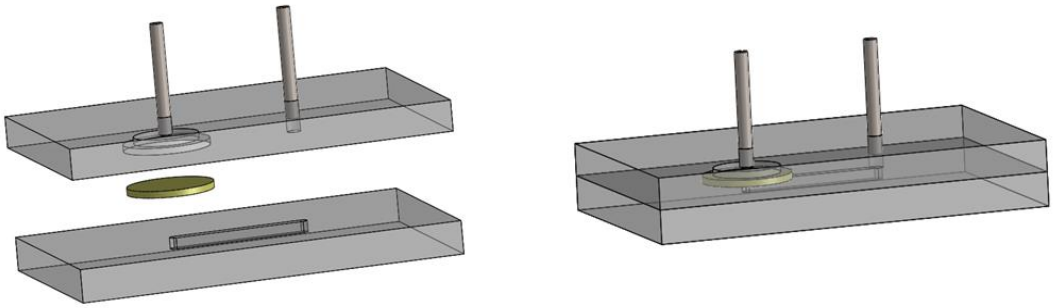

Figure 3.5. Diagram of the construction of the glass filter solid phase chip.

filter material between two laser-cut PMMA blocks. A CO_2 laser (Universal Laser Systems) was used to cut the access ports, filter pocket, and microchannel in the PMMA blocks. The filter pocket was created by laser etching a well into the PMMA with a shallower ring around the lip which serves to seal off the edges and force the fluid to pass through the filter. The two halves of the block are sealed together using a double-sided pressure sensitive adhesive (467 MP, 3M). Tubing connections are made by inserting 22 gauge stainless steel tubing into the access ports and bonding using a UV cure adhesive (3106, Loctite, Westlake, OH). These connectors are press-fit into access ports located on the PDMS fluidic control chip.

3.2.2.1 Filter material

Two types of glass filters were used as the solid phase membrane: borosilicate glass and quartz (GF/D and QM/A, respectively). To test the extraction efficiency of the different filter materials, 100 ng and 200 ng samples of prepurified human genomic DNA were added to a chaotropic salt buffer (Qiagen, Venlo, Netherlands) and passed through the filters at 100 µl/min. The filters were then rinsed with 80% ethanol and dried for 2

minutes with pressurized air at 10 psi. Finally, the DNA is eluted from the filters with 100 µl of purified water. The collected DNA was quantified using the fluorescence method described in later sections.

3.2.2.2 Flow rates

To determine the effect of flow rate on the extraction efficiency of the NA extraction chip, a syringe pump was loaded with a known concentration of DNA sample in a binding buffer. The syringe was connected to the solid phase filter chip and the fluid pumped through the filter at different flow rates. The residence time was kept the same for all flow rates by pumping the samples at higher flow rate samples several times through the filter. Consequently, the molecules at all flow rates would spend the same amount of time in proximity to the filter surface.

Following the binding step, the filters were washed with ethanol to remove excess salt and impurities. The filter was then dried by pumping air through the filter at a pressure of 10 psi for 2 minutes to remove residual ethanol, and then the DNA was eluted with 100 µl of purified water. The quantity of DNA eluted was determined using fluorescence as described in later sections.

3.2.3 Nucleic Acid Quantification Methods

To determine the effectiveness of the microfluidic nucleic acid extraction, the quantity of nucleic acid recovered from the system must be measured. Several methods have been developed to quantify the amount of nucleic acid, and three of the primary techniques were used to verify results in this work.

The first method uses a spectrophotometer (Nanodrop, Wilmington, DE) to measure the nucleic acid absorption of UV light. Nucleic acid has a specific UV

absorption spectrum, with the wavelength of interest being 260 nm. Light is passed through a sample and the instrument measures the absorption and relates it to the concentration of nucleic acid in the sample. Because of the specific absorption profile, the spectrum can also be used to determine the purity of the nucleic acid by examining the ratio of characteristic absorption wavelengths. For the case of nucleic acids, a ratio of absorption at 260 nm to 280 nm approximately between 1.8 and 2.0 indicates sufficiently pure nucleic acid. Contaminants left in the sample that absorb UV light in this spectral range can negatively impact readings, and care must be taken to ensure that the absorption spectrum from the carrier buffer be subtracted from the sample spectrum so that only the absorption of nucleic acids is taken into account.

A second method of nucleic acid quantification uses fluorescent dyes. Ribogreen and Picogreen (both from Invitrogen) are two such fluorescent dyes that give a linear response to the presence of nucleic acid and were used to quantify DNA and RNA, respectively. The quantification process begins with making a standard curve by diluting a known concentration of DNA or RNA to concentration values that surround the region of interest. The linear relation that results can be used to directly determine the nucleic acid concentration of an unknown sample from its level of fluorescence. For the studies in this work, fluorescence was measured on a 96-well microplate reader (BioTek).

The final quantification method used in this work is using real-time PCR. When a fluorescent dye is added to the PCR reagent mix, the fluorescence emission of the amplified product can be monitored after every amplification cycle. An increase in fluorescence indicates more strands have been duplicated, with the fluorescence making an exponential increase in intensity after a certain number of cycles, referred to as the

crossing point. Samples that begin with a larger quantity of target nucleic acid molecules will have an earlier crossing point than samples with lower concentration. Nucleic acid concentrations can be determined by comparing the cycle number of unknown sample crossing points to crossing points from known concentrations. The instrument used for these measurements is the LightCycler (Roche) which monitors the amplification of the DNA in real time using an intercalating fluorescent dye.

All three quantification methods have drawbacks and benefits. Spectrophotometry has low signal to noise ratios at low concentrations and is thus unreliable for samples that are dilute. However, spectrophotometry is very rapid and requires little handling, modification, or extra reagents. Fluorescence readings are adversely affected by the presence of autofluorescing agents and chemicals that interfere with the binding of the dyes to the molecules of interest, but fluorescence is superb at handling very low concentrations. PCR is very sensitive to contamination by PCR inhibitors and requires specialized equipment and strict laboratory techniques, but gives the best indication of the usability of the extracted sample for downstream analysis since much of the nucleic acid analysis for microfluidic systems includes PCR amplification of the target prior to detection and study.

To ensure the accuracy of the three measurement systems described above, samples with known quantities of nucleic acids were compared using the three nucleic acid quantification methods: spectrophotometry, fluorescence, and real-time PCR crossing point analysis.

3.2.4 Extraction Protocols

The standard chemical protocols to extract nucleic acid from a biological sample follow the same basic steps, independent of sample source and target molecule. Differences will be discussed later. First, the sample is mixed with reagents that work to release the nucleic acid into solution, which usually involves the lysis of target cells. The lysis buffer also contains a high concentration of a chaotropic salt (guanidinium thiocyanate or guanadinium hydrochloride) which will act as the selective binding agent in subsequent steps. Following lysis, the sample mixture with binding salts contacts the solid phase silica surface. The nucleic acid is reversibly bound to the solid phase and the remaining sample mixture is discarded. A wash step is then incorporated where an alcohol-based solution is flowed over the solid phase to rinse off any remaining cellular debris or proteins that might interfere with downstream amplification or analysis. After the wash step, the filter is dried, leaving only nucleic acid bound to the surface of the filter. The nucleic acid is then released from the solid phase using a buffer or pure water.

For extracting RNA from viruses, the basic protocol is followed with a few additions. Usually a stabilizing reagent (such as B-mercaptoethanol) is included with the lysis buffer to protect the more fragile RNA from degrading during the extraction process. Also, following the wash step, RNAse-free DNAse is used to digest any DNA that might have been extracted during the purification process, leaving only RNA for analysis.

To extract RNA from bacteria, the cell lysis step also needs to include a method for breaking the more robust cell wall. In this case lysozyme is used to perform an enzymatic process to disrupt the cell wall, enhancing the bacterial lysis process.

Extracting nucleic acid from blood samples provides an additional challenge. Proteins that are abundant in blood samples interfere with the extraction process and hinder amplification of target DNA strains by PCR. Consequently, blood extraction protocols begin with a proteinase digestion to remove proteins.

3.2.5 Microfluidic Control System

Performing multiple purification protocols on a single chip is accomplished by using a programmable instrument that controls the on-chip flow sequence. A manifold that interfaces directly with the PDMS chip is mounted onto an instrument that electrically triggers the pneumatic operations for the on-chip fluid handling tasks. The manifold is a plate embedded with barbed fittings at locations that match the pneumatic control ports on the bottom side of the PDMS chip (see Figure 3.6). The chip is loaded onto the instrument by pushing the chip down onto the manifold, creating press-fit seals between the manifold fittings and pneumatic ports.

The instrument contains 24 electrically actuated mini solenoid valves (Lee Company). Control of the valve actuation is accomplished using a USB I/O digital controller (Elexol) connected to a PC running a LabView control program. The LabView program (see Figure 3.7) has a mode for manual manipulation of fluid on the chip used for protocol development and troubleshooting. Up to 4 protocol sequences can also be stored and implemented in an automatic mode, allowing for hands-free extraction of nucleic acids.

A cleaning step was included in the program to allow for multiple tests on a single PDMS chip. A solution of RBS Neutral (Sigma-Adrich) is flushed twice over the system followed by three flushes of nuclease-free water (Qiagen). The programmable nature of

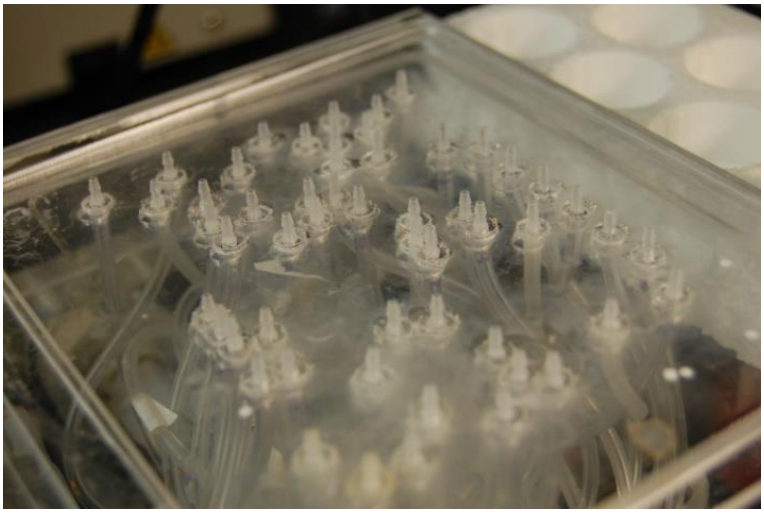

Figure 3.6: Barbed fitting manifold for interface between PDMS chip and control instrument facilitating rapid microfluidic chip replacement.

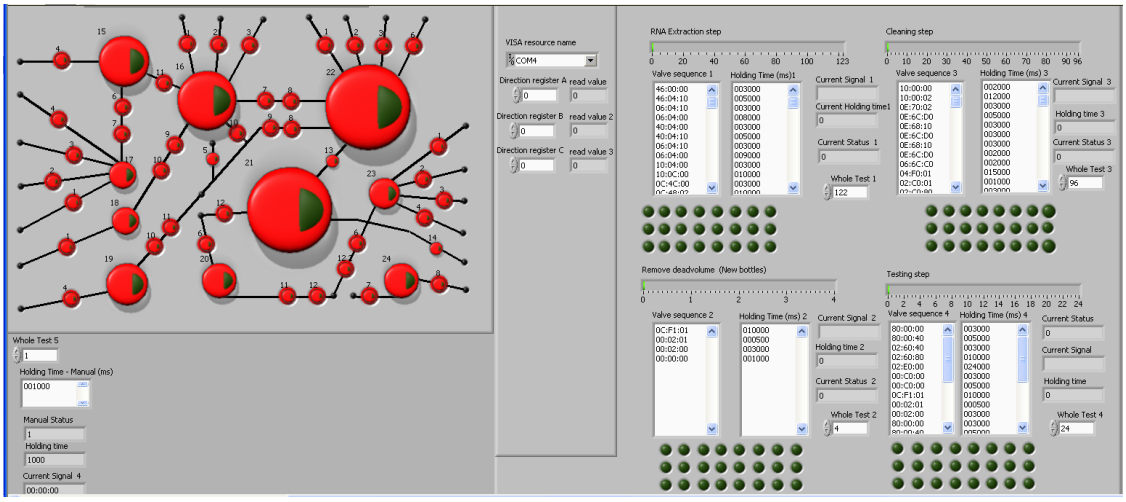

Figure 3.7: Screen shot of LabView control program showing manual mode (left) and 4 selectable automated protocol sequences (right).

the device allows for other disinfectants and cleaning agents to be introduced into the PDMS device, and the entire PDMS chip is also manifold-mounted for easy replacement for sensitive tests where disposable units are desired.

3.2.6 Surface Modification

Further optimization of the RNA extraction system was done by employing several surface coatings to PDMS chip to mitigate nonspecific binding of target molecules to the channel surfaces. Surfaces were coated with sodium polyphosphate (NaPP), P-108 pluronic, P-20, and polyvinyl periladone (PVP). To perform these coatings, approximately 1% w/v solutions of the coating chemicals were continuously pumped through the extraction chip for several hours, and finally the chip filled with the coating solution was put in a 60 ˚C oven overnight. Following coating of the channels, known 100 ng samples of RNA were extracted in the microfluidic chips and compared to standard extraction techniques.

3.2.7 RNA Extraction

Initial extraction protocols developed for the system were developed for extraction of RNA. Optimization of protocol parameters progressed by adapting the steps contained in the RNeasy Mini Kit (Qiagen 74104). Volumes were adjusted to keep mixing ratios the same and process steps were altered to incorporate chip-based pumping through the filter membrane instead of centrifugation.

For initial verification of RNA extraction process parameters, known concentrations of RNA from a standard stock (Invitrogen) were used as the sample. An RNA-containing solution was placed at the sample inlet port of the PDMS device. A protocol (Appendix B) for on-chip mixing of the sample with reagents was used to bind

the RNA to the glass filter, wash off any contaminants, and subsequently release the RNA in an elution of nuclease-free water. RNA extraction efficiencies were determined using a fluorescent Ribogreen RNA quantification kit obtained from Invitrogen. Fluorescence data were obtained using a 96-well plate reader (Bio-TEK). RNA extraction was determined to be successful if the system produced a linear response to the input concentration of RNA at levels on the order of what was seen by the control (Qiagen commercial spin kit). It was not anticipated that the microfluidic system would exceed the extraction efficiency of the commercial kit. Rather, the innovation of the microfluidic system would be demonstrated in its versatility and ease of use.

Following successful demonstration of RNA from prepurified samples from the system, RNA from raw biological samples was demonstrated by performing lysis and RNA extraction from *E. Coli* bacteria cells (New England Biolabs). The cells were incubated in cell culture medium and growth was monitored using optical density measurements to ensure viability. The *E. Coli* cells were then loaded into the automated system where they were enzymatically lysed, and RNA was extracted and quantified.

Viral RNA was also extracted from cultured samples for the detection of Foot and Mouth Disease Virus (FMDV). FMDV samples in tissue culture fluid were used as the sample. The extraction system was programmed according to the virus protocol listed in Appendix B. The presence of extracted viral RNA was verified using spectroscopy on a nanodrop instrument. Success in this case was determined by the ability to amplify the purified RNA by means of RT-PCR, and detected VIA gel electrophoresis.

3.2.8 DNA Extraction

The DNA extraction process was also established with prepurified human genomic DNA used as the input sample. For these tests 100 µl samples of purified DNA with total DNA mass of 0, 50, 100, 200, and 400 ng were drawn into the device and mixed with the appropriate reagents. Purified genomic DNA samples were provided as a gift from Carl Wittwer's lab in the Department of Pathology at the University of Utah. Other reagents were obtained from the DNeasy Blood & Tissue Kit (69504 Qiagen).

To perform the extraction tests, 100 µl of the known sample was drawn into a pipette tip, which was then inserted into the inlet port of the microfluidic chip. The DNA extraction protocol (Appendix B) was initiated, pulling the sample into the microfluidic chip, mixing it with reagents, and extracting the DNA using the same basic binding, washing, and eluting steps described for RNA extraction. The DNA extraction was quantified using fluorescence (Picogreen, Invitrogen) and verified by performing PCR on the eluate using a LightCycler instrument (Roche).

Following verification of the ability to recover DNA, whole blood from a volunteer was used as the extraction sample and DNA was again extracted in the system and quantified using fluorescence and PCR. The criterion for successful DNA extraction on the microfluidic system again was set as the ability to elicit a linear response to input concentration, at levels on the order of those seen in commercial standards.

3.3 Results

3.3.1 Microfluidic Chip Fabrication

The microfluidic chip was successfully fabricated from PDMS. The chip and control platform are shown in Figure 3.8. Forty-one pneumatic valves are connected to

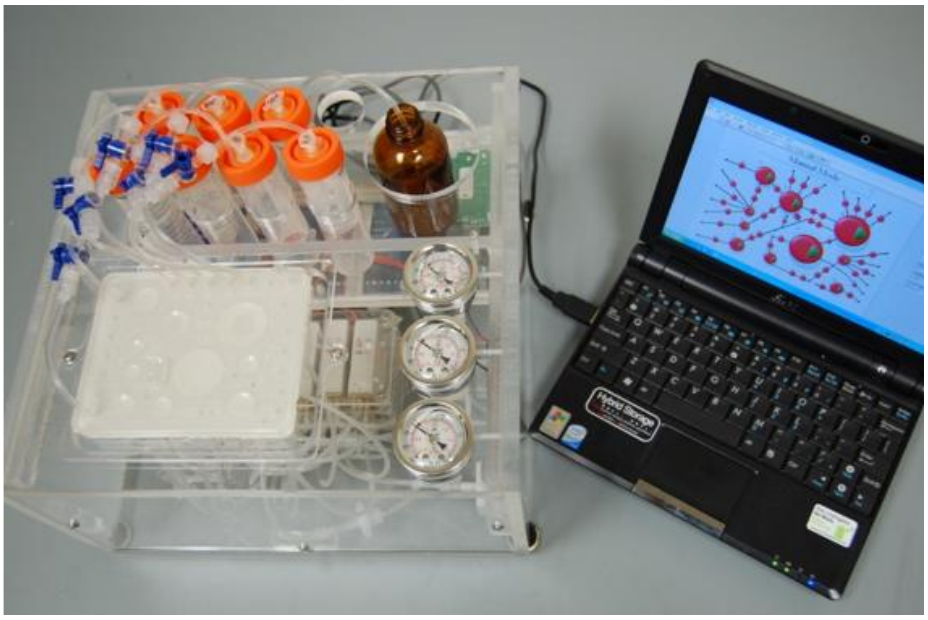

Figure 3.8: Completed PDMS extraction chip and control mechanism. This compact device uses electric vacuum and pressure pumps along with a bank of solenoid valves to control a PDMS microfluidic chip. A LabView control program allows easy adjustment of the protocol to handle a variety of sample inputs.

the on-chip membrane valves through a manifold connector. An on-board compressor and vacuum generator supply the different air pressures required to operate the on-chip pumps and valves. Reagent and waste reservoirs also connect to the PDMS chip through tubing with barbed fittings. A notebook computer with a LabView program control the processing sequence.

Masked corona bonding was successful at selectively bonding the layers together except at the interface between the membrane and the valve seat. All 41 on-chip valves were successful at sealing the channels for valve supply pressures greater than pumping pressures. Volumes pumped by the metering pumps were measured using a micro-pipettor and were found to vary from the desired volume by a maximum of 5% for the larger pumps and a minimum of 2.7% for the smaller pumps.

3.3.2 Silicate Solid Phase Membrane Extraction Yield Characterization and Improvement

In order to improve the extraction efficiency of nucleic acid recovery in the microfluidic purification system, the effect of several parameters were adjusted and studied: solid phase material, flow rates, elution volume.

3.3.2.1 Filter material

Two different types of filter material were used as the solid phase in the construction of the solid phase extraction chips: borosilicate glass microfiber filters and quartz filters. The borosilicate glass filters consistently had higher extraction efficiencies than the quartz as shown in Figure 3.9.

3.3.2.2 Flow rates

The effect of sample flow rate through filters made of both borosilicate glass and quartz was tested. Flow rates from 1 to 50 μl/min were tested and the results are displayed in Figure 3.10. Surprisingly, the lower flow rates yielded significantly less DNA than higher flow rates. As the flow rate increases, from zero, the yield increases to a point and then seems to approach an asymptote or even decrease at the high end of the flow rates tested. As this seems to disagree with results published in the literature; it is likely that the physical geometry of the filter chip inhibits DNA binding at low flow rates, perhaps by allowing the fluid to pass through a single, low-resistance flow path through the filter and reducing the effective surface area onto which the nucleic acid can be bound. More investigation is recommended to determine the cause of the discrepancy, but for the current work, the flow rates achieved by the PDMS chip through the filter corresponded to higher extraction efficiencies, so no further optimization was attempted.

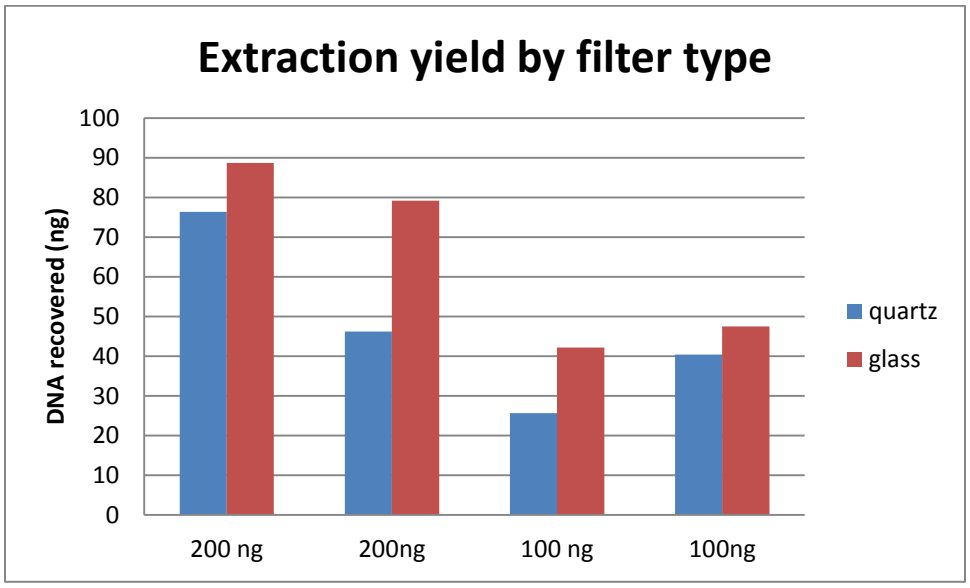

Figure 3.9: Comparison of extraction efficiencies of quartz and glass filters.

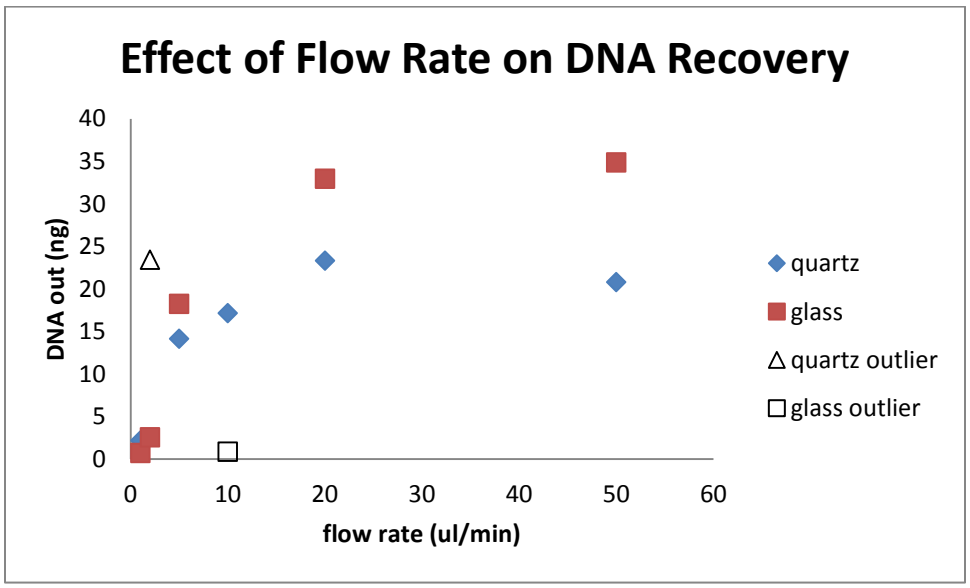

Figure 3.10: Figure showing affect of elution flow rate and different solid phase material on extraction efficiency.

3.3.2.3 Elution volume

When the DNA is eluted from the solid phase filter, only a certain fraction of the bound DNA is released. Elution profiles have shown [5, 6] that earlier elution fractions have a higher concentration of nucleic acid, with the rate of nucleic acid release decreasing as more fluid passes the solid phase. Elution fractions were examined by collecting two sets of five 35 µl (approximate) elution volumes from the extraction chip. The first elution volume was significantly less as the internal dead volume of the system had to be filled before the fluid actually went through the filter. Results in Figure 3.11 indicate that the peak concentration of elution happens between 15 and 70 µl with the amount of DNA decreasing after that. Using only two volumes from the elution pump chamber will thus yield the highest concentration of nucleic acid, but additional 35 µl fractions will continue to elute more DNA from the SPE filter.

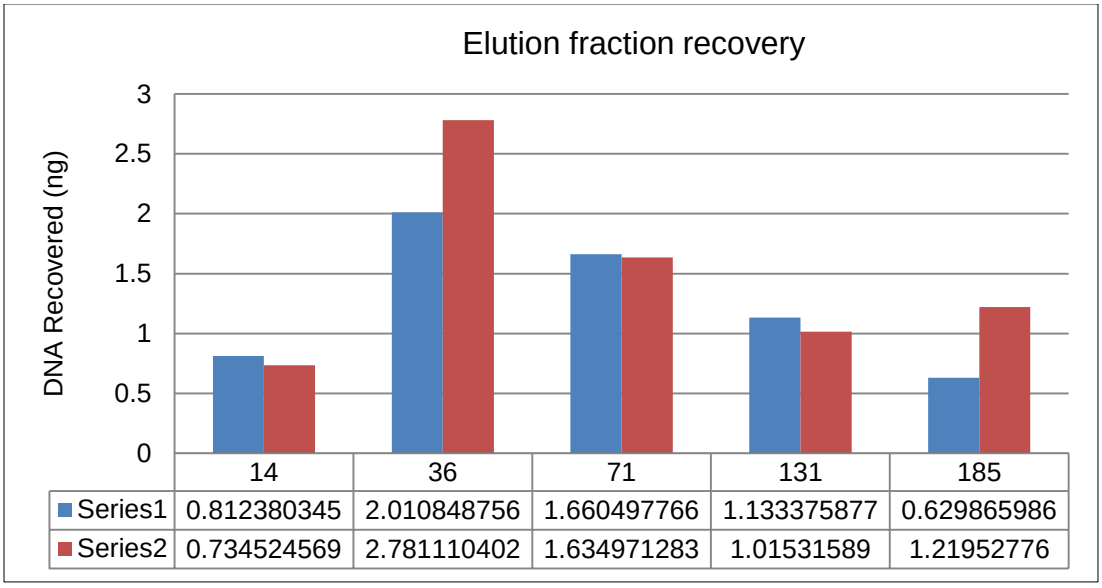

	14	36	71	131	185
Series1	0.812380345	2.010848756	1.660497766	1.133375877	0.629865986
Series2	0.734524569	2.781110402	1.634971283	1.01531589	1.21952776

Figure 3.11: Elution fractions. Bars represent the amount of DNA recovered with each successive 35 µl elution volume.

3.3.3 Nucleic Acid Quantification Methods

Fluorescence, spectroscopy, and PCR crossing point analysis all correctly identified the amount of DNA, and can thus be used interchangeably to quantify the extraction results. The inclusion of samples extracted using the microfluidic system and their successful quantification using the different methods indicates that the system adequately eliminates chemical contaminants, as shown in Figure 3.12. We see that all three quantification methods give strong qualitative evidence to the presence and purity of nucleic acids, as well as correlated, accurate quantitative measurements.

3.3.4 Microfluidic Control System

An instrument was constructed that contains a vacuum pump, a pressure pump, 24 solenoid valves, and a digital I/O controller. The controller connects via USB to a computer running a LabView control program.

Protocol sequences were developed to adapt to the established chemistry used to extract RNA or DNA from different samples as explained above. Table 3.1 highlights the differences between extraction protocols on using the automated system.

3.3.5 Surface Modification

Binding of the nucleic acid to the PDMS surfaces was minimized using various coatings and solution stabilizers. Results from such coating tests are presented in Figure 3.13 and extraction yields are compared to the commercial system. RNA recovery yields from a sodium poly-phosphate (NaPP) coated system approached those from the commercial spin kit. However, these high-yield products displayed some NaPP contamination that interfered with reverse-transcript polymerase chain reaction (RT-PCR) analysis methods. Other coatings actually reduced the extraction efficiency of the

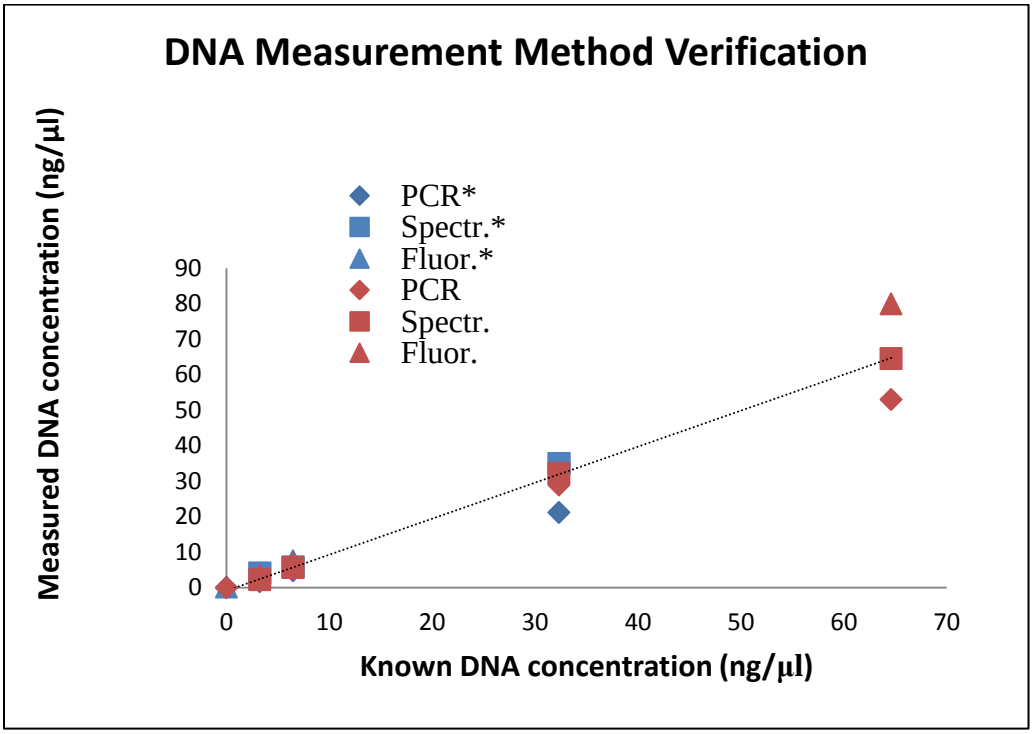

Figure 3.12: Quantification of known quantities of DNA by three different methods shows a close 1:1 relation between known concentration and measured concentration for all measurement techniques. Blue data points were measured with known concentrations spiked into a negative control extraction system output to verify that the system does not output trace contaminants that affect nucleic acid measurement. The dotted line indicates known values.

Table 3.1: Summary of protocol steps as performed by the microfluidics automated control program

Protocol	DNA extraction	DNA extraction from blood	RNA extraction from FMDV	RNA extraction from *E. Coli* (with hybridization)	RNA extraction
Number of process steps	42	64	112	166 (224)	85
Process time (minutes)	7.2	21.6	17.5	53.2 (62)	9.3
Number of reagents required	4	6	6	8(12)	6

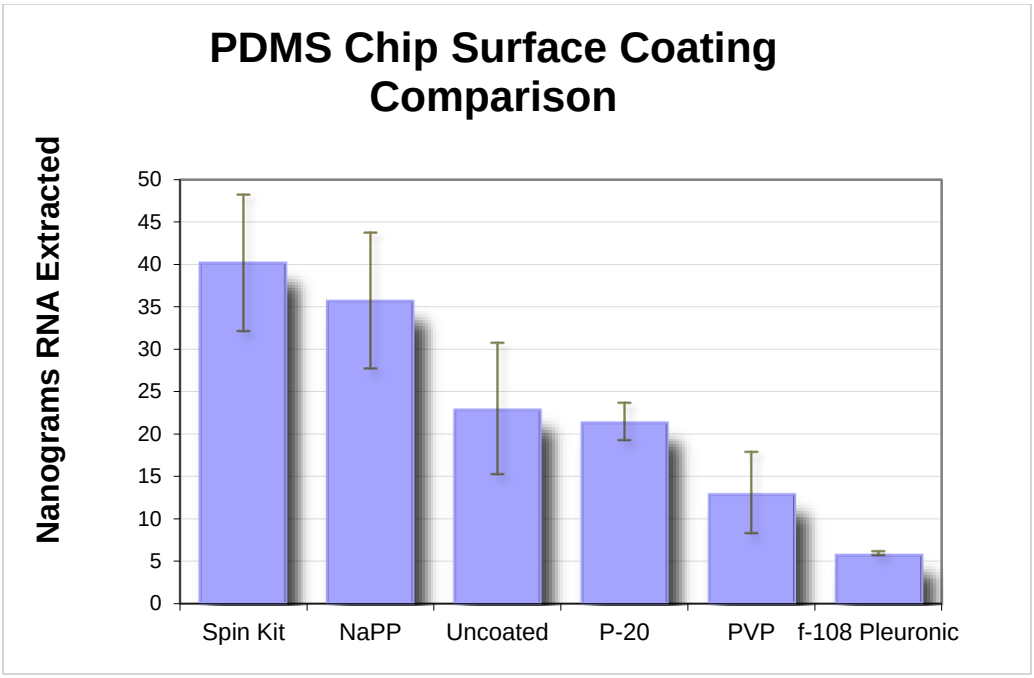

Figure 3.13: RNA recovery yields from automated extraction system with different chip surface coatings.

chip. NaPP could still be beneficial for applications that do not require PCR as the detection method. It was used with some success in tests performed by collaborating researchers (Integrated Explorations, Guelph, ON, Canada) using the microfluidic device to extract RNA for electrochemical detection.

Coatings for the microfluidic chip were not used for further nucleic acid extraction tests because the improvement with NaPP came with an unacceptable incompatibility with PCR.

3.3.6 Nucleic Acid Extraction

3.3.6.1 Extraction of RNA

The device was used to demonstrate successful RNA recovery at yields approaching results attained by a commercial spin kit (Qiagen). Known concentrations

of RNA from an RNA standard stock (Invitrogen) were used as the sample. RNA extraction results are determined using a fluorescent Ribogreen RNA quantification kit obtained from Invitrogen. Fluorescence data are obtained using a 96-well plate reader.

The device was used to demonstrate successful automated recovery of prepurified RNA at yields approaching results attained by a commercial spin kit. RNA is extracted from different starting concentrations with the microfluidic system demonstrating an extraction efficiency of approximately 50% compared to the commercial standard as seen in Figure 3.14.

3.3.6.2 Extraction of RNA from E. Coli bacteria

The ability of the extraction system to purify bacterial RNA was tested by using *E. Coli* 0157:H7 verotox negative bacteria as the sample. Bacteria were obtained from

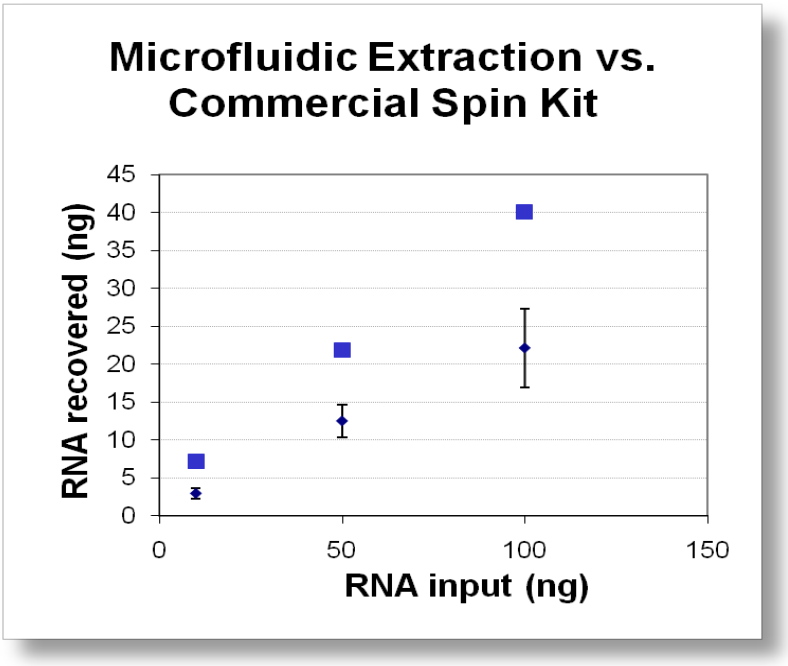

Figure 3.14: Nucleic acid extracted from the automated microfluidic system (diamonds with error bars) vs a commercial kit (squares).

New England BioLabs and cultured in cell growth medium until they reached the exponential growth phase. The number of bacterial cells was measured using optical density techniques. Seven million bacteria cells were used as the sample input to the microfluidic extraction devices. An automated protocol listed in Appendix B performed the necessary steps to lyse, extract, and purify the bacterial RNA, similar to the above-mentioned protocols, with the exception of the addition of a lysozyme to break the cell walls and the need for RNA protection reagents. A total of 193 ng of RNA was recovered as quantified using fluorescence techniques.

As a secondary evaluation of the ability of the system to purify RNA from bacteria samples, the micfoluidic system was tested at Integrated Explorations Inc., a biolab in Guelph, Ontario Canada. The robust nature of the system was demonstrated by extracting RNA from raw biological samples (*E. Coli* cells) as shown in Table 3.2. A 10-fold increase in the number of cells proved to produce less than double the recovery of RNA, indicating a nonlinear relationship between amount of bacteria supplied and the extraction yield. Factors that could possibly contribute to this include incomplete lysis of all cells, saturation of the solid phase during binding, RNA loss during washing step, or incomplete elution of target molecules. Further investigation and optimization would be required to use the extraction chip as a quantitative measurement tool, but the current results are adequate for detection purposes.

3.3.6.3 RNA extraction from virus samples

The automated RNA extraction protocol was modified to follow established steps for extracting viral RNA from biological samples. The system was tested in India by Indian Immunologicals LLC. Cultured FMDV samples were used as system inputs.

Table 3.2: RNA extraction yields from four samples of *E. Coli* cells that were lysed on-chip. Successful extraction demonstrates that the system is capable of extracting nucleic acid from raw biological samples

Sample	Cells Input	Total RNA Retrieved
E. Coli 0157:H7	70 million cells	429ng
E. Coli 0157:H7	70 million cells	374ng
E. Coli 0157:H7	56 million cells	253ng
E. Coli 0157:H7	7 million cells	276ng

Successful extraction was analyzed by both spectroscopic and RT-PCR detection. Table 3.3 shows Nanodrop readings of the concentration of RNA in the 35 μl elutions. The first column indicates the strain of virus and the run number identification. The last column is the ratio that signifies the purity of the extracted RNA. The 260/280 ratios in the table are consistently above the desired 1.8 which indicates a pure sample.

To verify that the readings do, in fact, represent the presence of viral RNA, RT-PCR was carried out on a plate cycler. Figure 3.15 shows results where RNA extraction results from the microfluidic device (MFD) were amplified using RT-PCR and verified by performing gel electrophoresis. Lane 6 is a positive control where the viral RNA was extracted using the Qiagen RNEasy Kit, and amplified on a plate cycler. Lanes 1-4 have distinct bands in the correct location indicating that the microfluidic system successfully extracted viral RNA. The weak band in lane 2 and the nonexistent band in lane 5 are signs that there are intermittent failures in the system.

3.3.6.4 DNA extraction

The nucleic acid extraction capabilities of the microfluidic system were again explored by using the solid phase extraction principles to purify DNA as well. Similar to RNA extraction, known quantities of DNA were obtained and used as sample inputs to the system. Figure 3.16 shows the DNA extraction efficiency compared to a commercial

Table 3.3: List of microfluidic extraction runs and RNA quantitation for each run using Nanodrop measurements

Target/Microfluidic Extraction Run	Nucleic Acid Conc. (µg/ml)	A260	A280	260/280
O IND R2/75 MFD1	69.300	1.732	0.372	4.65
O Manisa MFD2	86.200	2.154	0.471	4.58
O TNN 24/84 MFD3	18.900	0.473	0.103	4.58
O TNN 24/84 MFD4	15.400	0.386	0.108	3.57
O R2/75 MFD5	27.900	0.698	0.21	3.33
O R2/75 MFD5	27.700	0.691	0.202	3.42
O TNN 24/84 MFD 7	6.900	0.174	0.025	7.02
O TNN 24/84 MFD 9	11.100	0.278	0.023	11.96
O IND R2/75 MFD 10	7.200	0.179	0.034	5.23
O TNN 24/84 MFD12	0.183	4.577	1.332	3.44
O TNN 24/84 MFD13	0.031	0.78	0.31	2.52
O TNN 24/84 MFD14	0.087	2.162	0.885	2.44
O IND R2/75 MFD15	0.100	2.487	1.054	2.36
O IND R2/75 MFD16	0.126	3.149	0.83	3.79
O IND R2/75 MFD17	0.097	2.412	0.557	4.33
O IND R2/75 MFD21	38.0	0.951	0.441	2.16
O IND R2/75 MFD22	60.6	1.516	0.72	2.11
O IND R2/75 MFD23	48.7	1.217	0.531	2.29
O IND R2/75 MFD24	26.3	0.658	0.292	2.25

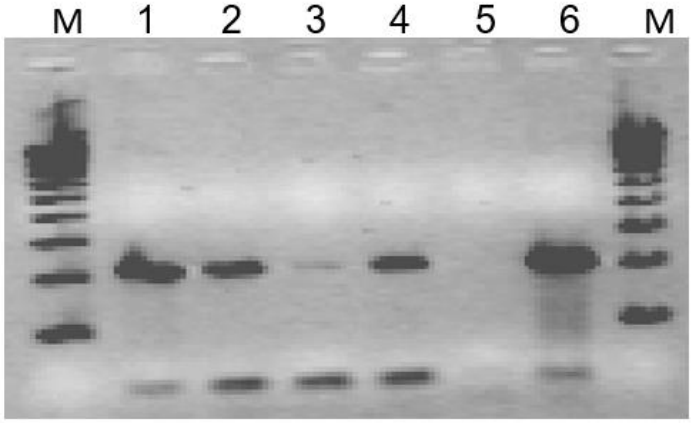

Figure 3.15: Gel electrophoresis of RT-PCR amplification of extracted RNA products from FMDV samples using automated microfluidic system. M: 100 bp DNA Ladder, Lane 1 to 6 RT & PCR with standard kit. Lane 1: O TNN 24/84 MFD Run 4. Lane 2: O IND R2/75 MFD Run 5. Lane 3: O TNN 24/84 MFD Run 3. Lane 4: O IND R2/75 MFD Run 1. Lane 5: O IND R2/75 RNA recovery in MFD. Lane 6: O IND R2/75 Positive control.

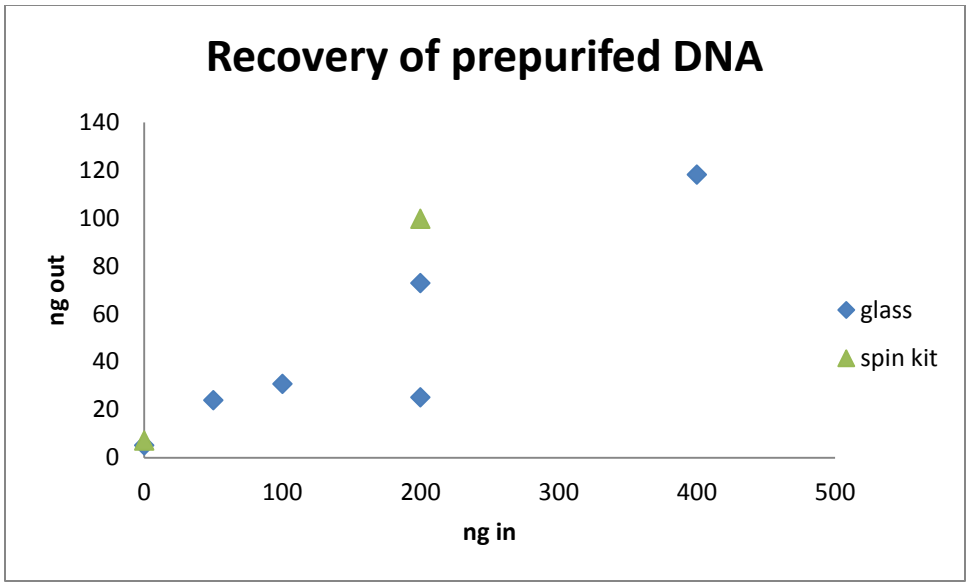

Figure 3.16: DNA recovery using microfluidic automated nucleic acid extraction system compared to commercial system.

laboratory kit (Qiagen DNA kit).

To ensure that the eluent is free of contaminating chemicals introduced by the extraction process, nucleic acid-free control samples sent through the extraction system were spiked with varying amounts of purified DNA in known quantities. Different amounts of whole human blood were used as the samples for nucleic acid extraction process, and results were again quantified using real-time PCR crossing-point analysis. Results were compared to extractions performed on standard commercial centrifugation kits. The glass filter from one of our devices was used to replace the filter in a commercial spin column, and the filter from the spin column was placed in one of our filter casings in order to compare our solid phase filter to the one used in the commercial kit. Results in Figure 3.17 show that while the extraction efficiency of the microfluidic device is slightly lower than commercial standards, the device is capable of extracting PCR-amplifiable DNA from a whole blood sample in an automated system. When the

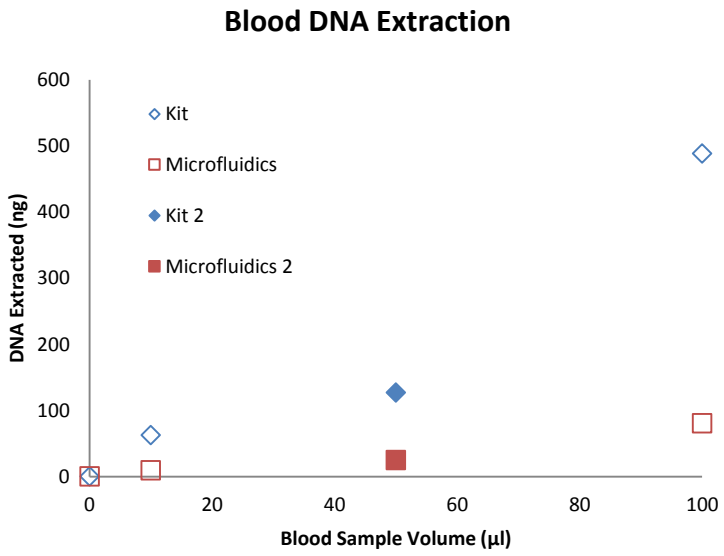

Figure 3.17: Extraction of DNA from whole blood samples performed on-chip compared with standard spin kit extraction progress. Kit 2 series indicates a spin kit test with the column filter replaced with the filter material used in the microfluidics. Microfluidics 2 is a test performed on the microfluidic chip with the filter material replaced with the material from the spin kit extraction columns.

filters were switched, both systems extracted slightly less genetic material than what would be expected based on the linear response observed in other tests.

The glass microfiber filter solid phase proved effective and is easily incorporated into an automated nucleic acid extraction system to extract PCR-amplifiable product from raw blood samples in less than 20 minutes.

3.3.6.5 Summary of nucleic acid extraction from multiple sample types

A system capable of varied extraction conditions and targets is desirable for the creation of a versatile sample preparation device. Table 3.4 gives a summary of total amounts of nucleic acid recovered from the representative extraction tests performed on the automated microfluidic system described in previous sections. Successful extraction of nucleic acids was demonstrated more by the ability of the system to produce detectible

Table 3.4: Nucleic acid extracted from multiple sample types

Sample	**Total nanograms NA Retrieved**
E. Coli 0157:H7	429 ng RNA
FMDV virus	539 ng RNA
Stock RNA	35.7 ng RNA
Whole Blood	22.0 ng DNA
Stock DNA	118 ng DNA

levels of the target NA, as opposed to having a mandated extraction efficiency or quantity threshold. Input amounts and conditions varied for each sample type in the table, so no conclusions should be drawn as to the relative quantitative ability of the system to process the different sample types. Rather this table illustrates the qualitative ability of the system to readily extract nucleic acids form different input samples and target molecules in an automated fashion.

3.4 Conclusions

The developed NA extraction system has proven capable of handling a variety of sample preparation tasks in an effort to make automated nucleic acid sample preparation more practical and available. Such work is a step towards a universal sample preparation unit that can handle many kinds of samples from viruses to tissue samples and provide rapid, meaningful results from a lab-on-a-chip platform. The RNA detection abilities were demonstrated for two main applications. The first was the detection of *E. Coli* RNA to monitor drinking water supplies for harmful bacteria where RNA is a more appropriate genetic material for detection. RNA was also extracted from viral samples in tissue

culture fluid to demonstrate another form of pathogen detection. These applications will open the door for future pathogen screening and detection tests. The same system was shown to be capable of extracting DNA from whole blood samples. The project results therefore show that the developed system meets the need for fast, simple, and adaptable sample preparation systems.

3.5 References

1. A. J. de Mello and N. Beard, Lab on a Chip **3** (1), 11N-20N (2003).

2. W. H. Grover, A. M. Skelley, C. N. Liu, E. T. Lagally and R. A. Mathies, Sensors and Actuators B (Chemical) **B89** (3), 317-325 (2003).

3. D. A. Bartholomeusz, R. W. Boutté and J. D. Andrade, Microelectromechanical Systems, Journal of **14** (6), 1364-1374 (2005).

4. Y. Chenying, W. Wei and L. Zhihong, presented at the 2009 4th IEEE International Conference on Nano/Micro Engineered and Molecular Systems (IEEE-NEMS 2009), 5-8 Jan. 2009, Piscataway, NJ, USA, 2009 (unpublished).

5. T. Poeckh, S. Lopez, A. O. Fuller, M. J. Solomon and R. G. Larson, Analytical Biochemistry **373** (2), 253-262 (2008).

6. X.-W. Chen, Z.-R. Xu, B.-Y. Qu, Y.-F. Wu, J. Zhou, H.-D. Zhang, J. Fang and J.-H. Wang, Analytical and Bioanalytical Chemistry **388** (1), 157-163 (2007).

CHAPTER 4

OSCILLATORY FLOW PCR WITH EVAPORATION CONTROL ON A POLYCARBONATE CHIP

4.1 Abstract

An oscillatory flow PCR module is presented for integration with the automated nucleic acid extraction system. A disposable, multilayer polycarbonate oscillatory flow PCR chip is fabricated with evaporation control to keep fluid loss to under 10% over 40 cycles. Temperature zones on the chip are created by making contact with external aluminum heating blocks. Fluid temperatures are computed using numerical simulations. Successful on-chip PCR is demonstrated.

4.2 Introduction

Nucleic acid amplification is a process by which a specific sequence of a strand of DNA or RNA is copied multiple times to produce a larger quantity of the target sequence. Of the methods of amplification, PCR has grown in popularity since its inception in 1987[1] because of its simplicity. In PCR, DNA sequence primers attach to the beginning and end of specific sequences of nucleotide bases of a single strand of DNA in an annealing process that takes place at about 60 ˚C. Elevating the temperature to an intermediate range around 72 ˚C activates an extension process where a polymerase enzyme begins at the primers and zips along the strand, inserting corresponding nucleotide bases to convert the single strand into a double strand of DNA. The temperature is then elevated above the melting temperature of the DNA at around 95 ˚C where the DNA molecule denatures into two single strand segments, and the process is repeated by following the same temperature cycle.

PCR is well suited for application to microfluidic devices because of the direct realization of several proposed microfluidic benefits: lower volumes of costly reagents and less thermal inertia for rapid thermal cycling. There have been several reviews

published in the last decade that explore the progress made in the adaptation of PCR to the microchip. There are hundreds of microfluidic devices, and most microfluidic PCR chips can be placed into two broad categories: stationary chamber-based chips with integrated temperature controllers and continuous flow PCR chips. Stationary chips offer good flexibility in temperature and cycle control but generally rely on more expensive silicon processing manufacturing techniques. Continuous flow chips generally have faster temperature ramp rates because only the fluid temperature needs to change, eliminating the thermal inertia of surrounding chip components. However, continuous flow chips have a fixed number of cycles based on channel geometry, offering little room for process adaptation.

A subset of continuous flow PCR chips that relies on oscillatory flow between temperature zones has arisen that attempts to include the flexibility of the stationary chamber devices with the low thermal mass seen in continuous flow chips. Using this architecture, a fluid droplet is shuttled back and forth between different temperature zones on the chip. This chapter presents a disposable polycarbonate oscillatory flow PCR chip that allows control over cycle times and temperatures. The chip is integrated with the nucleic extraction system presented earlier by using the same instrument and control software for pumping the PCR droplet between temperature zones.

4.3 Materials and Methods

The overall approach to developing an oscillatory PCR chip involved 3 stages: (1) Fabrication of an appropriate, cost effective chip, (2) Modification of the chip to overcome evaporation and sample loss, (3) Simulation of the chip to determine appropriate operating conditions. The motivation and rationale for these steps follows.

The creation of this oscillatory PCR chip began with the choice of substrates. Inexpensive, disposable devices are desirable for PCR chips to reduce the risk of cross contamination between tests. Plastics present fabrication cost advantages and can also have favorable optical properties. However, the elevated temperatures associated with PCR present a stability problem for many common thermoplastics. Polycarbonate was selected as the material for the chip substrate because it is optically transparent, relatively inexpensive, and has a sufficiently high glass transition temperature (150˚C) to withstand the elevated PCR annealing temperature.

Another disadvantage to using a plastic substrate is that it is an insulator. The relatively low thermal conductivity (k=0.2 w/m^2 K) impedes the heat transfer desired to quickly ramp the fluid temperature through the PCR thermal cycle. This low thermal conductivity can be circumvented by having the heat source in contact with the fluid, but it is difficult to embed on-chip heaters and temperature probes and maintain low production costs. Fluid temperature feedback in microchannels has been achieved using embedded temperature probes,[2, 3] temperature dependent fluorescent dyes,[4] and non-contact interferometry.[5] The difficulty in creating an inexpensive rapid plastic oscillatory PCR chip lies in having the ability to quickly and accurately adjust the internal fluid temperature using an external heat source.

The approach used in this work mitigates the thermal insulating effect of the polycarbonate substrate by using thin walls in good thermal contact with external heating blocks. Verification of internal fluid temperatures without direct feedback is achieved using numerical simulations to model the transient thermal state of the fluid. Parameters such as wall thickness, material thermal properties, and external heater temperature will

be varied in the simulation to determine optimum chip characteristics to achieve the fluid temperatures needed for PCR. Transient analysis will determine the cycle times required. Numerical results will be compared with measured surface and fluid temperatures gathered using topographical thermal imaging and embedded thermocouples. The parameters developed using these models are then used experimentally and successful PCR is demonstrated.

4.3.1 Chip Fabrication

Microfluidic devices for PCR need to be disposable to prevent cross-contamination between assays. Even trace amounts of target nucleic acids left from previous test runs can be amplified during the PCR process to detectable levels. Consequently, a simple laminated plastic chip design is used in this work to produce inexpensive, disposable PCR chips. The microfluidic PCR chip is then mounted onto a temperature controlled heater manifold to produce the regions at temperatures required for PCR.

Two versions of the microfluidic chip were created: a simple three-layer chip with a serpentine chip, and a more complex version with seven layers that incorporates an evaporation control scheme.

4.3.1.1 Three-layer chip fabrication

The microfluidic PCR chip is fabricated using three laminate layers of polycarbonate (Lexan FR83, Sabic Polymershapes Pittsfield, MA). As noted earlier, polycarbonate is an ideal material because its glass transition temperature is well above the maximum temperature required for PCR (~95 ˚C), so it can be used in PCR applications. Even though polycarbonate has a high glass transition temperature,

multilayer devices can still be easily created using heat to laminate layers together for rapid prototyping.

Figure 4.1 illustrates the process of creating a multilayer polycarbonate chip. The first step in chip fabrication is to cut the channel from the middle layer of polycarbonate. The serpentine nature of the channel geometry adds difficulty to cutting this middle layer as the interdigitated thin polycarbonate fingers that are produced are easily displaced from their intended position. Even small finger displacement leads to device failure in the final chip because the small cross-section channels are easily sealed by a slight dislocation of the channel walls. To prevent this dislocation, the middle layer is supported by a layer of adhesive during the cutting step and subsequent bonding to the top layer. The adhesive tape layer is applied to a sheet of polycarbonate (a). The

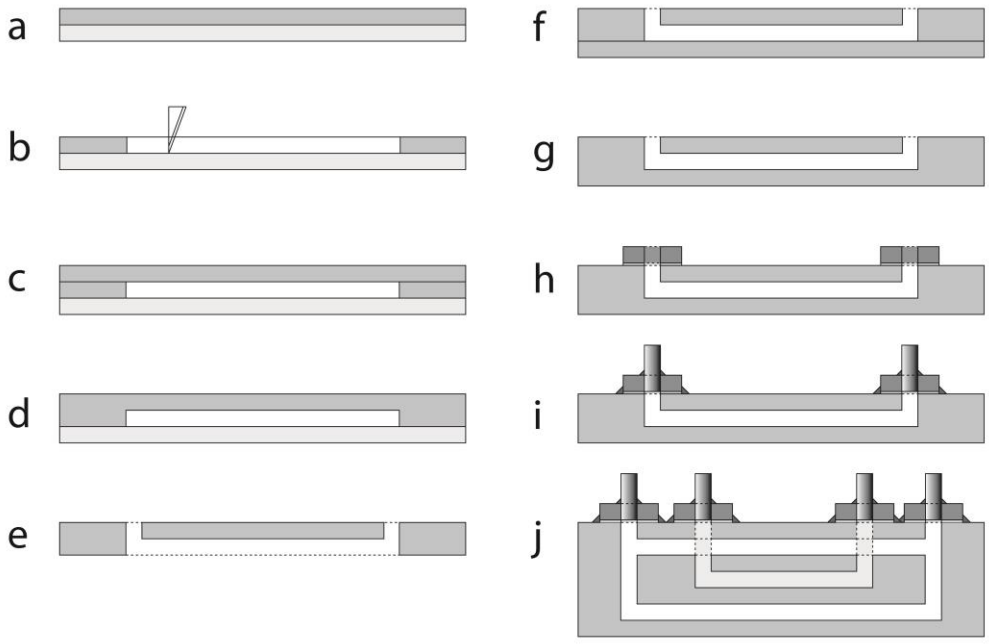

Figure 4.1: Schematic of multilayer chip fabrication method.

polycarbonate/tape assembly is then cut using a knife plotter (Graphtec) to cut through the polycarbonate but leave the supporting adhesive tape layer intact (b). The polycarbonate left where the fluid channel will be is then manually removed with tweezers, leaving an empty channel.

Following the cutting of the fluid channel, the top layer of polycarbonate is thermally bonded to the middle layer using a heat press set to 175˚C (c). The top polycarbonate layer is placed in contact with the polycarbonate side of the middle layer polycarbonate/tape assembly. The layers are sandwiched between two pieces of smooth paper backing and put into the heat press, with the tape layer down. The heat press is kept at 175 ˚C, just over the glass transition temperature of 150 ˚C, and the two layers are bonded for 2 minutes with slight pressure. This produces a good bond between the two layers (d), but minimizes melting to maintain the cross-section geometry of the fluid channel. Access holes are then cored into the top layer for the fluid inlet and outlet (e).

The adhesive tape support layer can then be removed from the middle layer because the bond between the middle and top polycarbonate layers now provides the support for the thin channel walls. A bottom layer of polycarbonate is then placed in contact with the now exposed middle layer(f), and the chip assembly is again placed in the heat press in the manner stated before to bond the bottom layer to the middle(g). The resulting chip has an enclosed serpentine channel in a disposable polycarbonate three-layer chip assembly. Custom access ports made from laser-cut acrylic are then attached to the cored port holes in the top layer with UV-cured adhesive (h-i).

4.3.1.2 Seven-layer evaporation control chip fabrication

The seven-layer version of the oscillatory flow PCR chip is fabricated using the same process as the three-layer device, but with two extra polycarbonate layers on the top and bottom surfaces shown in Figure 4.1 (j) and Figure 4.2. The intermediate layers create an extra fluid layer on either side of the sample fluid layer in the middle of the chip. The new fluid layers share a common inlet and outlet port.

4.3.1.3 Chip surface inoculation

Following chip fabrication, the channel walls were passivated to reduce non-specific adsorption of target molecules to the polycarbonate surface. To passivate the surface of the channels in the polycarbonate chip, 0.1 % solution (w/v) of bovine serum albumin (BSA) was pumped through the chip at a linear rate of approximately 1 mm/sec

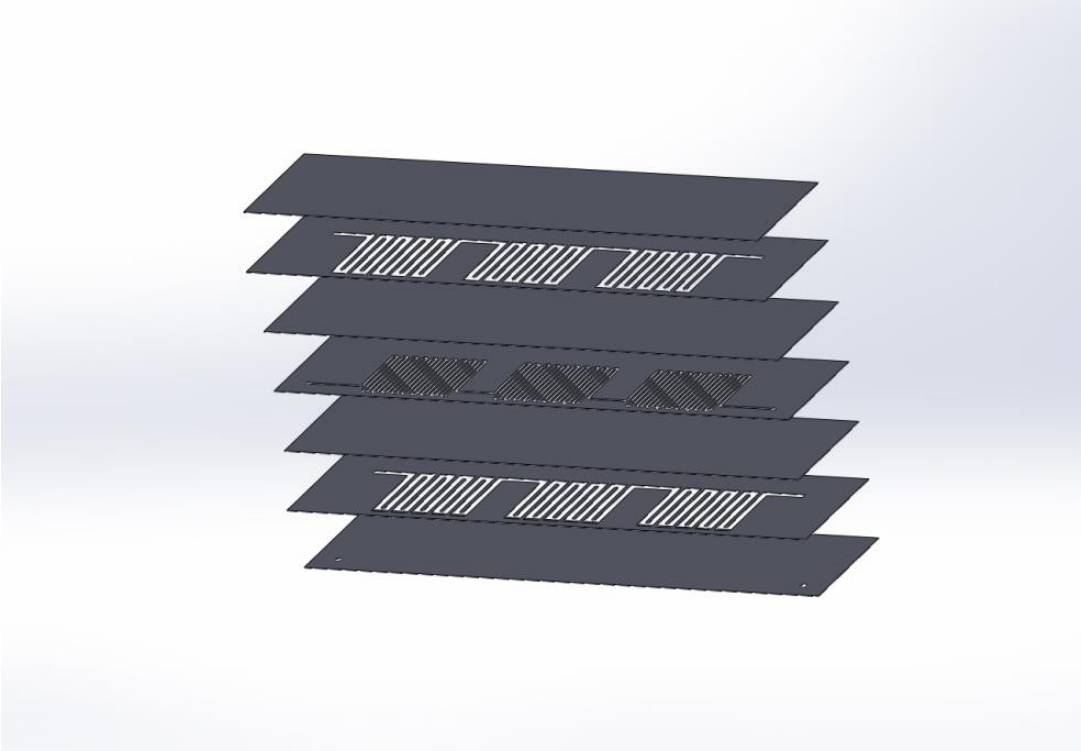

Figure 4.2: Diagram of seven-layer stack for fabrication of evaporation control chip.

for 1 hour. The BSA-filled chip was then incubated at 40 ˚F for 24 hours to allow BSA to coat all binding sites on the interior channel walls. Prior to use in experiments, the BSA was pumped out and the channels dried by a flow of air.

4.3.2 Temperature Control

The temperature zones for the PCR chip are controlled using three aluminum heater blocks. Each block is attached to a flexible film resistive heater (Omega) and has an embedded thermocouple for temperature feedback. The heater and thermocouple are connected to a commercial PID to monitor and control the heater block assembly temperature. Voltage to the heaters is provided by a DC power supply. The heater blocks are housed in a polycarbonate casing which separates the heater blocks with a small air gap (approximately 1 mm). The chip is held in contact with the heater blocks by a polycarbonate lid layer attached with bolts. Figure 4.3 is a photograph of the PCR

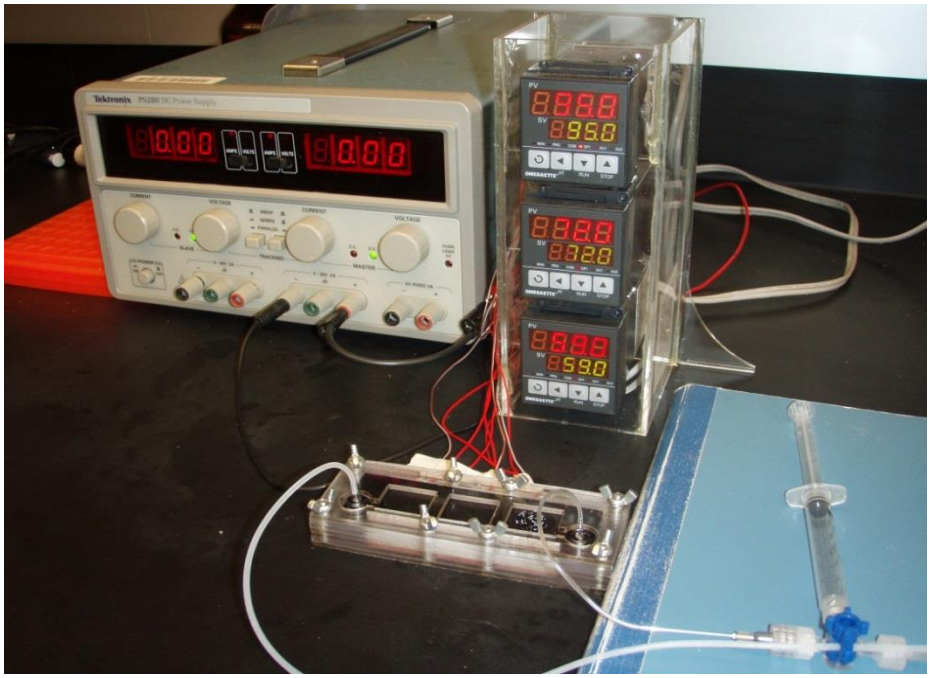

Figure 4.3: Photograph of heater control setup.

chip module setup including the 3 commercial PID controllers and the chip holder assembly.

4.3.3 Temperature Modeling

The critical step in performing PCR is ensuring that the fluid reaches the proper and precise temperature to facilitate the three steps of PCR: denaturation of the target DNA strand, annealing of the primer to the target sequence, and extension of the primer along the strand to create a copy of the target sequence. The precise requirements for the temperature at which these steps occur dictates a rigorous analysis of the PCR chip temperature profile and transient analysis to optimize the PCR protocol and ensure that the fluid has sufficient residence time in each temperature zone to reach the proper temperature and complete each step in the PCR cycle.

To help determine the best operating parameters, first, a 3-dimensional steady state simulation of the thermal conditions outside the chip was performed. This provided the boundary conditions needed to determine the internal temperature conditions of the chip. Next, 1-dimensional, steady state solutions are determined for a range of intra-channel fluid temperatures to yield a first approximation for the initial conditions applied in the transient temperature simulation. A 1-dimensional transient numerical solution is then implemented to determine the minimum residence time necessary for the fluid in each temperature zone to reach the desired temperature.

4.3.3.1 Determination of convection coefficient: h

The first modeling step is the determination of the boundary conditions needed to calculate the internal fluid temperature; specifically the rate of heat leaving the top surface of the chip, which is dependent on the convection coefficient, *h*. A common

method for determining *h* for natural convection involves using Nusselt number correlations based on the geometry and fluid properties. These empirical correlations were generally developed for larger systems with higher Rayleigh numbers than what is found in the system discussed in this work. Also, the geometric conditions of the PCR chip assembly require determination of the natural convection coefficient specific to this system. As the empirical convection coefficients are inappropriate for the conditions in this work, convection coefficients here are determined from 3-dimensional multiphysics modeling using Comsol multiphysics software. The fluid of interest for determining the convection coefficient is the air above the chip surface. The heated chip surface warms the air which lowers the air density, causing it to rise from buoyancy forces. The geometry modeled for this system was a block of air shown in Figure 4.4.

.

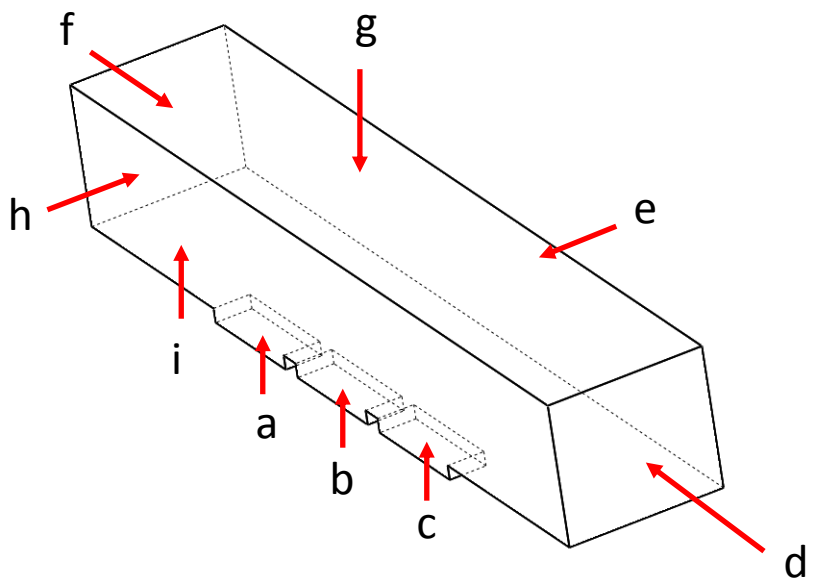

Figure 4.4: Geometry used for natural convection modeling.

The size of the block of air to be modeled was chosen based on guidance from the software manufacturer to place boundaries sufficiently far away from the heating surface. These recommended boundary distances were verified by incrementally increasing the size of the geometry until simulated heat flux results from the surface of interest remained constant. The final geometry used for the simulations was stable with a 0.74% change in heat flux with a 16.7% change in geometry dimensions.

Symmetrical flow and adiabatic boundary conditions were used on the boundary representing the plane of symmetry (face h). Fixed temperatures were used at the surface of the chip temperature zones (faces a, b, and c). The other solid surfaces were modeled as thermal insulators (face i and all unlabeled faces). Those solids surfaces were constrained as no-slip walls for laminar flow. The top air boundary (face g) was a heat outflow and a laminar outlet at ambient pressure. The side air boundaries (faces d, e, and f) are set to ambient temperature and laminar inflow with no pressure.

A body force based on the gravity acting on the temperature-induced density gradient was added to the air in the simulated domain to create the density driven flow in a natural convection environment. The model was used to calculate I for a series of surface temperatures that cover the range expected for PCR experiments. The numerical simulation was iterated with successively finer mesh elements until the change in the results varied less than 1%.

4.3.3.2 1D steady state solution

For a first approximation of the temperature state in the PCR chip and the fluid inside the channel, a1D steady state analytical solution for a composite wall is used. Multiple layers are used to represent the polycarbonate layers, fluid layers, and the heater

block. The thicknesses of the layers and material properties are adjusted to attain optimal PCR temperature control.

The boundary conditions of the composite wall are a fixed temperature at the boundary representing the contact between the chip and the heater control manifold and a free convection boundary at the top surface exposed to room temperature. The variable of interest is the temperature of the heater control manifold. The goal is to determine what temperature to set as the manifold operating temperature to achieve the proper fluid temperature inside the channel.

To calculate the temperature at points in the wall, we need to find the heat flux *q*, which can be determined using the thermal resistance of the entire composite wall coupled with the boundary conditions. The heat equation for the composite wall is:

$$q'' = U(T_i - T_o) \tag{3.1}$$

where q'' is the heat flux per unit area, T_i is temperature at the inner surface of the wall, T_o is the temperature at the outer surface, and U is the overall heat transfer coefficient in the wall given by

$$U = \frac{1}{t_1/k_1 + t_2/k_2 + \cdots + t_n/k_n} \tag{3.2}$$

where t_{1-n} and k_{1-n} are, respectively, the thickness and thermal conductivity of each layer of the PCR chip. Any layer can be omitted in the simulation by setting the thickness of that layer to zero. The temperature at the outer surface is found by combining the heat equation in the wall with the convection heat equation at the surface:

$$q'' = h(T_o - T_\infty) \tag{3.3}$$

where T_∞ is the ambient temperature and h is the convection coefficient. Solving for the

temperature at the outer surface yields:

$$T_o = \frac{hT_\infty + T_i U}{h + U} \tag{3.4}$$

In the numerical simulation, the unknown temperature T_i at the inner surface is given a guessed initial value below the expected value for the temperature at the heater manifold/PCR chip interface. The temperature at the outer surface is then calculated from equation 3.4. Then the heat flux q'' can be calculated from equation 3.1, which can then be used to calculate the temperature at all interior points. The average temperature in the middle PCR chip layer is then compared to the desired fluid temperature. If the temperatures are not equal to within the desired tolerance, the guessed inner surface temperature is adjusted and the process repeats until the correct fluid temperature is reached.

This approach provides the steady-state temperature profile for the temperature through all layers of the PCR chip. This temperature profile (like that in Figure 4.5) provides the initial conditions for solving the transient temperature profile to determine the required residence time for the fluid to reach the desired temperature.

4.3.3.3 Transient temperature analysis

A transient temperature analysis of the PCR chip is performed by using a finite difference approximation of the differential heat equation with no heat generation:

$$\frac{\partial}{\partial x}\left(k\frac{\partial T}{\partial x}\right) + \frac{\partial}{\partial y}\left(k\frac{\partial T}{\partial y}\right) + \frac{\partial}{\partial z}\left(k\frac{\partial T}{\partial z}\right) = \rho C_p \frac{\partial T}{\partial t} \tag{3.5}$$

The form often seen of this equation assumes constant properties throughout the material. In the case of the composite wall in this study, there are abrupt changes in the thermal conductivity at the boundaries of the different materials. Thus, the differential heat

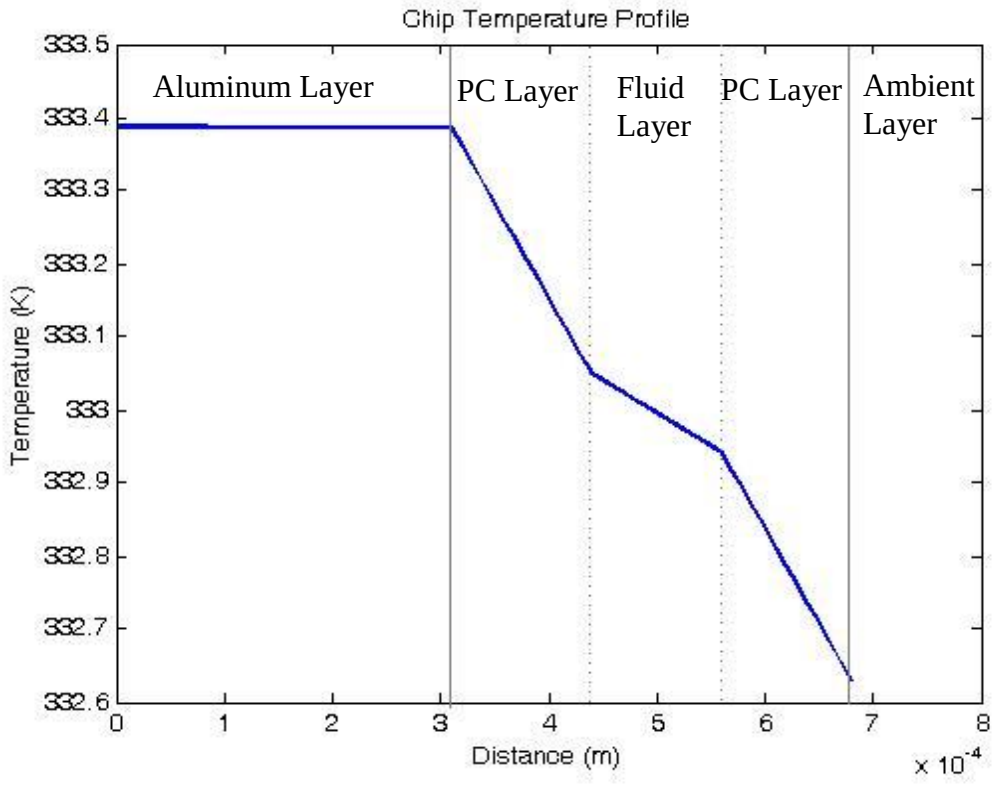

Figure 4.5: Graph of a steady-state temperature profile solved for a 3-layer PCR chip.

equation must be solved assuming that the thermal conductivity varies with *x*. The equation can also be simplified because the planar geometry of the system allows the assumption that heat flows only in the *x* direction (normal to the chip surface) to remove any *y* and *z* dependence. These assumptions result in the following form of the heat equation:

$$k\frac{\partial^2 T}{\partial x^2} + \frac{\partial T \partial k}{\partial x^2} = \rho C_p \frac{\partial T}{\partial t} \tag{3.6}$$

Equation (3.6) is then converted to a finite difference approximation using a forward time, center space configuration.

$$\sigma_i^{m+1} = \alpha_i \Delta t \left(\frac{\sigma_{i-1}^m - 2\sigma_i^m + \sigma_{i+1}^m}{\Delta x^2} \right) + \frac{\alpha_i \Delta t}{k_i} \left(\frac{k_i - k_{i-1}}{\Delta x} \right) \left(\frac{\sigma_{i+1}^m - \sigma_{i-1}^m}{2\Delta x} \right) \quad (3.7)$$

where σ is the temperature at position i and time m, Δt is the time step and Δx the distance between position nodes. The variable thermal conductivity term does not use a center space configuration in equation 3.7. In the composite wall configuration, using the centered space finite difference approximation for the thermal conductivity derivative does not accurately reflect the step function nature at the material interfaces. Consequently a backward space finite difference scheme is applied for the thermal conductivity derivative only.

Boundary conditions for the transient thermal model included a constant temperature at the heater block and a convection coefficient at the chip surface.

4.3.4 Temperature Testing

Verification of the numerical temperature simulations was performed using infrared thermography. An infrared thermal camera (FLIR 420) was used to capture the surface temperature of the chip. The camera was mounted to look down at the surface of the PCR chip on the heater block assembly. The chip surface was coated with a thin layer (approximately 30 μm) of matte black acrylic paint. The emissivity of the paint was measured following the camera manufacturer's instructions to be 0.95.

The temperatures of the heater blocks were adjusted from 50 ˚C to 100 ˚C and surface temperatures of the three-block heater assembly were recorded at 10 ˚C increments. These measured surface temperatures were compared to calculated surface temperatures based on the simulated values for heat flux and convection coefficients.

Temperature uniformity to within approximately 1°C over the surface of interest was desired. Heat sink compound was employed between the heater block surface and the plastic chip to ensure good thermal contact and reduce temperature deviations.

4.3.5 Pumping/Integration

The pumping method used for moving the plug of fluid between temperature zones uses the same metering diaphragm pumps used for the nucleic acid extraction chip. The pumping chip is fabricated in PDMS using the three-layer technique already described. Inlet and outlet tubes from the polycarbonate PCR chip are connected to two ports on the pumping chip. Diaphragm pump volumes are calculated such that a single stroke pushes the PCR fluid from one temperature zone to the next. A pressurized air line provides an elevated back pressure to the entire pump/PCR chip system to keep the PCR fluid from boiling at the high temperature zone. The pumping module for the PCR chip is controlled using the same instrument and software used for the nucleic acid extraction chip, creating an integrated extraction/amplification system.

4.3.6 PCR Process Parameters

The ability of the oscillatory flow PCR system to amplify nucleic acids was demonstrated by thermal cycling a PCR sample based on an engineered, relatively short DNA strand obtained as a gift from BioFire Diagnostics Inc. PCR chemistry conditions are indicated in Table 4.1.

The template was an engineered DNA sequence of 184 base pairs in the following sequence: CTCGCAAATGACTGGCTAAAAGTCTGATTAACCGATAGGTCATTCA GATTCATTTATGTAGCTTTATTATCCTAAATCTCCACTTCCACTGAGCTGGGTC

Table 4.1: Description of PCR reaction chemistry used for functional testing of polycarbonate oscillatory flow PCR chip

PCR Mix Reagent Description	Volume (ul)	Final concentration
10X dntp's	1.5	1.5 X
30mM MgCl2 10X PCR Buffer	1	1 X
10X LC Green	1	1 X
10X Primer Mix (5uM)	1	0.5 μM
Klen Taq	0.8	0.4 U/μl
Template	2	
Water	2.7	
total	10	

GTCCCTATCCTTATTGCACTACTATCTTTAGTTTACGAATATGGTTGTTTAAAT ATGAGTCCGTGTTGACCTGAATAGCGAGG. The forward primer used had sequence ATAGGTCATTCAGATTCAGTTTATGTA and the reverse primer was CAGGTCAACACGGACTCATATT. The melting temperature for the sequence is 83 ˚C.

For thermal cycling on the chip, the first temperature zone is set to 60 ˚C and the second and third temperature zones are both set to 95 ˚C. The short nature of this specific DNA target sequence does not require an intermediate extension temperature. The fluid is pumped between the two temperatures, 20 seconds at 60 ˚C and 10 seconds at 95˚C for each cycle.

4.3.7 Gradient PCR

To verify the chemistry, eight samples of the PCR mix with template were placed in the wells of a 96-well plate. The plate was thermocycled on a gradient thermocycler (BioRad S1000) with annealing temperatures ranging from 55 ˚C to 70 ˚C. The plate underwent 40 cycles of 30 seconds at the annealing temperatures followed by 10 seconds

at the denaturation temperature. Following temperature cycling, the plate was fluorescently imaged and analyzed using high resolution melting analysis (Light Scanner, Idaho Technologies).

4.3.8 Melting Analysis

Melting analysis is performed by including a dye that fluoresces in the presence of DNA. As the temperature increases to the point where the DNA denatures, the dye fluorescence declines rapidly. For the 184 base-pair engineered DNA sequence, the melting temperature was previously calculated to be at 83 ˚C and experimentally verified by performing real time PCR and melting analysis on a commercial instrument (Light-Cycler, Roche).

4.3.9 Evaporation Control

While the small volume of PCR fluid on the microscale is advantageous for decreasing thermal cycling times, evaporation can be a major concern. The high temperatures associated with PCR (especially with the denature step) and the high surface to volume ratios of the droplet cause significant evaporation rates. Also, a thin polycarbonate film is not a perfect barrier to water vapor. Polycarbonate has a permeability of 1400 barrers[6] at STP, which correlates to a loss of approximately 1 μl (10% of a 10 μl sample) over the approximate time span of a 40 cycle PCR amplification run using the oscillatory flow PCR chip. The fluid loss is expected to be even higher at elevated temperatures. While information on the permeability of the polycarbonate to water vapor at elevated temperature is scarce, Hanada et al. indicate an approximate 10 fold increase in water vapor transmission rates for a 40˚C increase in temperature for 120

μm polycarbonate membranes.[7] The chip conditions at the elevated PCR temperatures (especially the denature temperature) predict a significant loss of fluid by permeation through the thin polycarbonate chip layer.

Losing even small percentages of fluid can affect the delicate PCR chemistry balance and reduce PCR efficiency. Several attempts have been made to mitigate the evaporation effects in microchip PCR including surrounding the droplet in oil,[8] embedding capillary channels in PDMS,[9] and increasing the pressure in the channel.[10] Evaporation control was attempted using several oil-based methods in relation to the chip under development.

Effective evaporation control was achieved on the polycarbonate chip by including an evaporation control layer on the top and bottom surfaces of the polycarbonate chip. The evaporation control layers are filled with water and pressurized with the same back pressure used in the fluid layer of the chip.

4.3.10 Chip Coating

With evaporation effectively reduced, on chip DNA amplification still demonstrated primer-dimerization, an ineffective amplification of the target sequence. To improve PCR performance, the channel surface of a seven-layer evaporation control chip was coated with bovine serum albumin (BSA) to inoculate nonspecific binding sites and reduce possible target molecule or PCR reagent adsorption to the channel walls.

For PCR on the coated, evaporation control chip, samples were loaded and pumped between two temperature zones. Forty cycles were performed with denaturation taking place for 10 seconds at a temperature zone set for 97.5 ˚C, annealing and extension taking place for 20 seconds at 60 ˚C.

4.4 Results

4.4.1 Chip Fabrication

Three-layer (Figure 4.6) and seven-layer (Figure 4.7) chips were fabricated using the lamination method described above. Tubing was connected to the access ports to load samples and interface with the control system. The chips held approximately 20 μl of fluid per temperature zone. A laser-cut polycarbonate stack was fabricated to house the aluminum heater blocks for the heating module. Figure 4.8 shows the heater module with wire leads for the thermocouple embedded in the aluminum and the thin film heater attached to the aluminum blocks.

4.4.2 Numerical Simulations

4.4.2.1. 3D modeling to determine convection coefficient

Simulations were performed on COMSOL multiphysics modeling software to determine the convection coefficient *h* for the chip geometry with multiple temperature zone configurations. Flow and body force profiles for one such configuration are visualized in Figure 4.9.

It was observed that the middle temperature zone produced less upward flow relative to the neighboring temperature zones when held at the same temperature. This

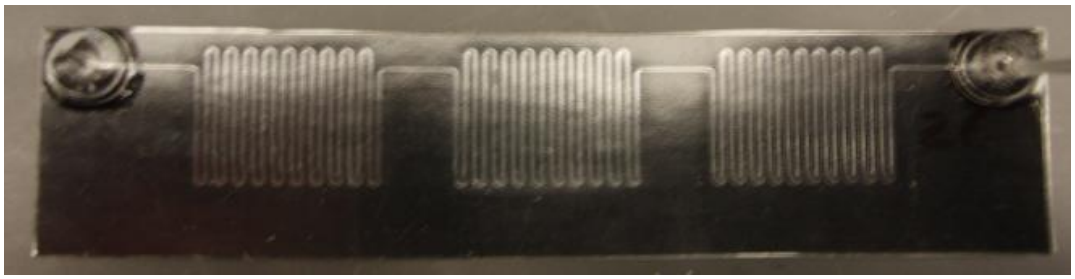

Figure 4.6: Polycarbonate PCR chip with serpenting channels to transmit fluid to three distinct temperature zones.

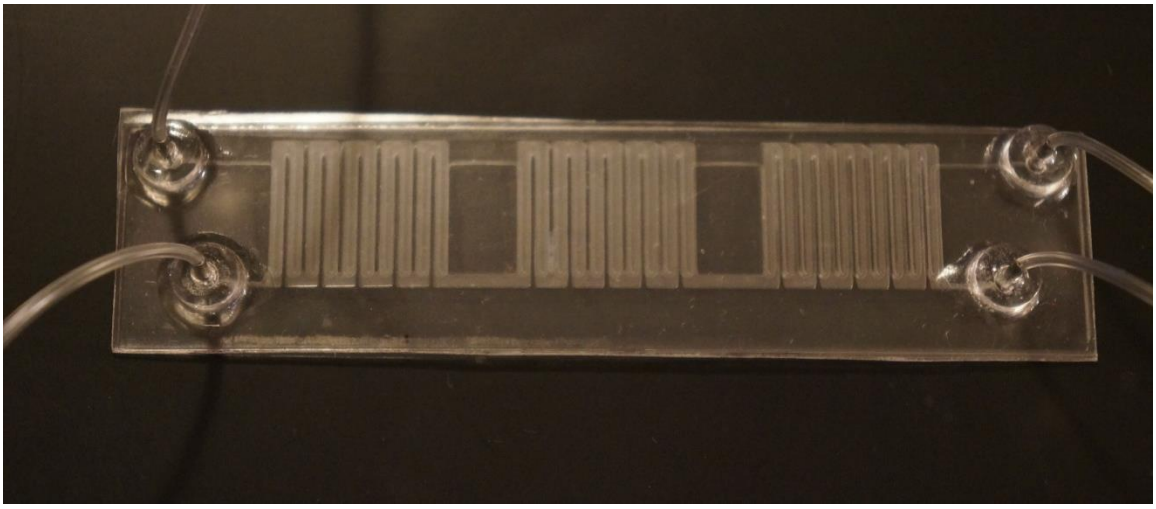

Figure 4.7: Photograph of fabricated seven-layer evaporation control chip with wider channels for pressurized water above and below the sample fluid layer.

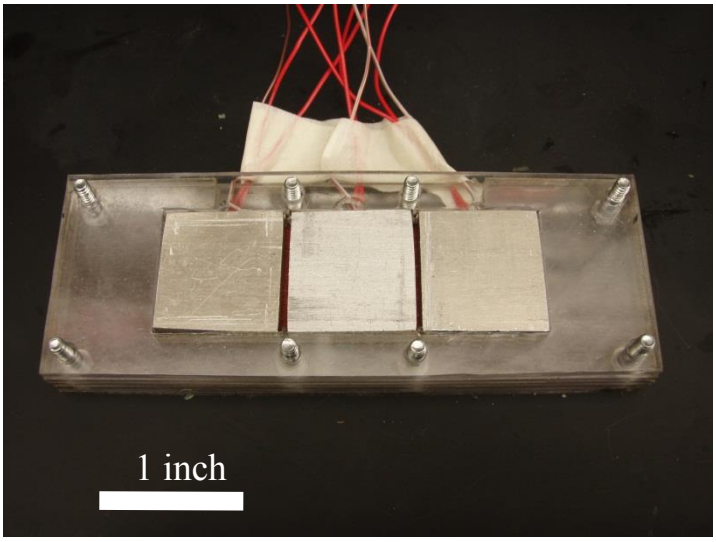

Figure 4.8: Heater block module for temperature zone creation.

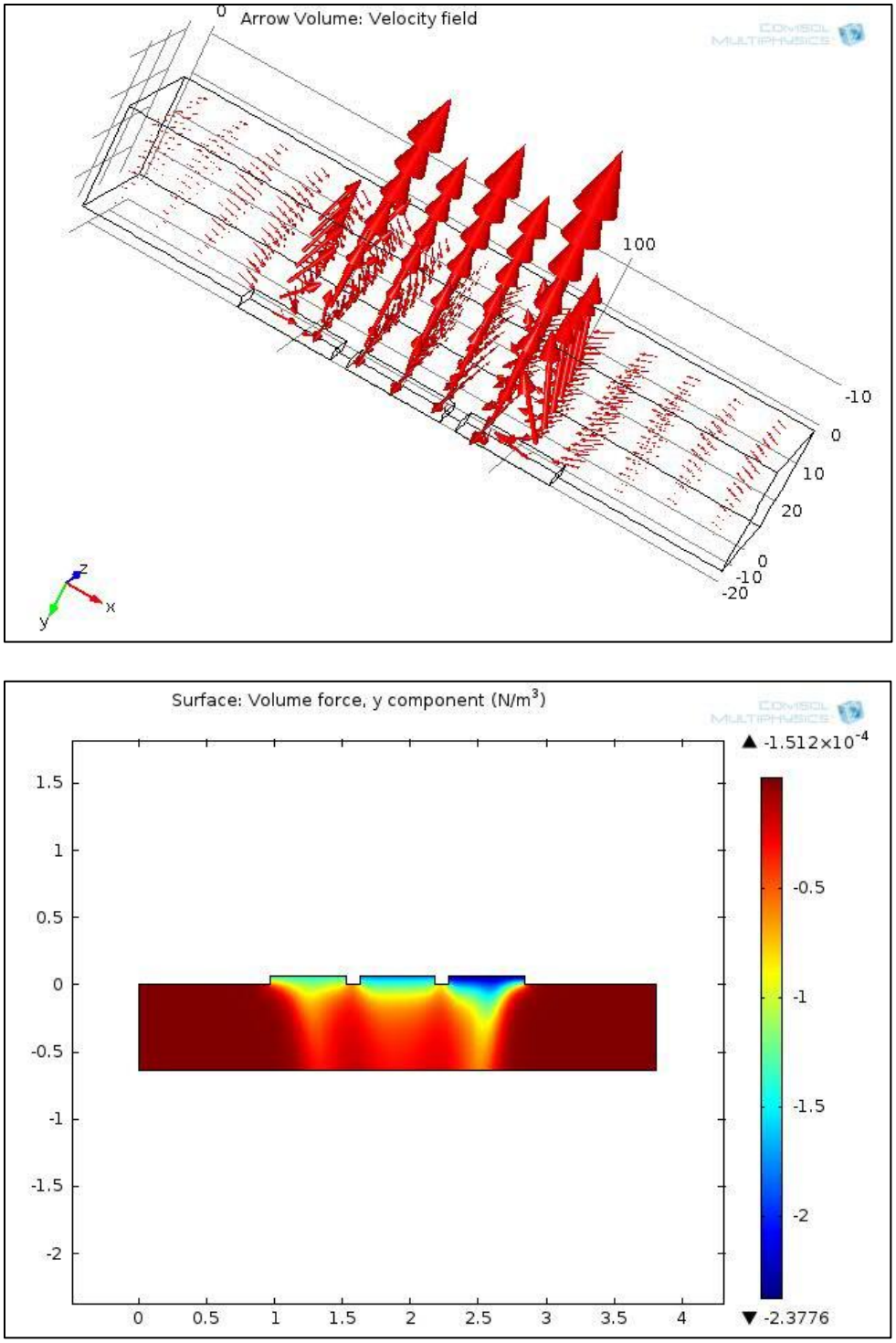

Figure 4.9: Flow and body force profiles for the fluidic chip (a) Velocity magnitude vectors of air flow above the fluidic chip and (b) body force based on buoyancy in cross section at line of symmetry.

effect is likely due to the outside zones being exposed to inflows of cool air from three sides, while the middle zone is insulated on two sides by the other temperature zones. However, this effect was found to have negligible impact on the determined convection coefficient, with differences of less than 0.5% observed from zones of the same temperature at different locations on the chip.

The average convection coefficient for free convection heat transfer from the chip surface was calculated from the heat flux per unit area q''_{conv} leaving the surface as determined by the simulations. Results for h and q''_{conv} are summarized in the first three columns of Table 4.2 for several chip surface temperatures.

The small amount of heat loss from the chip surface due to natural convection makes radiation effects important for this system. Indeed, calculated heat loss to the environment based on radiation, q''_{rad} proves to be a larger proportion of the total heat flux than that caused by convection effects. For such calculations, ambient temperatures (T_∞) were set to 20°C. An effective convection coefficient h_{eff} was calculated based on the combined heat flux q''_{total} from both radiation and convective effects. While h_{eff} thus includes a 4th power function of temperature with the radiative heat flux, the total heat

Table 4.2: Simulated and calculated values for heat flux and convection coefficients based on chip surface temperature.

Surface Temp ˚C	***h* (W/m^2 K)**	***q"*$_{conv}$ (W/m^2)**	***q"*$_{rad}$ (W/m^2)**	***q"*$_{total}$ (W/m^2)**	***h*$_{eff}$ (W/m^2 K)**
60	6	240.6	278.5	519.1	13
72	6.3	328.7	384.5	713.2	13.7
90	6.8	474.6	565.8	1040.4	14.9
100	7	559.9	678.8	1238.7	15.5

flux can be closely approximated by a linear function over the temperature range of interest. This will be shown to be advantageous when applying boundary conditions to calculate the transient temperature conditions in the system.

4.4.2.2 Agreement with calculated temperature

Table 4.3 shows good agreement between thermographically measured surface temperature and the calculated surface temperature to within 1˚C over the range of interest.

4.4.2.3 Temperature uniformity over chip surface

Thermography temperature data from the total area of each chip temperature zone provide information on the temperature uniformity. Thermal images were taken of the PCR chip contacting the heater blocks in two different manners: direct clamping from the top plate of the heater assembly, and direct clamping coupled with a layer of heat sink compound.

Chips without heat sink compound were shown to demonstrate a larger variance in temperatures, both between temperature zones set at the same temperature, and within a single temperature zone. The middle temperature zone showed better temperature uniformity than the outside temperature zones regardless of the presence of heat sink

Table 4.3: Agreement between calculated and measured chip surface temperatures

Set Block Temperature (˚C)	**Measured surface temp (˚C)**	**Calculated surface temp (˚C)**	**Difference (˚C) (absolute value)**
60	59.8	59.62	0.18
70	69.3	69.05	0.25
80	78.5	78.83	0.33
90	87.9	88.59	0.69
100	97.4	98.36	0.96

compound, likely due to more uniform physical contact based on the distribution of the clamping bolts. Figure 4.10 shows the temperature distribution on the surface with and without heat sink compound. Table 4.4 summarizes the statistics for the temperature zones all set to the same temperature (110 ˚C) with or without heat sink compound. Figure 4.11 shows the simulated effects of changing geometric parameters in the system. The first graph shows the temperature of the sample fluid over time under heating and cooling conditions with changes to the thickness of the sample fluid layer. The second

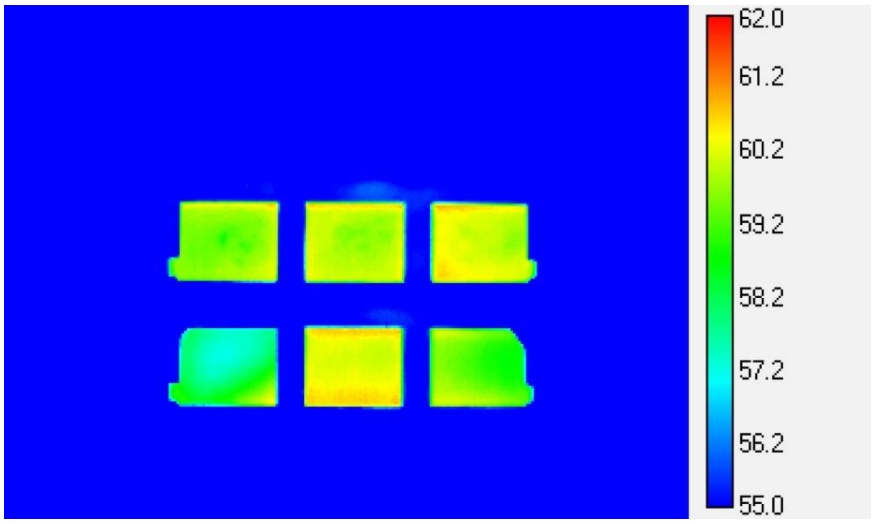

Figure 4.10: Thermographic image showing temperature uniformity over the chip surface whith and without heat sink compound.

Table 4.4: Effect of heat sink compound on temperature uniformity

	Zone 1	**Zone 2**	**Zone 3**
Ave. Temp ˚C (no compound)	100.4	106.0	98.4
St. dev.	2.7	.4	3.3
Ave. Temp ˚C (with compound)	105.7	106.6	105.3
St. dev.	0.7	0.5	0.7

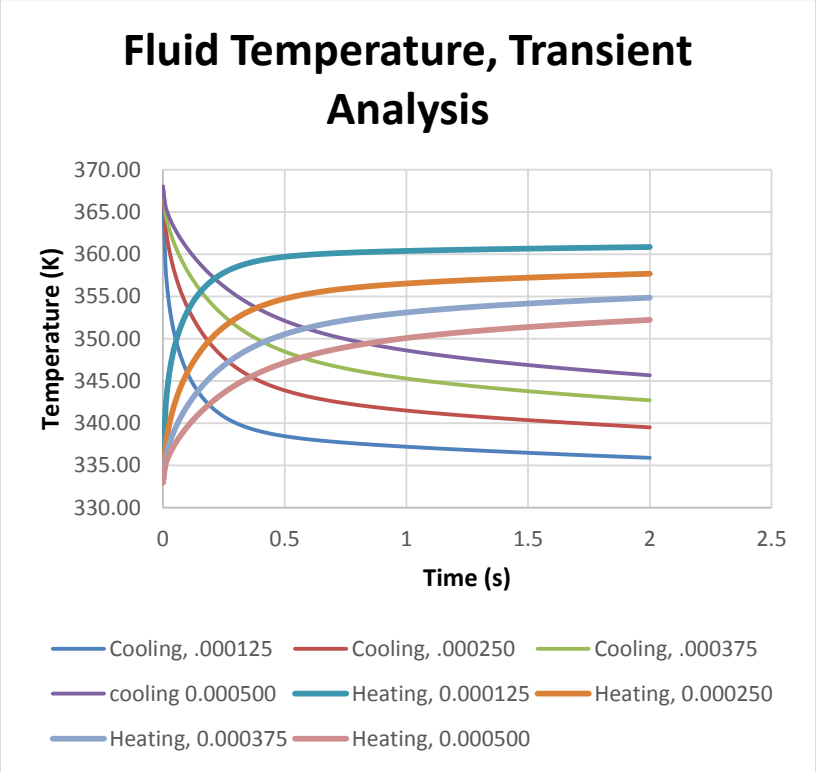

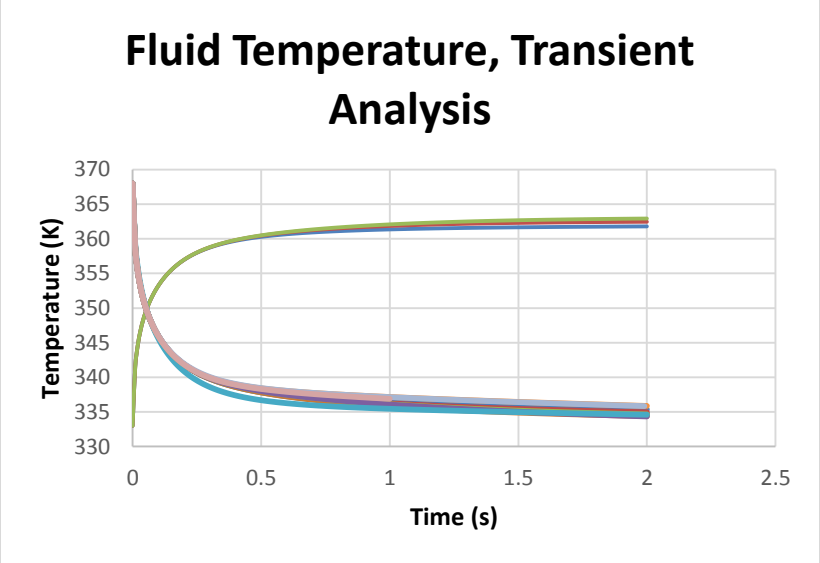

Figure 4.11: Transient heating and cooling analysis of sample fluid with adjusted parameters. Legend in (a) indicates whether it was a heating or cooling operation and the thickness of the fluid layer in meters.

graph shows the effect of adjusting other parameters such as insulating layer thickness, evaporation control layer thickness, convection coefficient, etc. These parameters each had a much smaller effect on the heating and cooling rates of the target fluid.

The simulation results indicate that keeping the sample fluid layer as thin as possible is the best way to keep the temperature ramp rate high, with other layer thicknesses being less important. The sample fluid can cool from 95˚C to the desired 64.7 ˚C in less than .5 seconds. Heating rates are similarly rapid.

4.4.3 Evaporation Control

Several approaches were used to reduce evaporation in the polycarbonate chip. First, mineral oil droplets of two different sizes (5 µl and 20 µl) were placed on either side of a plug of water inside a three-layer polycarbonate chip. In another test, the top and bottom surfaces of a chip were coated with mineral oil. These two efforts showed at best a 25% evaporation rate over 35 cycles, which was little improvement over control cycles (see Figure 4.12) The seven-layer evaporation control PCR chip was with

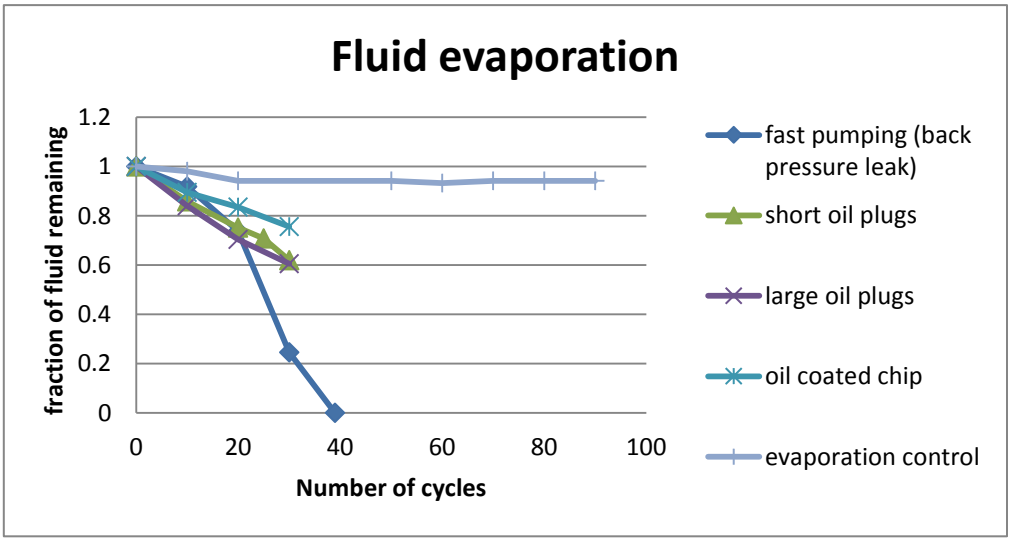

Figure 4.12: Fraction of fluid remaining inside PCR chip after multiple cycles.

equalized pressure and humidity on either side of the polycarbonate membrane was shown to greatly reduce evaporation: less than 10% over as many as 60 cycles. This shows that oil droplets do not work as effective evaporation deterrents for systems made of materials that are not good vapor barriers. However, equalizing the pressure and humidity on either side of the fluid channel prevents fluid from evaporating through the thin channel wall of the polymer chip.

Initial Tests of PCR amplification on the polycarbonate oscillatory flow PCR chip were carried out on three-layer chips. Melting curves for amplicon produced by the chip are shown in Figure 4.13. The red line (02-08-13-t1) is a PCR reaction control performed on commercial PCR equipment (LightCycler). The single sudden drop in fluorescence and single peak in the derivative plot at the expected temperature of approximately 81°C indicates proper PCR amplification.

The other lines in Figure 4.13 have multiple fluorescent drops indicated by multiple peaks in the derivative plot. These peaks indicate different lengths in the strands of DNA molecules present. The likely cause of this is primer-dimerization, where primers bind to each other and the PCR reaction replicates small primer chains, rather than the sequence of interest. Dimerization can be caused by multiple factors including improper temperature conditions, chemical imbalances, or other forms of interference with the annealing or extension PCR steps. Good temperature control in the current system evident by the agreement between simulations and measurements indicated that chemical problems with the PCR reaction rather than temperature anomalies were likely the main cause of these incorrect amplification products.

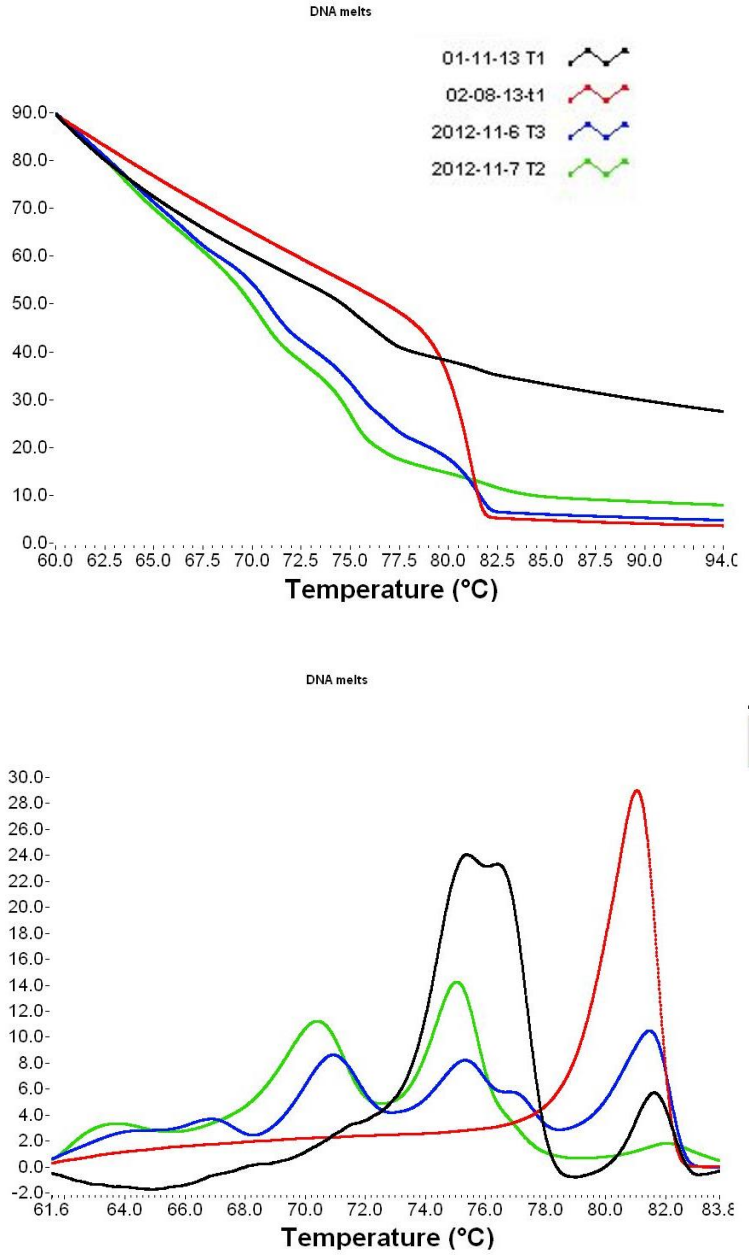

Figure 4.13: Fluorescence and fluorescence derivative plots for high resolution melting analysis The fluorescence plot (top) shows the relative intensity of the emitted fluorescence (y-axis) as the temperature is increased (x-axis). The fluorescence decreases as the DNA strands unwind at elevated temperature. The fluorescence derivative plot (bottom) is the negative derivative of the fluorescence plot. This serves to highlight abrupt changes in fluorescence caused by strands of the same molecule denaturing at the same melting temperature.

4.4.4 Amplification

4.4.4.1 Gradient PCR

Melting analysis performed on the gradient PCR test samples indicates that the template amplified at all temperatures tested, with the highest amplification coming on samples with annealing at a temperature of 64.7 ˚C (see Figure 4.14). Figure 4.14 also shows that the sample at the annealing temperature of 64.7 ˚C had the lowest small melting curve derivative peaks at other temperatures. These other peaks indicate primer dimerization, where the primers attach to a section of a DNA strand (or primer) other than the one targeted and amplify incorrect sequences. This condition is detrimental to PCR efficiency and can lead to false positive tests and is caused by temperature or chemical variations from the PCR recipe standard. Based on these results, PCR for this molecule is effective with annealing temperatures below 64.7 ˚C. However, all temperatures produced relatively minor dimerization peaks, indicating a relatively stable process with respect to temperature.

4.4.4.2 Amplification on evaporation control chip

Because temperature was ruled out as the cause of PCR reaction failures, the next step in producing good PCR product was to decrease evaporation rates to stabilize the reagent concentrations. This was done using the seven-layer evaporation control chip. Following BSA coating of a seven-layer evaporation control chip, amplification was performed on chip with 40 cycles alternating between 95 ˚C for 10 seconds and 65 ˚C for 20 seconds. Successful amplification was demonstrated in 20 minutes with the proper melting temperature observed without dimerization products as evidenced by Figure 4.15.

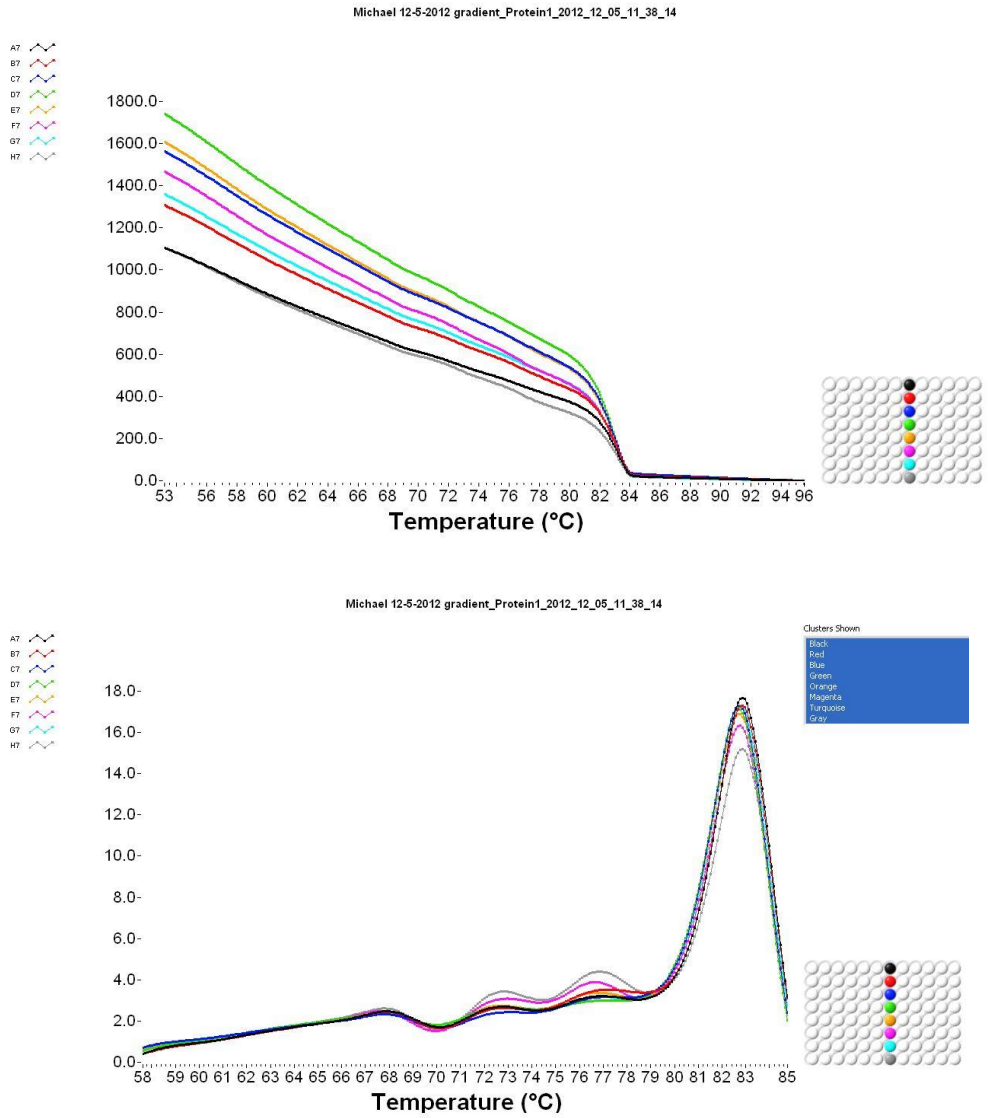

Figure 4.14: High resolution melting curve and negative derivative plot of gradient PCR performed at a range of annealing temperatures.

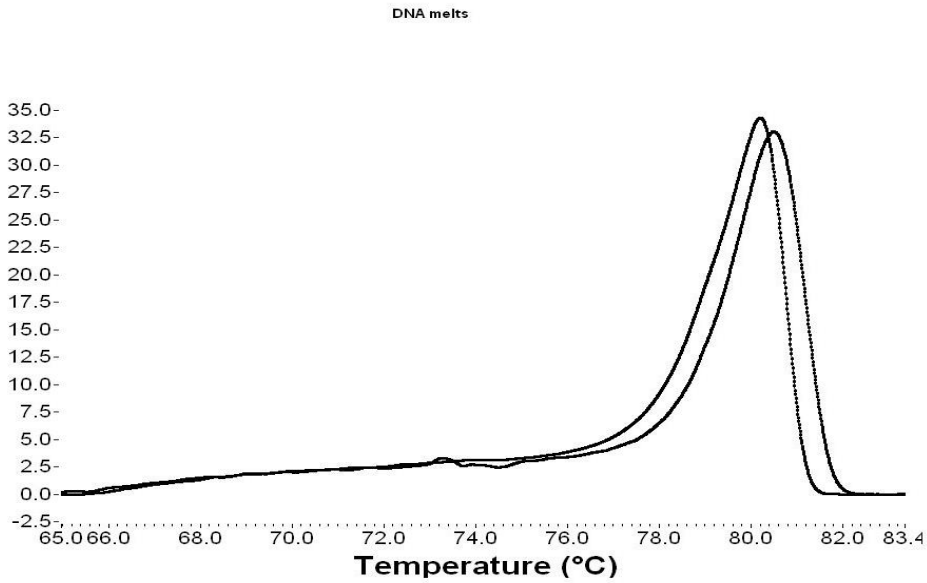

Figure 4.15: Plot of negative derivative of melting curve indicating dimer-free amplificaiton of DNA template for two amplification tests.

Verification that the amplicon produced by the on-chip PCR is correct was also carried out by performing a gel electrophoresis shown in Figure 4.16. Bright bands were evident with the same number of base pairs as a positive control amplified using a water bath PCR method.

Amplification of the target molecule was successful using the BSA-coated chip as evidenced by the electropherogram lanes 2 and 6 matching the positive control in lane 8. For those tests, the samples were pumped through the temperature zones and cycled by hand, prior to the instigation of full automation. Though fainter, lanes 1 and 7 which correspond to totally automated also showed bands at the correct position. The smearing of material at the bottom of the lanes indicates some primer dimerization. The likely cause is changes in the pumping distance for each cycle that expose portions of the fluid

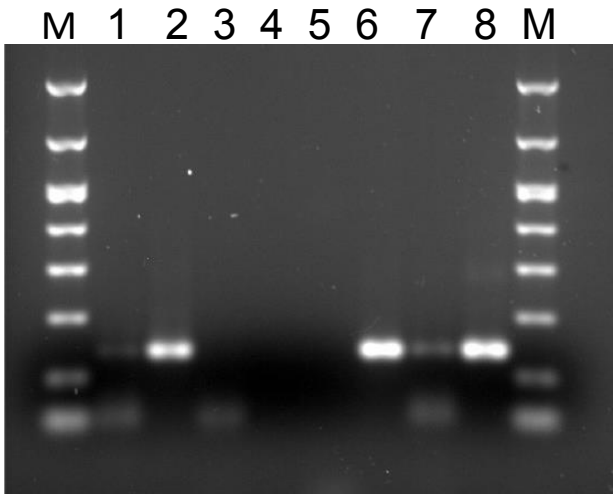

M: DNA Ladder
Lane 1: Automated shuttle PCR
Lane 2: Evaporation control, BSA-coated
Lane 3: Automated shuttle PCR
Lane 4: Not amplified
Lane 5: negative control
Lane 6: Evaporation control, BSA-coated
Lane 7: Automated shuttle PCR
Lane 8: Positive control

Figure 4.16: Electropherogram of DNA amplicon showing successful on-chip amplification.

plug to regions of incorrect temperature. However, the amplification was successful to the point that a melting curve would detect the presence of the target molecule.

4.5 Conclusions

A disposable oscillatory flow PCR chip was fabricated using multilayered thermally laminated polycarbonate sheets. Temperature conditions were numerically simulated and experimentally verified. A unique scheme for evaporation control was implemented. Successful amplification of DNA was achieved in 40 PCR cycles in approximately 20 minutes.

4.6 References

1. K. B. Mullis, Scientific American **262** (4), 56-61 (1990).

2. M. Bu, T. Melvin, G. Ensell, J. S. Wilkinson and A. G. Evans, Journal of Micromechanics and Microengineering **13** (4), S125 (2003).

3. Q. Xiang, B. Xu, R. Fu and D. Li, Biomedical Microdevices **7** (4), 273-279 (2005).

4. D. Ross, M. Gaitan and L. E. Locascio, Analytical Chemistry **73** (17), 4117-4123 (2001).

5. D. C. Leslie, E. Seker, L. A. Bazydlo, B. C. Strachan and J. P. Landers, Lab on a Chip **12** (1), 127-132 (2012).

6. S. Metz, W. Van de Ven, J. Potreck, M. Mulder and M. Wessling, Journal of Membrane Science **251** (1), 29-41 (2005).

7. T. Hanada, I. Shiroishi, T. Negishi and T. Shiro, presented at the OPTO, 2010 (unpublished).

8. Z. Yi and W. Tza-Huei, presented at the 23rd IEEE International Conference on Micro Electro Mechanical Systems (MEMS 2010), 24-28 Jan. 2010, Piscataway, NJ, USA, 2010 (unpublished).

9. A. Polini, E. Mele, A. G. Sciancalepore, S. Girardo, A. Biasco, A. Camposeo, R. Cingolani, D. A. Weitz and D. Pisignano, Biomicrofluidics **4**, 036502 (2010).

10. J.-Y. Cheng, C.-J. Hsieh, Y.-C. Chuang and J.-R. Hsieh, Analyst **130** (6), 931-940 (2005).

CHAPTER 5

CONCLUSIONS AND FUTURE WORK

5.1 Conclusions

A system for automated extraction and amplification from a variety of samples was developed. The system built off of advancements to 3-layer PDMS microfluidic chip manufacturing to provide a device capable of complex fluid handling tasks. The programmability of the device allowed for hands-off processing of nucleic acids. A novel integratable shuttle PCR chip design was fabricated and successfully reduced evaporation rates and amplified DNA.

Reviewing the state of the art in microfluidic nucleic acid extraction devices and investigating the capability to create an automated system provides several clear conclusions:

- There is a need for versatile nucleic acid sample preparation systems that can process pure RNA or DNA from a variety of sample types in a way that can be done by nonexperts.
- Three-layer PDMS components and devices were fabricated and proved to be effective in portable microfluidic systems with minimal external equipment.
- The gas permeability of the membrane provided a unique pumping, bubble injection, and bubble removal mechanism that was effective at low-flow pumping in dead-end channels, trapping air bubbles, and enhancing mixing by over 40%.
- A system was created that performs automated extraction of RNA or DNA from multiple sample types to make sample preparation more practical and available.
- The Utah system is capable of extracting detectible levels of RNA from *E. Coli* bacteria and FMDV virus samples. It likewise can be used to extract human genomic DNA from blood.

- The LabView control interface for the extraction system is capable of handling multiple protocols to adjust the specifics of the test to be performed.
- A multi-layer laminate oscillatory flow PCR chip was fabricated for integration with the extraction system.
- The oscillatory flow PCR scheme provides flexibility in cycle parameters while keeping thermal inertia low for rapid cycle times.
- Thin polycarbonate PCR chips are prone to evaporation of sample fluid at the high PCR temperatures. This evaporation can effectively be minimized by layering the fluid channel between layers of water pressurized equal to the sample fluid.
- BSA coating of polycarbonate PCR chips prevents PCR reagent loss and permits dimer-free PCR amplification.

Advancements in membrane-based component integration were instrumental in the selection of PDMS as the substrate for the main fluid handling chip for the nucleic acid extraction system. This system has proven capable of handling a variety of sample preparation tasks in an effort to make automated nucleic acid sample preparation more practical and available. Such work is a step towards a universal sample preparation unit that can handle many kinds of samples from viruses to tissue samples and provide rapid, meaningful results from a lab-on-a-chip platform. The RNA detection abilities were demonstrated for two main applications. The first is the detection of *E. Coli* RNA to monitor drinking water supplies for harmful bacteria where RNA is a more appropriate genetic material for detection. RNA was also extracted from viral samples in tissue culture fluid to demonstrate another form of pathogen detection. These applications will open the

door for future pathogen screening and detection tests. The same system was shown to be capable of extracting DNA from whole blood samples. This project satisfies global demand for fast, simple, and adaptable genetic testing systems.

Detection of DNA or RNA often requires amplification through PCR. To integrate an amplification module with the extraction system, a disposable oscillatory flow PCR chip was fabricated using multilayered thermally laminated polycarbonate sheets. Temperature conditions were numerically simulated and experimentally verified to produce temperature ramp rates as high as 60 ºC/s. A unique scheme for evaporation control was implemented. Successful amplification of DNA was achieved in 40 PCR cycles in approximately 20 minutes.

5.2 Contributions

Contributions made over the course of completing this project are summarized in the following list:

- Utah system extraction unit for nucleic acid purification
- Multiscale rapid prototyping PDMS casting mold creation process with masked corona bonding
- Disposable glass fiber extraction chips
- Matlab code for solving 1D steady state, and 1D transient temperature analysis for a fluid layer in a composite wall geometry with varying layer thickness and material properties
- Numerical temperature analysis to determine convection coefficient for free convection for low Rayleigh number horizontal heated surface
- Numerical temperature analysis for transient temperature profiles inside

multilayer, variable material microfluidic device

- Novel sample evaporation control for polymer film chips to reduced evaporation to less than 6% over 40 cycles
- LabView program for interface and control of extraction unit
- Successful automated amplification of DNA template in 40 cycles in ~20 minutes.

5.3 Future Work

While the system presented in this work has proven effective at extracting nucleic acids from multiple sample types, there are still several areas recommended for improvement in future iterations of the system and related research.

Multiple sample types were used in the extraction system, but they were all in liquid form. Work still needs to be done in demonstration of the current system's ability to extract nucleic acids from an increased number of sample types. Some raw sample mediums of interest such as stool, soil, or other solid material present difficult challenges for use in microfluidic systems. Small channels could easily be blocked by excessive amounts of solid matter. A filtration mechanism added to the sample input will further increase the versatility of the sample preparation system. Filter material or integrated fabricated filter features could be chosen such that large particles in impure samples could be screened out in the sample input well, while smaller particles and organisms that don't pose the risk of channel blockage would pass through. Demonstration of extraction of the target molecule from soil, food, or stool samples would indeed demonstrate versatility of the sample preparation system.

Akin to filtration, a sample preconcentration step would help detect minute

quantities of the target molecule when it would normally get lost among the more prevalent DNA and RNA molecules in the sample. As an illustration, contrast the demonstrated ability of the current system to extract human genomic DNA from blood versus the goal to find the nucleic acid signature of a scarce pathogen found in the blood stream. The more plentiful genetic material from the host and other organisms in the blood stream would compete for solid phase binding sites. The relatively dilute target (often with orders of magnitude fewer molecules) could end up fading into the background noise of the detection system. A preconcentration step that would rid the sample of unwanted organisms or genetic material would greatly increase the specificity of the extraction system.

The difficulty in implementing a preconcentration step for a system that purports to be agnostic to sample type is that it is not feasible to sort mechanically solely on cell size. The size of the target would change based on the application as would the size of the unwanted background debris. Fortunately, the control chip is already designed for modular components, and perhaps future work could focus on interchangeable mechanical filter modules with different pore sizes that can be used as the initial sample input section.

The mechanical separation method seems a better fit with the goal of universality than other preconcentration technologies such as functionalized magnetic beads that attach to target molecules using specific antibodies. While the functionalized beads perform well, they are highly specific to a single organism and require skilled handling for implementation.

Another recommended advancement to improve the extraction system would be

to fully integrate the extraction and PCR modules into a single disposable device. The current modular method has a benefit in that some customers may have a detection or analysis method that does not require amplification. However, the sensitive nature of biomolecular tests begs for extreme care in avoiding cross-contamination, so reusable chips pose a threat. The current PDMS extraction chip could technically be considered a disposable, but the materials and fabrication process are more costly than what would be seen in a thermoplastic chip.

Other suggested work for the future does not include such drastic changes to the system's over-all design. Instead work can focus on realizing an expanded role of features already in place in the current system. For example, the flexibility of the oscillatory PCR chip has not been fully explored. The fluid temperature behavior has been characterized, but the ability of the system to amplify nucleic acids has only been proven on a single molecule. The flexible nature of the automated PCR chip could be explored by performing RT-PCR on the chip. Also longer DNA strands could be amplified and protocols with tighter temperature tolerances could be performed to explore the limits of the PCR chip.

Finally, integration of an analysis or detection module onto the system would make it a complete sample-in answer-out system. The main focus of the research to this point has been solely on extraction, purification, and amplification of the target, as there is already a wide range of devices that detect or analyze nucleic acids. However, simply because the main focus is on extraction does not mean that analysis cannot be an offered module for the system. Analysis could be integrated with the PCR module, where real time monitoring of fluorescence of the PCR process would be able to indicate the

presence of amplified target. The capability to perform such analysis would require little more than a light transmitter and fluorescence detector. LabView, which already controls the instrument function, can readily control and monitor the detection equipment at the same time.

These recommendations will further improve a system that has demonstrated an ability to simplify nucleic acid extraction. This system has demonstrated improvements in components and subsystems that can be used by nonexperts. It has also proven to be a practical technology, used by nonexperts in the field in Canada and India, far from the supervision of the system creators. As the future work continues to expand on the past demonstrations of versatile nucleic acid extraction, this sample preparation system will be on the cutting edge of the transition to a commercially viable technology as it benefits researchers, clinicians, patients, and the public at large.

APPENDIX A

MICROFLUIDIC SAMPLE PREPARATION: CELL LYSIS AND NUCLEIC ACID PURIFICATION

Kim, Jungkyu, Michael Johnson, Parker Hill, and Bruce K. Gale. "Microfluidic sample preparation: cell lysis and nucleic acid purification." *Integrative biology* 1, no. 10 (2009): 574-586. – Reprinted by permission of the Royal Society of Chemistry

CRITICAL REVIEW www.rsc.org/ibiology | Integrative Biology

Microfluidic sample preparation: cell lysis and nucleic acid purification

Jungkyu Kim,†[a] Michael Johnson,†[b] Parker Hill[a] and Bruce K. Gale*[b]

Received 24th March 2009, Accepted 10th August 2009
First published as an Advance Article on the web 25th August 2009
DOI: 10.1039/b905844c

Due to the lack of development in the area of sample preparation, few complete lab-on-a-chip systems have appeared in recent years that can deal with raw samples. Cell lysis and nucleic acid extraction systems are sufficiently complex even before adding the complexity of an analysis system. In this review, a variety of microfluidic sample preparation methods are discussed and evaluated. Microsystems for cell lysis are discussed by grouping them into categories based on their lysis mechanisms: mechanical, chemical, thermal or electrical. We classify the nucleic acid purification techniques according to the mechanism that links nucleic acids to substrates: silica-based surface affinity, electrostatic interaction, nanoporous membrane filtration, and functionalized microparticles. The techniques for microfluidic cell lysis and nucleic acid purification are compared based on the ease of microfabrication and integration, and sample flexibility. These assessments can help us determine the appropriate sample preparation technique for generating a true lab-on-a-chip.

Introduction

Microfluidic systems using nucleic acids for biomedical analysis, environmental sensing, and biological research have been developing at a rapid rate. As part of this movement, there is a large push to fully integrate analysis systems onto a single biochip—thus reducing laboratory time, human interaction, and reagent and equipment costs. The primary focus of these research and development efforts has been on the sensing and analysis platforms that make the critical measurements, and a wide variety of these systems have been developed. For example, nucleic acid analysis chips have been developed that rely on techniques such as: polymerase chain reaction (PCR), capillary electrophoresis, fluorescence *in situ* hybridization (FISH),[1] surface plasmon resonance (SPR),[2,3] surface enhanced raman scattering (SERS), micro/nano-cantilevers,[4] nanowires,[5] nanopores,[6] and dozens of other technologies. Recent nanomechanical biosensors can be used for applications in ultrasensitive detection of: DNA hybridization,[7,8] biomarker transcripts of human RNA,[1] and viruses.[9] Several research groups have already demonstrated successful solution-phase silicon nanowire (SiNW) sensing of DNA,[10] viruses,[11] small molecules[12] and proteins.[13,14] All of these methods, though, require off-chip sample preparation steps. As microscale sample preparation techniques have lagged behind the development of sensing and analysis techniques, the viability of these integrated devices for widespread use in clinical or environmental situations is still limited. Nevertheless, substantial progress has been made in the development of microscale nucleic acid preparation techniques, which will be the subject of this work.

Nucleic acid sample preparation is highly labor intensive and time consuming with multiple steps required to collect DNA or RNA from raw samples such as whole blood, urine, saliva, serum, tissue from biopsies, spinal fluid, and stool.[15–17] To solve the sample preparation challenge and simplify the steps in the sample preparation process, macroscale sample preparation techniques are typically modified and implemented into microfluidic systems that interface with downstream components. The integration of sample preparation typically reduces the total analysis time and cost by reducing the

[a] *Department of Bioengineering, University of Utah, Salt Lake City, UT 84112, USA. E-mail: jungkyu.kim@utah.edu; Fax: 801-585-9826; Tel: 801-585-3176*
[b] *Department of Mechanical Engineering, University of Utah, Salt Lake City, UT 84112, USA. E-mail: bruce.gale@utah.edu; Fax: 801-585-9826; Tel: 801-585-3176*
† These authors contributed equally to this work.

Insight, innovation, integration

Various nano-biosensors have been developed and used for detecting and genotyping nucleic acid samples. As this field expands, there is the wish to develop totally integrated systems ("Lab-on-a-chip" or micro Total Analysis Systems (TAS)). Sample preparation is a critical research field in creating these integrated systems. Microfluidic sample preparation minimizes total assay times, labor and contamination issues. For these reasons, a microfluidic sample preparation system is needed in order to realize microTAS or a Lab-on-a-chip. This article presents the state of the art of microfluidic sample preparation including cell lysis and nucleic acid extraction for implementation in an integration system. Each technique for microfluidic lysis and extraction are compared and discussed to provide perspectives in this field.

 This journal is © The Royal Society of Chemistry 2009

samples and reagents consumed and takes advantage of high reaction rates at the microscale. Another benefit stems from having an enclosed system performing the entire analysis from sample-in to answer-out, which reduces the chance for cross-contamination. Advances in this field will facilitate an increase in the spread and scope of nucleic acid analysis, leading to more insight and discovery of underlying biological phenomena. These insights will be generated by the ability of next-generation analysis systems to rapidly process multiple samples simultaneously using microfludic-based extraction systems. The large amounts of data will not require costly robotics that limit their use to large labs, but they will be available to small, benchtop or portable units that will allow rapid analysis in the field or at the clinic. Thus, research costs will also fall, allowing more ubiquitous research to be performed. Integrated, small-scale nucleic acid purification will also allow for ''take-home'' systems that will allow for a steady stream of data to be generated by home users that can be scoured by researchers for trends and new information. These home based systems will provide help in the tracking and detection of infectious disease and pandemics that have garnered so much attention lately. Thus, these benefits inspire a closer inspection of current on-chip sample preparation techniques.

Generally, the nucleic acid sample preparation process can be separated into two primary steps: (1) cell or tissue lysis, and (2) nucleic acid extraction or separation. Current techniques for both macroscale and microscale cell lysis and nucleic acid extraction will be reviewed to indicate the state-of-the-art.

Conventional sample preparation

Microfluidic DNA extraction procedures are derived from lab protocols typically used by biologists. Conventional processes may include sample filtration, centrifugation, distillation, dilution and extraction. For example, when a whole blood sample is being analyzed, a typical nucleic acid extraction process might proceed as follows. Citrate buffer is added to the sample, which is then mixed and centrifuged. The supernatant is discarded and additional buffer is added, mixed, and again the tube is centrifuged. After the new supernatant is discarded, the pellet is resuspended in a solution of SDS detergent and proteinase K, and the mixture is incubated at 55 °C for 1 h. The sample is then extracted once with a phenol/chloroform alcohol solution, and after centrifugation the aqueous layer is removed to a fresh microcentrifuge tube. The DNA is precipitated in ethanol, resuspended in buffer, and precipitated in ethanol a second time. Once the pellet is dried, buffer is added and the DNA is resuspended by incubation at 55 °C overnight. This is a lengthy procedure and is not directly applicable to high-throughput methods, which require smaller

Jungkyu Kim

Jungkyu Kim received his PhD in Biomedical Engineering from University of Utah in 2009. He has been working in the area of microfluidics fabrication technique, microfluidic sample preparation and Lab-on-a-chip development for personalized medicine and bacteria detection. He is currently a postdoc researcher in Electrical Engineering at University of California, Berkeley.

Michael Johnson

Michael Johnson received his BS degree in Applied Physics from Brigham Young University in 2006. He is currently a PhD student in Mechanical Engineering at the University of Utah. His graduate research focuses on microfluidic devices for biomedical applications.

Parker Hill

Parker Hill is completing a BS degree in Bioengineering from the University of Utah. His undergraduate research focuses on cell lysis and nucleic acid extraction on microfluidic devices.

Bruce K. Gale

Bruce K. Gale, currently Director of the Utah State Center of Excellence for Biomedical Microfluidics and an Associate Professor of Mechanical Engineering at the University of Utah since 2001, has been working in the area of microfluidics and micro-total-analysis systems (μ-TAS) for the past decade. His interests include lab-on-a-chip devices that require a variety of microfluidic components for the completion of complex and challenging medical and biological assays.

reaction volumes to reduce the cost of reagents and the amount of waste generated. To simplify this conventional method, several companies such as Qiagen, GE Healthcare, Invitrogen and Progmega have developed silica column kits for nucleic acid purification. The supplied lysis methods and nucleic acid binding columns provide a fast (around 30 min), cost-effective way to purify nucleic acids. But, these methods still need centrifugation and manual pipetting by a researcher. In addition, this system takes too much time, setup and labor to be adapted for high-throughput systems. In particular, centrifugation processes are almost impossible to implement in most microfluidic systems, due to the small length scales (including rotational arm lengths needed for high centrifugal forces) and the desire to avoid complex moving parts. Much microfluidics research has been aimed at developing miniaturized and sensitive detection techniques that will overcome these drawbacks and incompatibilities. On the macroscale, the time necessary for DNA purification was greatly reduced by the shift from conventional extraction-based processes to those using solid-phase extraction (SPE) on silica or ion exchange resins. Since most of these techniques have been implemented on the microscale in some way, we will review these techniques by exploring primarily their microscale implementations.

Sample preparation using microfluidic techniques

Based on miniaturization concepts and physicochemical mechanisms, a variety of methods have been implemented to accomplish chip-scale extraction from biological samples. Most biological samples consist of a complicated mixture of compounds, and researchers do not completely understand how some molecules promote or prohibit the analytical process. Thus, before examining the desired molecules a separation step is implemented to remove these potentially problematic materials. If the target molecules exist inside the cell, the cells must be broken down to release the desired molecules, which must then be isolated. Specifically integrated steps of cell lysis and nucleic acid extraction must be implemented to enable the high-throughput, focused, nucleic acid analysis that will lead to biological understanding and insight. Current microfluidic research that has developed components and protocols that accomplish lysis and extraction on a scale amenable to integration will therefore be the focus of discussion.

Cell lysis in a microfluidic system

There are many current methods for lysing cells that are used within microsystems, which will be categorized in this work into four major groups. (1) Mechanical lysis employs cellular contact forces to crush or burst the cells. (2) Thermal lysis uses high temperatures to disrupt the cell membrane. (3) Chemical lysis uses a chemical buffer or enzymes to break down the cell membrane. (4) Electrical lysis induces cell membrane porosity with a low-strength electric field or complete lysis of the cells with a stronger field. This work examines current cell lysis components being explored in each of these four categories. The effectiveness of these techniques are discussed, and some fabrication methods are explained to help understand how a method might be manufactured and integrated with other sample preparation and nucleic acid analysis systems.

Mechanical lysis. Cell lysis occurs when the cell membrane (and/or cell wall) is disrupted in some way allowing the contents of the cytoplasm to be released. Perhaps the most conceptually simple method to achieve lysis is to use a mechanical force to tear or puncture the membrane. A few of the numerous different cell membrane disruption methods using physical contact will be reviewed here. One method for mechanical lysis is to force the cell through a filter with openings too small for a whole cell to pass through, thus shearing the cell membrane. This causes the cell to rupture and the contents to spill out. Improvements to this method have been demonstrated by fabricating the device so that the walls of the filter have sharp nanoscale barbs.[18] These channel walls have scalloped ''microknives'' created using a modified DRIE process as shown in Fig. 1(A-1). Use of these microbarbs increased the amount of lysis compared to filtering cells through a similarly sized filter with smooth walls. Another basic method is simply to burst the cells by deforming the cell to the point that the membrane bursts.[19] One such method uses a polydimethylsiloxane (PDMS) membrane to crush cells and break their membranes.[20] The fluid channel through which the cells flow is shaped to have a curved cross section on one side while the other side is a flat membrane separating the fluid channel from a pneumatic control channel shown in Fig. 1(A-2). The pneumatic control channel can be pressurized to force the membrane to expand into the fluid channel and crush any cells trapped there. This basic design is used in a chip that can pull cell-containing fluid from a reservoir, seal the cell solution into a chamber with valves, and lyse the cells by crushing them with the membrane before sending the lysed solution to the outlet. As the pressure on the cells is slowly increased from ambient, the cells flatten out as they are compressed and deformed. Once pressure approaches 25 kPa in the system, the cells begin to split open and spill their internal cellular structures. Complete lysis is evident as the pressure approaches 30 kPa. Kim *et al.*[21] use a strictly mechanical method for lysing cells in a spinning microfluidic CD device. The driving mechanical principle to break up the cells involves friction and collisions between the cells and granular particles—such as glass beads—in the solution. The solution containing cells and particles are placed into an annular channel on a microfluidic CD-like chip. The disc is rotated at high speeds around a horizontal axis. The device was tested with several different cell types—mammalian cells, bacterial cells, and yeast cells—and was seen to be effective at lysing all of them. A related CD cell lysis device is presented by Kido *et al.*[22] which shows more promise of potential integration with other steps of nucleic acid analysis. In this case, small, moving ferromagnetic discs on the CD are actuated by an oscillating magnetic field to stir the grinding beads and lyse the cells. Sonication is another form of mechanical cell lysis that differs from the physical contact methods already described by employing ultrasonic agitation to create pressure waves with enough energy to disrupt the cell, causing it to lyse.[23–27] Taylor *et al.* integrate sonication into a microfluidic system and show that increasing the fluid pressure enhances the coupling between the ultrasonic horn tip and the liquid region, which leads to more efficient cell lysis.[28] A fluidic chamber was in contact with the ultrasonic horn through a flexible interface.

This journal is © The Royal Society of Chemistry 2009

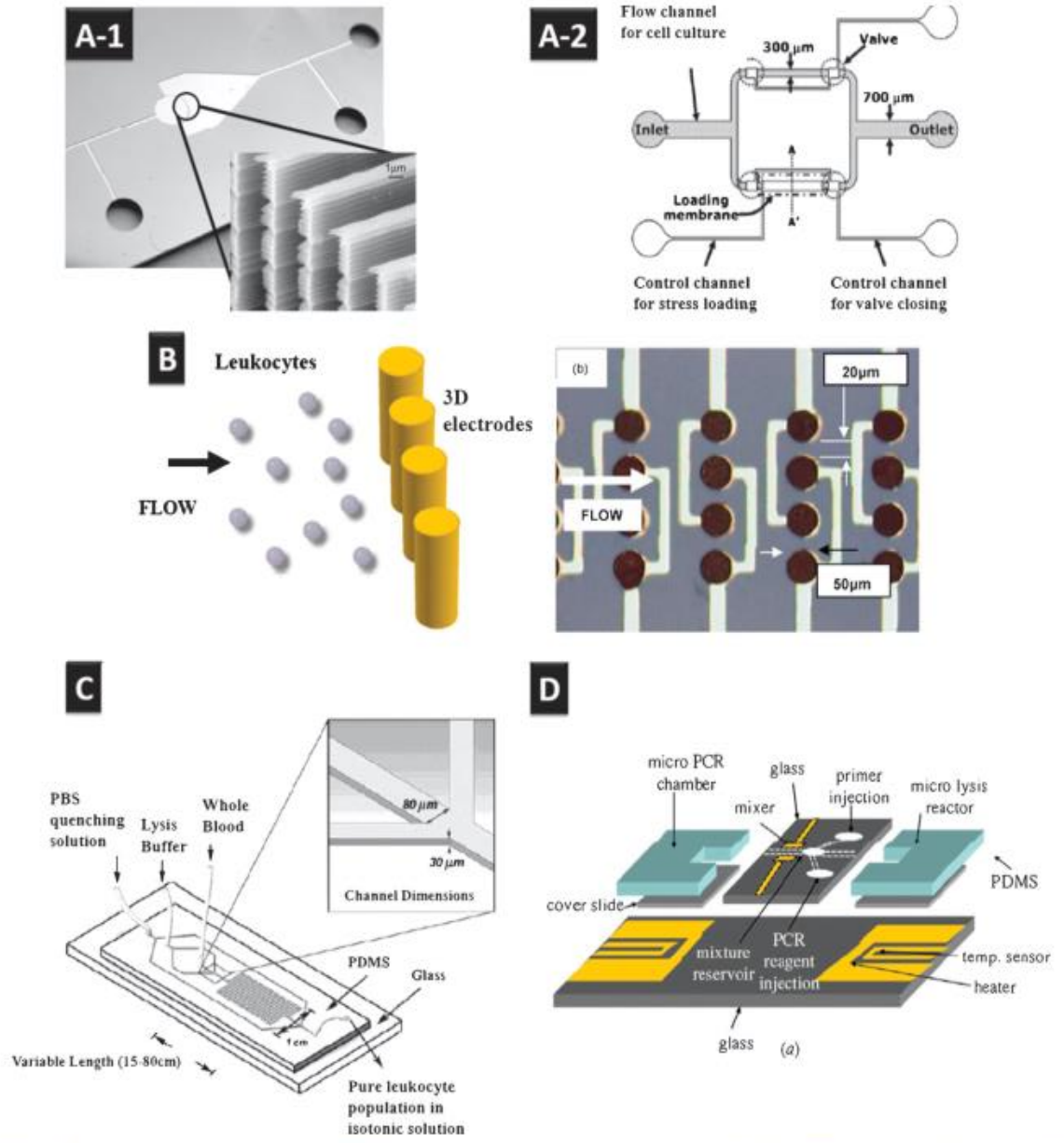

Fig. 1 Microfluidic cell lysis systems using different energy sources to accomplish cell disruption. (A-1) Sharp microbarbs were fabricated in a microfluidic channel. When the cells passed though the microbarb filter, the membranes were ruptured and the cells were lysed.[18] (A-2) Top-view schematic of a compression force lysis device. Cells from the inlet are trapped in the fluid channel chamber at the bottom of the figure by pneumatic valves at either end. Pressure applied to the loading membrane applies a compression force that bursts the cells.[20] (B) 3-D schematic and top view of an electrical cell lysis system. Cylindrical electrodes used to increase the electric field strength were fabricated by electroplating and embedded in a microfluidic channel for leukocyte cell lysis.[67] (C) Schematic of a simple chamber and serpentine microfluidic channel for chemical lysis. Whole blood enters the system and meets and mixes with a lysis buffer. PBS buffer then dilutes the lysis buffer solution.[45] (D) Schematic of a microfabricated PCR chamber with integrated thermal cell lysis reactor using a thin-film heater to attain 95 °C.[33]

The fluidic chamber included a filter to trap spore cells and debris for study. While sonication involves an increase in external equipment, its non-invasive nature shows promise for integration. A final physical mechanism for cell lysis involves the use of lasers. Cell lysis has been demonstrated as the focused laser beam forms a plasma, produces a shock wave, and creates bubbles by cavitation which expand and collapse, thus lysing the cell.[29]

Thermal lysis. Thermal lysis is one of the more well-established lysis techniques in nucleic acid preparation, and is common in laboratory settings. At high temperatures

proteins within the cell membranes are denatured, irreparably damaging the cell and releasing the cytoplasmic contents. The most common method of inducing this thermal damage is immersion of a sample tube in a boiling water bath for 40 s.[30] This short exposure at 100 °C is sufficient to cause significant damage to the cell membrane without damaging the nucleic acids. Prolonged heat treatment risks causing irreversible denaturation of superhelical DNA.[31] This lysis method is less commonly integrated with microfluidic systems, but is now being used more commonly with PCR-based assays. Liu *et al.* used a method of on-chip cell concentration to preconcentrate cells in a PCR chamber.[32] The concentrated cells were then exposed to the first PCR thermal cycle and lysed sufficiently to amplify the DNA present by PCR. The heat for thermal lysis and PCR was applied by a single embedded resistive heater and required no additional chemical reagents with a whole blood sample, making a cost-effective system. This system is effective for single samples, but cannot be used as part of a continuous flow assay or with downstream analysis techniques that require a sample free of protein and other cellular contaminants. Lee *et al.* improved the flow capabilities of the chip by fabricating a glass chip with a PDMS-based cell lysis reactor, a sample driving module, an electrokinetically driven micromixer, and a PCR chamber as shown in Fig. 1(D).[33] Microelectrodes deposited on the lower glass substrate control the flow of cellular material through the chip while two sets of micro-heaters and micro-temperature sensors control and monitor the temperature of the lysis and PCR chambers. Yeung *et al.* further developed the use of thermal lysis for PCR and alternative assays using a chip with a single silicon and glass-based microchamber for thermal lysis, DNA amplification by asymmetric PCR, and electrochemical detection of the target DNA.[34] This process again shows effective use of thermal lysis in a microfluidic device, but its considerable operator steps and inability to function as a continuous flow device give it limited use in micro-total analysis system (μ-TAS) applications.

Continuous flow sample preparation using thermal lysis has been applied on the macro-scale and may have implications for microfluidic systems.[35,36] Zhu *et al.* use peristaltic pumps to drive pre-concentrated bacteria through two copper coils, the first of which acts as the lysis chamber and the second of which cools the sample to terminate enzymatic processes. Bacteria are sufficiently lysed after passing through the lysis coil for a brief 20 s, allowing DNA plasmid extraction from 17 l of *E. Coli* in just 45 min. This method requires a temperature of only 70–80 °C for bacterial lysis, a relatively low temperature when compared with conventional protocols. This continuous thermal lysis protocol has potential for microfluidic applications. However, the success of this method is dependent on several preparation steps, including freezing and reconstitution of the sample in Tris-EDTA(TE) buffer, treatment with lysozyme to disrupt the peptidoglycan bacterial cell wall, and downstream plasmid isolation and purification. The requirement of lysozyme for the feasibility of this method is an important consideration, as often thermal lysis is used as an alternative to chemical or enzymatic lysis, especially where downstream contamination is an issue or on-site cold storage is not feasible. Another consideration for thermal lysis is the high power requirements for heating, which might not be feasible for portable systems. An advantage of performing thermal lysis on a microfluidic chip is that the reduced heat capacity of smaller sample volumes works to reduce the needed power. Recently, an optothermal technique was applied for a microfluidic cell lysis system using a laser source and gold nanorods. The absorbance of the 808 nm laser differed as the aspect ratio of gold rods was changed. The optimal rod shape (aspect ratio 3) was found to produce efficient heat absorption for optimal lysis.[37] By incorporating this system with a Compact Disk (CD) microfluidic platform, cell lysis and nucleic acid sample preparation were successfully performed on a single device.[38]

Chemical lysis. In chemical lysis, buffers or other lytic agents are employed to break down the cell wall and/or membrane. The wide range of sample cell types and target molecules accounts for the variety of chemicals used in lysis protocols. Ammonium chloride, known as Red Blood Cell Buffer (RBC) acts on erythrocytes only and is ineffective in lysing none-rythrotic mammalian cells.[39] Non-ionic and ionic detergents disrupt cell membranes by solubilizing membrane proteins and lipids and creating pores. Triton X, a non-ionic detergent, acts more slowly and is primarily used in sample preparations for downstream assays requiring protein structure and function to be maintained. SDS, an ionic detergent, acts more quickly to totally denature proteins, and is primarily used in protein assays such as determination of molecular weight by SDS PAGE. It is also used in sample preparations for nucleic acid, as SDS denatures DNAse and RNAse enzymes.[40] As detergents act on cell membranes, they are incapable of bacterial lysis without a pretreatment to destroy the cell wall, and often follow an enzymatic degradation step such as treatment with lysozyme. Chaotropic salts are most commonly used in nucleic acid preparations. At high concentrations guanidinium thiocyanate and guanidinium chloride lyse cell membranes by disrupting protein intermolecular forces. They denature RNAses as well as membrane proteins, and so are valuable in nucleic acid extraction. The high salt concentration also allows the salt bridge that forms to extract RNA in silica environments.[41–43] Because of the large number of chemical lysis techniques that have been implemented, we limit this review to novel uses of chemical means in microfluidic devices with insights leading to more integrated systems. Shilling *et al.* have created a chip that uses chemical means to lyse cells and extract and detect proteins.[44] While proteins are not the focus of this study, the cell lysis technique could be adapted to nucleic acid preparation systems. The device is fabricated using a simple lamination scheme. A sample containing the cells is injected into a fluid channel where it meets with another solution containing a chemical lysing agent. After the two fluids join, they flow down a long channel that gives the lysing agent time to diffuse into the cell sample and disrupt the cell membranes. The protein of interest leaves the disrupted cells and diffuses out into the channel. The fluid then comes to a T-junction where it splits. The unlysed cells along with those that have had their membrane disrupted exit one channel while the lytic agent, along with some of the captured proteins, go in the other direction towards the detection channel. This device

This journal is © The Royal Society of Chemistry 2009

illustrates the ability of chemical lysis techniques to operate in a continuous flow mode, which will enable high-throughput devices. While the cell lysis method used was specifically made and tested for *E. Coli* bacterial cells, it can be modified for a wide variety of cells. Another device employing a chemical method for lysing cells was presented by Sethu *et al.*[45] in a device fabricated using typical soft lithography techniques and is depicted in Fig. 1(C). A buffer solution containing mainly ammonium chloride is used to lyse the cells. A single inlet of this cell lysis solution is split into two channels that then meet to sandwich the sample solution, thereby increasing the surface area of contact between the lysis buffer and the sample cells. This mixture then goes through a long series of turns in a serpentine channel to enhance the mixing. After the cells have been lysed in the serpentine channel section, the solution is mixed with phosphate buffer saline (PBS) solution which dilutes the lysis buffer and returns the sample solution to its original physiological concentration. Almost complete DNA release is achieved at a channel length of 15.2 cm. Another method uses a microfluidic chip to perform rapid, controlled cell lysis for the exploration of cell signaling pathways.[46] The chip includes sections for heating and cooling control with fluid channels in PDMS bonded to a glass substrate. Segmented gas-liquid flow enhances the mixing between the cell sample and the lysis buffer so that lysis is fast enough to allow the time control needed for cell signaling analysis. Stachowiak *et al.* introduce a microfluidic system that lyses bacterial spores by solubilizing the coat proteins with a chemical (such as β-mercaptoethanol) that reduces the disulfide linkages.[47] Proteins are then evaluated to ensure lysis. Heo *et al.* demonstrate chemical cell lysis by trapping *E. Coli* cells in a hydrogel in a fluid channel and then passing a 1% (w/v) sodium dodecyl sulfate (SDS) solution through the channel for 20 min.[48] The trapped bacteria cells were dyed and exhibited strong fluorescence to indicate successful lysis. A device for chemical lysis of pico-liter cell samples was demonstrated to improve single cell analysis techniques.[49] A small volume of the cell sample containing a single cell and a picoliter volume of lysis buffer (PBS, SDS or guanidinium thiocyanate (GTC)) are combined in a PDMS picoliter reservoir where the cell is lysed and visualized with a dye. The large number of microfluidic systems that employ chemical means to lyse cells indicates the versatility of this method, which could well be adapted to suit a nucleic acid sample preparation system for a specific application.

Electrical lysis. Exposure of cells to strong electric fields can compromise cell membranes sufficiently to induce cell lysis. As cells are exposed to high-intensity pulsed electric fields (PEFs), membranes are destabilized and become transiently permeable to macromolecules.[50] As pulse length and electric field strength reach a critical value the cell is lysed by dielectric breakdown of the cell membrane.[51] Though the exact mechanism of increased permeability and lysis by PEF is not fully understood, it has been shown that cell lysis occurs due to an electrical effect, and not as a result of Joule heating or electrolysis of the solution.[52] The critical electric field value is the most important parameter for lysis by PEF, and varies between types of bacteria and mammalian cells due to deviations in cell shape and radius, though this relationship has been mathematically determined and is well understood.[53] In each case the applied electric field induced lysis when the cell membrane potential reached on average 1.1 V, usually requiring an external applied electric field of about 20 kV cm^{-1}.[54] Pulse length and number must also be set within critical parameters, with minimum DC square pulse thresholds as low as 4.5 μs for *E. Coli*. Pulses also have a maximum parameter based on the threshold value for electrolysis of the cell buffer solution. Alternative electroporation lysis methods use a high frequency AC current to give the same effect.[55] Cell lysis by PEF is well suited for microfluidics applications, and has been used with increasing frequency in μTAS.[55–59] The elimination of the high voltage generator required in macroscale electroporation is one of the main advantages of microfluidic applications of this lysis technique, as on-chip systems typically require only ~500 V to generate the equivalent electric field, due to the decreased distance between the electrodes. Applications typically differ in the geometry of the electrode configuration and the upstream or downstream components of the chip. One method used checkerboard or square-wall patterns of 25 platinum electrodes on a silicon chip to separate *E. Coli* from blood by dielectrophoresis before lysis. Dielectrophoresis was accomplished by using a 10 V, 10 kHz AC current, while lysis was performed by a series of 400–500 V, 50 μs pulses with polarity alternated every 20 pulses. This lysis method allowed downstream analysis of RNA, plasmid DNA and genomic DNA by hybridization assay, showing great utility as a μTAS device.[56] Another approach used poly(tetrafluoroethylene) (PTFE)-coated saw-tooth electrodes for lysis to minimize the distance between the electrodes and electrode damage during hydrolysis of the cell medium. Using this electrode geometry, cell lysis was achieved for plant protoplasts, yeast protoplasts and *E. Coli* when a DC square pulse of only 3.5–20 V was used. A 1–2 MHz AC current was also attempted, but cell lysis was only observed in plant protoplasts. This reduced voltage lysis system can be more easily integrated in microfluidic systems with electrical power limitations.[55] Later groups with chips based on a similar saw-tooth geometry were able to lyse mammalian cells with 74% efficiency using 8.5 V at 10 kHz AC current.[57] Other groups have further altered the electrode geometry to increase lysis efficiency. Lu *et al.* have similarly developed an electroporation chip for cell lysis depicted in Fig. 1(B).[58] The main difference in this system is that the electrodes in the device are three-dimensional cylinders, which provides more volume in which the electric field affects the cell membrane. One study established an electric field by inserting platinum wires in PDMS microfluidic reservoirs connected by a channel which narrows an order of magnitude in width to intensify the electric field and lyse the cells. The most effective geometry required 500 V to induce the needed electric field, and resulted in essentially 100% *E. Coli* lysis at that voltage.[59] Other methods use incubation with lytic enzymes to insure effective lysis.[60] Recently, an increasing amount of focus has turned to the use of electrical lysis for single-cell analysis as a high-throughput improvement on capillary electrophoresis.[61–64] Single cell assays are typically time sensitive, and electrical lysis is used due to the rapidity of single cell lysis

Table 1 Design considerations for a cell lysis component

Method	Fabrication techniques	Required controls	Lysis time	Comments/considerations
Chemical	Laser cut laminates, soft lithography (with SU8)	Flow control, temperature controls, valves	30–190 s	Reagent costs can be considerable. Chemistry needs to be modified for different cell types.
Electrical	Lithography, electrode deposition, glass bonding, electroplating, soft lithography	Voltage/current control	< 50 ms–20 min	Lower electric fields cause electroporation rather than lysis. Easily used with electrophoresis. Time for lysis depends on field strength.
Mechanical	DRIE, microfabrication, soft lithography	Flow control, Optical controls (laser), servo motors, pneumatic controls, ultrasonics	30 s–10 min	Good adaptability to different cell types. More involved fabrication and device operation.
Thermal	Microfabrication	Temperature controls, flow controls	2–5 min	Lysis can be sped up by increasing the pressure to prevent boiling at higher temperatures.

(<33 ms). An alternative form of electrical lysis involves using DC voltage to electrochemically lyse cells by generating hydroxide which cleaves the fatty acid groups and permanently breaks open the cells.[65,66] Electrical lysis systems will be increasingly used in microfluidic devices, as a reagent-free, faster and less expensive alternative to chemical treatment.

Comparison of lysis techniques. Table 1 summarizes some of the design considerations that are important for a cell lysis component and shows how the different techniques compare with one another. The table gives an overview of the four major lysis categories described above with the understanding that there could be specific devices or applications within those categories that do not agree with the generalized statement applied to the group as a whole. Knowing the typical fabrication techniques to create a cell lysis device will help understand what capabilities are required for manufacturing and how easily it could be produced in conjunction with later chip components. Information on the required controls will aid in determining if the device will work in the desired application environment. The lysis time is included in the table to help construct a picture of the time required for the system to operate. Finally, additional comments for consideration are included that might be specific to that cell lysis technique. The type of cell lysis component can be chosen depending on what constraints are imposed by the microfluidic system. For example, if a system is being designed to be highly portable, it might be important to choose a cell lysis component that doesn't require excessive external controls, so a chemical system might be a good choice. All four types of lysis components have proven to be effective for their applications and have helped to propel the industry towards complete lab-on-a-chip devices.

Microfluidic DNA extraction. Once cells or samples have been lysed, or the nucleic acid is freed from the sample, many microfluidic sensing systems require the nucleic acid to be purified or concentrated before delivery to the sensor. Thus, a number of nucleic acid extraction techniques have been developed as a component of μTAS systems. Microfluidic nucleic acid extraction techniques can be categorized in terms of the basic mechanism that gives rise to the nucleic acid separation: silica-based surface affinity, electrostatic interaction, nanoporous membrane filtration, and functionalized microparticles.

Silica-based surface affinity. Micro-solid phase extraction (μSPE) is the typical method used to prepare DNA samples for genetic analysis within microchips[68] as shown in Fig. 2(A). Nucleic acid is able to bind with silica or glass fibers in high ionic strength solutions due to decreases in the electrostatic repulsion. After washing with a non-polar solvent, DNA is eluted with a low ionic strength buffer. These procedures are well-known and commonly used in commercial nucleic acid extraction kits. In the first trials applying SPE in a micro-device, silica beads were held in a polyethylene sleeve with two glass fiber frits, and a silica capillary was connected to serve as the inlet and outlet of this device. A microdevice containing only a nanogram of silica resin has been shown to be effective for the adsorption and desorption of DNA in a chaotropic salt solution. In this system, all silica particles showed a high binding capacity and ~70% yield rate from white blood cell (WBC) lysates.[69] Using the same geometry, researchers immobilized silica beads, a sol–gel matrix and hybrid sol–gel/silica bead matrices within microchannels to find the maximum extraction efficiency and the simplest fabrication method. Comparing the extraction efficiency of the three different immobilization techniques, hybrid sol–gel/silica bead matrices were found to be the most effective, showing ~90% extraction efficiency from the λ-DNA experiment. In a more detailed study, the optimal loading buffer condition and flow rate were defined. Using these optimized procedures, genomic DNA was extracted from whole blood and bacteria with high yields in less than 15 min.[70,71] However, this hybrid sol–gel matrix exhibits bonding and shrinkage problems between the microchannel wall and the matrix. Due to these problems, the surface area, which is critical in the binding process with DNA, decreased and the purity of the eluted DNA sample also decreased. To compensate for these problems, tetramethylorthosilicate (TMOS)-based sol–gel matrices with micro-pores were developed and used to extract the DNA. The extraction efficiency of this system was about ~70% for genomic DNA from human blood. To show possible usage for clinical analysis, DNA and viral DNA were extracted from *B. anthracis* bacteria and human cerebral spinal fluid (CSF), respectively, and amplified without any inhibition.[72] Furthermore, a photo-polymerized silica-based column was fabricated with the sol–gel solution consisting of a monomer solution of trimethoxysilylpropyl methacrylate (TMSPM) and photo-initiator. A TMSPM-treated capillary was filled with

This journal is © The Royal Society of Chemistry 2009

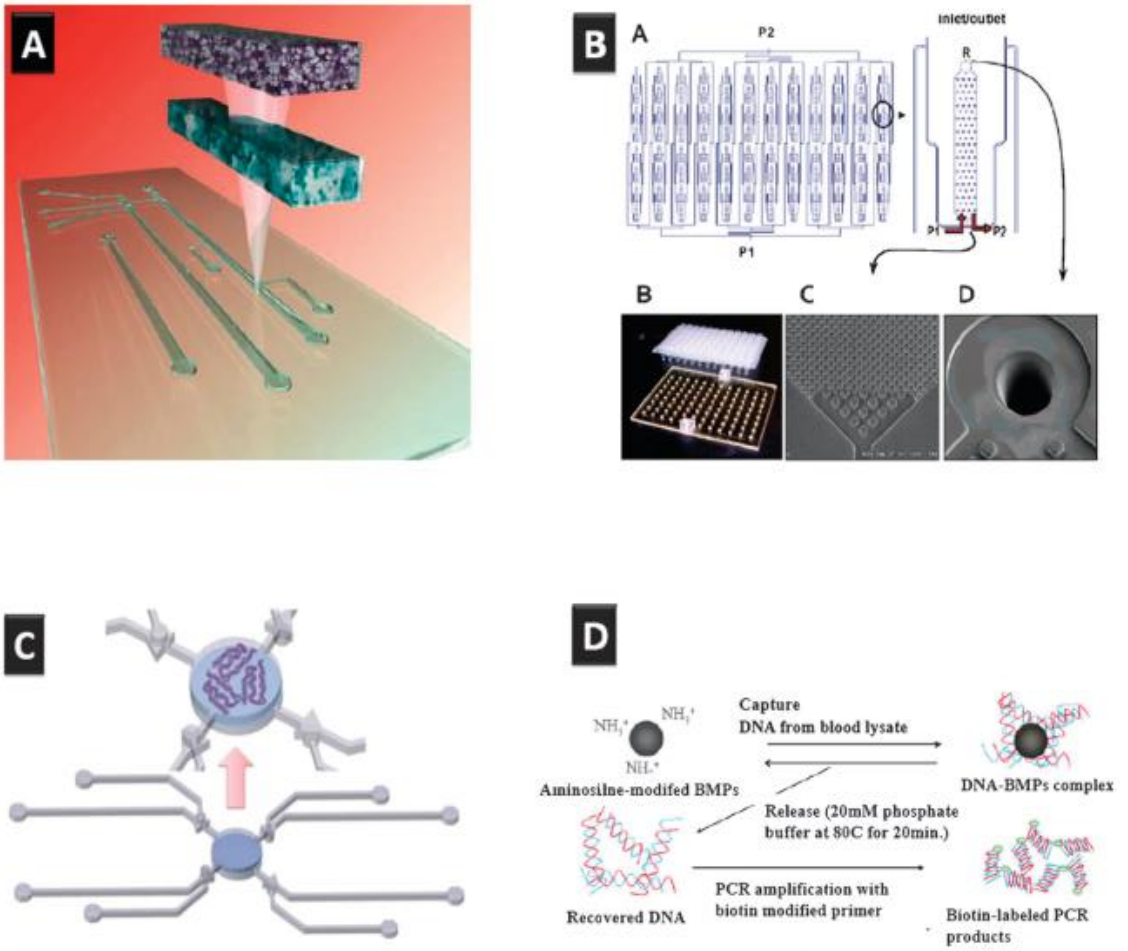

Fig. 2 Nucleic acid purification techniques. (A) Schematic of a nucleic acid purification microfluidic device including a magnified view of a silica-affinity binding column with its location on the chip indicated.[68] (B) Schematic of a 96-well PPC-SPRI microfluidic plate with nucleic acid immobilization beds fabricated with a LIGA process. The inserts show how the fabricated device looks with a commercial 96-well plate, and SEM micrographs of the inlet and outlet of the immobilization beds. The beds were photoactivated to make nucleic acids bind under the appropriate immobilization buffer.[87] (C) Schematic of a device for integration of a microfluidic system with a nanoporous membrane for nucleic acid immobilization and purification. The large circle at the center contains the aluminium oxide filter that traps the nucleic acid (indicated in the magnified inset above).[90] (D) Schematic of how magnetic microparticles functionalized with aminosilane are used to capture and release nucleic acid from blood samples.[95]

the sol–gel solution and then exposed to UV light on a specific part of the microdevice, leaving the TMPSPM material only in the area exposed to UV. To increase the extraction efficiency, the porous surface of the column was derivatized by 85% v/v TMOS. The extraction efficiency was about 85.6% when using purified genomic DNA, but using the same sample mixed with blood significantly decreased the DNA binding capacity and extraction efficiency to 59.9%.[73] To remove the protein in the sample effectively, a two-stage microfluidic device was developed in the same manner. By combining the DNA extraction column with a C18 (octadecyl) reversed-phase column that has a high affinity for hydrophobic proteins, the TMSPM/TMOS DNA extraction chip showed a high protein removal rate and DNA extraction efficiency.[74] Using a simpler SPE concept, Christel *et al.* reported the first purification of DNA using a microfabricated silicon chip. To increase the surface area for adsorption, a pillar-like structure was fabricated in a silicon microchip using reactive ion etching (RIE).[75] Using similar concepts, Cady *et al.* microfabricated microchannels in which silica-coated pillars were etched to increase the surface area within the channel by 300–600% when the etch depth is varied from 20 to 50 μm. DNA was selectively bound to these pillars in the presence of a chaotropic salt, followed by washing with ethanol and elution with low-ionic strength buffer.[76,77] With microfabricated silica structures on the wafer, the microfluidic device is able to make the extraction process simple and consistent. Recently, an integrated microsystem simultaneously implementing cell sorting, cell lysis and DNA purification steps was fabricated using surface micromachining and tested with a blood sample. For the DNA extraction step,

a porous silicon matrix was fabricated by an anodizing technique, followed by thermal oxidization to form silanol groups on the surface. These anodizing and functionalizing steps increased the silanol density, which provided an increase in adsorption sites for the nucleic acids.[78] A separate integrated silicon chip was developed and demonstrated extraction of human genomic DNA from a blood sample. The silicon chip consisted of a microfilter, micromixer, microvalve and microbinder to implement a sample preparation procedure from cell sorting to DNA extraction. For the microbinder component, thermal silicon dioxide was grown and then treated by O_2 + CHF_3 plasma in a plasma etching chamber. Using this chip, about 10 ng of gDNA was extracted from 1 μL of human blood.[79] Some of the critical research in SPE is to find the optimal chaotropic salt, pH and elution profile for nucleic acids. Among four different salts, GTC has promoted the highest adsorption on the silica surface. Usually, under low pH solution, nucleic acids have more affinity with silica surfaces, but at pH 6.0 and 8.0, adsorption isotherms showed nearly the same affinity. Based on the elution profile, about 50% of the adsorbed nucleic acid was collected in the first 5 μl of the elution buffer. These optimization data allow us to improve the effectiveness of nucleic acid extraction of microfluidic SPE systems.[80] Extending SPE research, researchers have developed an automated, parallel microfluidic DNA purification system with 26 access holes and 54 valves and validated it with a small number of bacteria cells (<28 bacteria cells).[81] By integrating a mechanical/chemical cell lysis system, genomic DNA was purified from gram positive and gram negative bacteria using microscale silica bead/polymer composites.[82] A more user friendly microfluidic cell lysis and DNA extraction system is introduced by Kim *et al*., including a modular microfluidic system with separate functional and flow control modules. In this system, the silica bead/glass-fiber-membrane hybrid module was connected to a microfluidic platform to control the sample flow. This microfluidic system can be used for multiple tests by replacing the silica module once the sample preparation test is done.[83] Furthermore, a fully integrated microfluidic genetic analysis system that included PCR and an electrophoretic detection system was shown and used to find the presence of infectious pathogens.[84] From these examples, it can be observed that the SPE methods have great flexibility and integrability for μTAS. The main challenge for SPE involves the difficulty in fabricating the device or immobilizing the silica structures inside the channels of a microfluidic device.

Electrostatic interactions for nucleic acid extraction. A variety of nucleic acid extraction techniques based on electrostatic interactions between DNA and modified surfaces have been demonstrated. The most basic rely on an amine surface coating. Amine groups below neutral pH have a positive charge (causing negatively charged DNA to bind), which decreases above neutral pH. However, this method can affect the DNA amplification step due to the high pH required for elution.[85] To overcome this pH problem associated with typical electrostatic methods, a chitosan surface coating was used to extract DNA from whole blood. Chitosan has a cationic charge at pH 5 and is easily neutralized at pH 9. High density microfluidic channels coated with chitosan were fabricated and tested with lysed whole blood samples. DNA was captured at pH 5.0 through electrostatic interactions with the chitosan and eluted using pH 9.1 Tris buffer. The recovery rate was found to be 68% for human genomic DNA.[86] PCR was demonstrated with the eluted DNA. Using a polymerization reaction under ultraviolet (UV) light, one can create a polycarbonate (PC) surface with positively charged carbonyl/carboxyl functional groups. A PC microfluidic chip fabricated using this technique with 20 μm diameter posts was developed and fabricated using a hot-embossing technique and the surface was activated by UV radiation to implement solid-phase reversible immobilization (SPRI). With the binding buffer consisting of 3% polyethylene glycol (PEG), 0.4 M NaCl and 70% ethanol, about 85% of gDNA was extracted from a lysed *E coli* sample within 25 min. As an extension of this research, a high-throughput nucleic acid extraction system was achieved by a 96-well PC-SPRI microfluidic bed as shown in Fig. 2(B). The loading capacity of nucleic acid from *E. coli* samples was 206 ng for gDNA and 165 ng for total RNA. The extraction efficiency was 63% for gDNA and 73% for total RNA. PCR and reverse transcript PCR (RT-PCR) were successfully performed without any inhibition.[87] Although the extraction system has proven adequate, the flow control system will need to be automated to make this a true high-throughput extraction system.

Nanoporous membrane filtration. A combination of sieving and electrostatic interactions to improve DNA yield has also proven useful. For example, a microfluidic DNA extraction system with a nanoporous membrane was proposed and tested with λ-DNA.[88,89] Elgort *et al*. demonstrated the use of nanoporous aluminium oxide membrane (AOM)-based purification of genomic DNA (gDNA) from human blood in which blood is lysed and gDNA is localized to the AOM surface by filtration and possible surface interactions. Lysis was performed using 1 μL of human whole blood that had been drawn into tubes containing dipotassium EDTA, sodium citrate, or sodium heparin as an anticoagulant for 1 min at room temperature in a 100 μL final volume of 200 mmol L^{-1} NaCl, 10 mL L^{-1} Triton X-100 and 2.5 mg mL^{-1} Proteinase K (50 U/mg; Sigma). The lysates were then filtered through an AOM disc mounted on a specialized filtration tube.[88] Based on this concept, Kim *et al*. were able to integrate the nanoporous AOM with microfluidic channels to extract the DNA depicted in Fig. 2(C). To understand the physical and chemical mechanisms of the AOM, different lysis and elution buffers were tested. Under high-salt conditions, the gDNA collection rate increased due to strengthened interactions between DNA, the surface and the aggregation of the gDNA itself. During elution, higher pH and anionic solutions had higher extraction efficiencies. Smaller nanopores were also found to increase the extraction efficiency with pure DNA samples, but mid-sized pores (100 nm) were found to be better when used with more realistic samples.[90] To enable high-throughput extraction, the membrane was patterned with SU-8 and integrated with PDMS microfluidic structures.[91]

This journal is © The Royal Society of Chemistry 2009

Functionalized microparticles/magnetic beads. Microparticles with DNA adsorbent surfaces have also been used in a variety of ways for DNA extraction. Magnetic particles coated with silica or functionalized carboxyl groups have been used to extract DNA from biological samples.[92–94] Magnetic beads with amine groups on the surface have been used to increase the DNA binding affinity as demonstrated in Fig. 2(D).[95] The lure of magnetic beads is that they can be used free floating in solution and then collected in one location using a magnetic field. In some cases, they can be used to eliminate the washing steps common with SPE extraction. A drawback to using magnetic particles in microfluidic systems is that appropriate micro-manipulating systems need to be implemented to control the magnetic field. In one case, a microfabricated magnetic device consisting of an embedded micro-coil structure was designed and fabricated using simple metal deposition. In comparison, a two-spiral micro-coil system was more effective at trapping beads and could move beads over 350 μm in the vertical direction and 500 μm in the radial direction. Also, the trapping efficiency of this system was about 84% with a 20 μl min^{-1} flow rate.[96] By adopting microfluidic technologies with functionalized magnetic beads, cells found in saliva were lysed and the DNA was purified within a single system designed to detect genetic disease. Silica coated magnetic beads were mixed with saliva samples and lysis buffer, and then a high salt buffer was flowed into the same chamber to perform affinity binding with the DNA. This system allowed cell lysis and DNA extraction within 10 min and was able to generate a high yield and good purification of DNA samples in an automated fashion.[97] Magnetic particles coated with sequence-specific probes were used to extract *E. Coli* genomic DNA in a microreactor integrated with a microheater and a temperature sensor. The denatured genomic DNA hybridized with a biotinylated DNA probe on the particle and then the hybridized gDNA was separated from the remainder of the cellular components by a wash step. The captured gDNA was released by heating the microreactor without a specific elution buffer.[98] Using this technique, one can extract species-specific DNA, but a few extra steps are required to functionalize the magnetic particles and more time is needed to effectively hybridize the target and the probe. In a similar concept, a totally integrated pathogen DNA sample preparation system was developed using a microfluidic compact disk (CD) platform. Cell lysis was accomplished rapidly using a laser system without any lysis buffer and gDNA extracted using biotinylated magnetic beads. The extraction efficiency produced results similar to that obtained with commercial DNA preparation kits.[38]

Comparison of nucleic acid extraction techniques. Table 2 provides a summary of some of the advantages and disadvantages of the different nucleic acid extraction techniques. The fabrication difficulty summarizes the relative level of facility requirements for chip fabrication. The extraction efficiency indicates what percent of input nucleic acid has been demonstrated to be extracted using that method. Integration difficulty compares the ability of each extraction technique to be connected with other microfluidic components such as lysis or analysis systems. Each of the different techniques has some clear advantages over the others, so the specific application of any given technique will depend on the application of interest. For example, some of the methods are more amenable to disposable components (physical filtration, magnetic beads), while others require expensive fabrication processes that limit disposability (microfabricated columns, magnetic particle control), but may be more useful for repeated use, or may be more easily integrated and have a smaller footprint. In any case, there is no method clearly superior to the others, possibly because they all rely on the same basic physics, so they will all likely find continued use in the future.

Microfluidic RNA extraction. As shown so far, nearly all microfluidic extraction systems are designed for DNA sample preparation. RNA sample preparation systems are relatively rare in the literature due to issues surrounding the stability (RNA typically has a half-life measured in minutes) and complexity (multiple types of RNA are found in cells) of RNA extraction, even though most DNA extraction methods will also bind RNA. While DNA is better known and more commonly used in biological assays, RNA has multiple advantages over DNA in some applications as a biological target material since it is more closely related to the proteins that are the cells' machinery. RNA is also important in identifying genetic diseases, measuring gene expression, and monitoring pathogenic diseases. Unfortunately, RNA sample preparation is a more complicated process due to challenges associated with contamination and degradation by ubiquitous RNase enzymes. Nevertheless, RNA extraction will become increasingly important in microfluidic systems, especially since microfluidic methods provide some key techniques to solving these RNA extraction challenges. Typically, approaches to RNA sample preparation can be categorized by the cell type from which the RNA is being extracted since protocols vary for eukaryotic and prokaryotic cells. For applications exploring the mRNA of eukaryotic cells that have a poly-A tail, paramagnetic beads coated with oligo-dT's have been used for capturing mRNA. For example, a simple Y-shaped microfluidic channel fabricated with a glass etching technique and then integrated with magnets was built to capture the beads. The capture efficiency of off-chip and on-chip extraction was low, but the amount of mRNA was enough for cDNA (complementary DNA) library construction using RT-PCR.[99,100]

Table 2 Comparison of nucleic acid techniques

Technique	Fabrication difficulty	Extraction efficiency	Assay speed	Integration difficulty
Basic SPE silica bead/sol–gel chamber	Medium	~90%	15 min	Low
Electrostatic effect	Medium	60–80%	25 min	Low
Physical filtration	Low	~90%	<10 min	Medium
Magnetic particles	High	~84%	10 min	High

Another application of probe-coated magnetic particles is to detect viral RNA. Magnetic beads were modified with streptavidin and biotinylated capture probes conjugated to the bead surface. In this approach, a liposome that had a reporter probe was added to hybridize with the captured probe. The bead is passed through the magnet embedded microfluidic channel and captured on the microfluidic surface. After washing unbound material away, the liposome is lysed to release the fluorescence molecules, providing signal amplification. This RNA capture technique was used for the rapid detection and identification of Dengue virus serotypes.[101] The challenge, though, is that magnetic bead methods need extra steps, materials and systems before they can be used in a μTAS system. To make a more practical extraction system, a microfluidic system was packed with a UV-initiated methacrylate-based porous polymer monolith (PPM) to purify mRNA from eukaryotic cells. A PPM provides a large surface area, good adhesion, and stability within a microfluidic channel. In addition, the surface of a PPM is easy to modify with various functional groups. To extract mRNA from eukaryotic cells, the surface of the PPM was functionalized with 20-mer oligo-dT's to interact with the poly-A tail found on mRNA. The extraction efficiency was about 70% and the results for yield, capacity and purity of the extracted sample were equivalent to that of commercial kits.[102] Unfortunately, these techniques are limited to cells that have the poly-A sequence on their mRNA and thus cannot be used with prokaryotes or for rRNA, increasing the usage for RT-PCR for pathogen detection. To extract both RNA and DNA on a single chip, and without relying on the poly-A tail, Witek *et al.* used a photoactivated polycarbonate solid-phase reversible immobilization (PPC-SPRI), as noted previously when discussing DNA extraction. The 96-well microfluidic plate and immobilization beds were fabricated with a LIGA process and the beds were photoactivated to make nucleic acids bind under the appropriate immobilization buffer. This high-throughput system showed 63% DNA and 73% total RNA recovery rates without any inhibition of PCR or RT-PCR.[87] The major drawback of this approach is the relatively expensive and challenging LIGA process that is needed, and the system still must be integrated with microfluidic control components. Using a high-throughput genome-wide transcriptome analysis, a multi-step microfluidic RNA purification system was built by packing silica beads into a microfluidic channel. To increase the recovery ratio and purity of RNA samples, three silica bead columns that optimized the size of silica beads and column pre-treatment were integrated with the microfluidic system. The RNA yield rate showed consistent increments as the number of cells increased from 50 to 1000, and the total time for processing was about 50 min.[103] Commercially available RNA prep kits usually use silica membrane tubes as the RNA binding substrate and require the centrifugation of the tube with 4–5 different reagents. This method has a high RNA recovery rate and uses relatively inexpensive materials. Using a silica membrane in a microfluidic RNA extraction chip, Micronics extracted RNA from human blood at levels comparable with RNeasy (Qiagen) and MagnaPure(Roche) kits,[104] but more research is needed to understand and implement this technique in a μTAS.

Perspective

The goal for the microfluidics community for the last decade or more has been to generate fully integrated systems that can complete an assay from sample-in to answer-out. There have been surprisingly few "complete" lab-on-a-chip systems in recent years that can deal with raw samples, and that is primarily because of the lack of development in sample preparation systems. The primary challenge with many of these systems is complexity. The nucleic acid extraction systems are sufficiently complex without adding the complexity of the analysis systems. Also, the manufacturing techniques for the extraction, lysis, and analysis components are not always compatible, so substantial design and manufacturing work has to be completed to make these components integratable. Since this is beginning to approach a development effort, as a variety of lysis and extraction components are now available, these efforts will likely fall to industry to fully flesh out and to make a true lab-on-a-chip. But as noted in this work, there are a few systems that have combined both lysis and extraction, and then linked the results to a microfabricated analysis system of one kind or another.[84] Thus, it can be done, though there is still substantial research to be completed on methods of integration, and the optimization of these systems. Also, genetic analysis typically involves a wide range of samples, so developing a sample preparation system that handles all of these different potential samples may be impossible, but a system that handles a wide range of samples equally well (bacteria, viruses, tissue, body fluids, low concentration solutions, *etc.*) would be extremely valuable. Also, many of the sample preparation techniques in the literature are quite complex, requiring multiple chemistry or processing steps, so a reduction in complexity is clearly a priority to maximize effectiveness and reliability. Even with these challenges, the number of complete nucleic acid analysis systems is expected to increase rapidly, and there are more fully integrated systems coming out each year. DNA analysis systems are clearly well ahead of systems focused on RNA, though RNA based devices may be available shortly.[87] Nevertheless, implementing RNA analysis in a fully integrated system has proven challenging. For example, in a recent state-of-the-art paper, RNA extraction was performed in one location and then the analysis was performed in another location thousands of kilometers away. Clearly, additional expertise and technology must be developed before true nucleic acid based lab-on-a-chip systems are routinely generated and become commercially viable.

As genetic material is common to nearly all organisms, genetic analysis is the most promising approach for identifying organisms or mutations in nearly every biological field. Thus, huge advances in understanding the basics of biology and population genetics will likely be enabled by rapid advances in small and highly parallel nucleic acid preparation technologies. As these technologies advance to allow full integration of cell lysis, nucleic acid extraction and analysis steps, access to nucleic acid testing will widen in clinics and labs, but also into areas not yet fully appreciated. For example, handheld or simple benchtop devices will lead to field measurements, which could be a great benefit in poor areas of the world where disease tracking is difficult. Environmental monitoring of

This journal is © The Royal Society of Chemistry 2009

infectious agents will also become a reality shortly, leading to early warning of contaminated water supplies or the presence of biowarfare agents. Small devices may also find their way into the home, where simple self diagnosis of certain diseases such as colds and flu could be performed, with the data sent to a doctor and researchers to track and verify the results and treatment. Small, efficient bedside nucleic acid analysis systems would make it easier for doctors in the clinic to rapidly determine the particular genetic makeup of an individual or an infectious disease organism, allowing rapid, effective therapies to be introduced more quickly, assuming the biology related to the genetic sequence is known. Even if the data is not collected at the bedside, hospital labs using high throughput genetic analyzers that both prepare and process samples, could become more regular users of genetic assays without requiring that samples be sent to distance reference labs. Such widespread genetic data collection could help researchers track infectious disease more readily, assuming appropriate assays were available. These developments will enable a more focused examination of individual biomolecules as well as a broadened picture of their effect on biological systems, both individual and communal, as genetic phenomena are more fully detected and mapped out.

Acknowledgements

The authors acknowledge financial support to complete this work from Early Warning, LLC and the University of Utah.

References

1 J. Zhang, H. P. Lang, F. Huber, A. Bietsch, W. Grange, U. Certa, R. McKendry, H. J. Guntgerodt, M. Hegner and C. Gerber, *Nat. Nanotechnol.*, 2006, **1**, 214–220.
2 P. Englebienne, A. V. Hoonacker and M. Verhas, *Spectroscopy*, 2003, **17**, 255–273.
3 B. Nguyen, F. A. Taniousa and W. D. Wilson, *Methods*, 2007, **42**, 150–161.
4 C. Ziegler, *Anal. Bioanal. Chem.*, 2004, **379**, 946–959.
5 J. Kong, N. R. Franklin, C. W. Zhou, M. G. Chapline, S. Peng, K. J. Cho and H. J. Dai, *Science*, 2000, **287**, 622–625.
6 C. Dekker, *Nat. Nanotechnol.*, 2007, **2**, 209–215.
7 S. L. Biswal, D. Raorane, A. Chaiken, H. Birecki and A. Majumdar, *Anal. Chem.*, 2006, **78**, 7104–7109.
8 J. Fritz, M. K. Baller, H. P. Lang, H. Rothuizen, P. Vettiger, E. Meyer, H. J. Guntherodt, C. Gerber and J. K. Gimzewski, *Science*, 2000, **288**, 316–318.
9 A. K. Gupta, P. R. Nair, D. Akin, M. R. Ladisch, S. Broyles, M. A. Alam and R. Bashir, *Proc. Natl. Acad. Sci. U. S. A.*, 2006, **103**, 13362–13367.
10 Y. L. Bunimovich, Y. S. Shin, W. S. Yeo, M. Amori, G. Kwong and J. R. Heath, *J. Am. Chem. Soc.*, 2006, **128**, 16323–16331.
11 F. Patolsky, G. Zheng, O. Hayden, M. Lakadamyali, X. Zhuang and C. M. Lieber, *Proc. Natl. Acad. Sci. U. S. A.*, 2004, **101**, 14017–14022.
12 W. U. Wang, C. Chen, K. H. Lin, Y. Fang and C. M. Lieber, *Proc. Natl. Acad. Sci. U. S. A.*, 2005, **102**, 3208–3212.
13 G. Zheng, F. Patolsky, Y. Cui, W. U. Wang and C. M. Lieber, *Nat. Biotechnol.*, 2005, **23**, 1294–1301.
14 E. Stern, J. F. Klemic, D. A. Routenberg, P. N. Wyrembak, D. B. Turner-Evans, A. D. Hamilton, D. A. LaVan, T. M. Fahmy and M. A. Reed, *Nature*, 2007, **445**, 519–522.
15 Y. Huang, E. L. Mather, J. L. Bell and M. Madou, *Anal. Bioanal. Chem.*, 2002, **372**, 49–65.
16 A. J. de Mello and N. Beard, *Lab Chip*, 2003, **3**, 11N–19N.
17 J. Pawliszyn, *Anal. Chem.*, 2003, **75**, 2543–2558.
18 D. D. Carlo, K.-H. Jeong and L. P. Lee, *Lab Chip*, 2003, **3**, 287–291.
19 H. Takamatsu, R. Takeya, S. Naito and H. Sumimoto, *J. Biomech.*, 2005, **38**, 117–124.
20 Y. C. Kim, J. H. Kang, S.-J. Park, E.-S. Yoon and J.-K. Park, *Sens. Actuators, B*, 2007, **128**, 108–116.
21 J. Kim, S. H. J. Jang, G. Jia, J. V. Zoval, N. A. Da Silva and M. J. Madou, *Lab Chip*, 2004, **4**, 516–522.
22 H. Kido, M. Micic, D. Smith, J. Zoval, J. Norton and M. Madou, *Colloids Surf., B*, 2007, **58**, 44–51.
23 T. C. Marentis, B. Kusler, G. G. Yaralioglu, S. Liu, E. O. Haeggstrom and B. T. Khuri-Yakub, *Ultrasound Med. Biol.*, 2005, **31**, 1265–1277.
24 A. A. Brayman, Y. Doida and M. W. Miller, *Ultrasound Med. Biol.*, 1992, **18**, 701–714.
25 L. B. Feril, T. Kondo, Q.-L. Zhao, R. Ogawa, K. Tachibana, N. Kudo, S. Fujimoto and S. Nakamura, *Ultrasound Med. Biol.*, 2003, **29**, 331–337.
26 P. Belgrader, D. Hansford, G. T. A. Kovacs, K. Venkateswaran, R. Mariella, F. Milanovich, S. Nasarabadi, M. Okuzumi, F. Pourahmadi and M. A. Northrup, *Anal. Chem.*, 1999, **71**, 4232–4236.
27 C. Ogino, M. F. Dadjour, K. Takaki and N. Shimizu, *Biochem. Eng. J.*, 2006, **32**, 100–105.
28 M. T. Taylor, P. Belgrader, B. J. Furman, F. Pourahmadi, G. T. A. Kovacs and M. A. Northrup, *Anal. Chem.*, 2001, **73**, 492–496.
29 K. R. Rau, P. A. Quinto-Su, A. N. Hellman and V. Venugopalan, *Biophys. J.*, 2006, **91**, 317–329.
30 J. Sambrook and D. W. Russell, *Molecular Cloning: A Laboratory Manual*, Cold Spring Harbor, New York, 2001.
31 J. Vinograd and J. Lebowitz, *J. Gen. Physiol.*, 1966, **49**, 103–125.
32 R. H. Liu, J. Yang, R. Lenigk, J. Bonanno and P. Grodzinski, *Anal. Chem.*, 2004, **76**, 1824–1831.
33 C. Y. Lee, G. B. Lee, L. J. L., H. F. C. and C. S. Liao, *J. Micromech. Microeng.*, 2005, **15**, 1215–1223.
34 S. W. Yeung, T. M. H. Lee, H. Cai and I. M. Hsing, *Nucleic Acids Res.*, 2006, **34**, e118.
35 K. Zhu, H. Jin, Y. Ma, R. Zhihui, C. Xiao, Z. He, F. Zhang, Z. Qinghong and B. Wang, *J. Biotechnol.*, 2005, **118**, 257–264.
36 K. Zhu, H. Jin, Z. He, Q. Zhu and B. Wang, *Nat. Protoc.*, 2007, **1**, 3088–3093.
37 K. h. Cheong, D. K. Yi, J.-G. Lee, J.-M. Park, M. J. Kim, J. B. Edel and C. Ko, *Lab Chip*, 2008, **8**, 810–813.
38 Y. K. Cho, J. G. Lee, J. M. Park, B. S. Lee, Y. Lee and C. Ko, *Lab Chip*, 2007, **7**, 565–573.
39 I. Yust, B. Frisch and N. Goldsher, *Am. J. Hematol.*, 1982, **13**, 53–62.
40 Z. Pang, A. Al-Mahrouki, M. Berezovski and S. N. Krylov, *Electrophoresis*, 2006, **27**, 1489–1494.
41 P. H. von Hippel and K. Y. Wong, *Science*, 1964, **145**, 577–580.
42 R. Boom, C. J. A. Sol, M. M. M. Salimans, C. L. Jansen, P. M. E. Wertheim-van Dillen and J. Van der Noordaa, *J. Clin. Microbiol.*, 1990, **28**, 495–503.
43 J. M. Chirgwin, A. E. Przybyla, R. J. MacDonald and W. J. Rutter, *Biochemistry*, 1979, **18**, 5294–5299.
44 E. Schilling, A. Kamholz and P. Yager, *Anal. Chem.*, 2002, **74**, 1798–1804.
45 P. Sethu, M. Anahtar, L. Moldawer, R. Tompkins and M. Toner, *Anal. Chem.*, 2004, **76**, 6247–6253.
46 J. El-Ali, S. Guadet, A. Gunther, P. K. Sorger and K. F. Jensen, *Anal. Chem.*, 2005, **77**, 3629–3636.
47 J. C. Stachowiak, E. E. Shugard, B. P. Mosier, R. F. Renzi, P. F. Caton, S. M. Ferko, J. L. Van de Vreugle, D. D. Yee, B. L. Haroldsen and V. A. Vandernoot, *Anal. Chem.*, 2007, **79**, 5763–5770.
48 J. Heo, K. J. Thomas, G. H. Seong and R. M. Crooks, *Anal. Chem.*, 2003, **75**, 22–26.
49 D. Irimia, R. G. Tompkins and M. Toner, *Anal. Chem.*, 2004, **76**, 6137–6143.
50 D. C. Chang, B. M. Chassy, J. A. Saunders and A. E. Sowers, *Guide to Electroporation and Electrofusion*, Academic Press, San Diego, CA, 1992.
51 W. A. Hamilton and J. H. Sale, *Biochim. Biophys. Acta*, 1967, **148**, 789–800.

52 W. A. Hamilton and J. H. Sale, *Biochim. Biophys. Acta*, 1967, **148**, 781–788.
53 H. Hülsheger, J. Potel and E. G. Niemann, *Radiat. Environ. Biophys.*, 1983, **22**, 149–162.
54 T. Grahl and H. Markl, *Appl. Microbiol. Biotechnol.*, 1996, **45**, 148–157.
55 S. W. Lee and Y. C. Tai, *Sens. Actuators, A*, 1999, **73**, 74–79.
56 J. Cheng, E. L. Sheldon, L. Wu, A. Uribe, L. O. Gerrue, J. Carrino, M. J. Heller and J. P. O'Connell, *Nat. Biotechnol.*, 1998, **16**, 541–546.
57 H. Lu, M. A. Schmidt and K. F. Jensen, *Lab Chip*, 2005, **5**, 23–29.
58 M. A. McClain, C. T. Culbertson, S. C. Jacobsen, N. L. Allbritton, C. E. Sims and J. M. Ramsey, *Anal. Chem.*, 2003, **75**, 5646–5655.
59 H. Y. Wang, A. K. Bhunia and C. Lu, *Biosens. Bioelectron.*, 2006, **22**, 582–588.
60 C. De la Rosa and K. Kaler, in *Proc. 28th IEEE EMBS Annu. Int. Conf.*, New York City, USA, 2006, pp. 4096–4099.
61 J. Gao, X. F. Yin and Z. L. Fang, *Lab Chip*, 2004, **4**, 47–52.
62 F. Han, Y. Wang, C. E. Sims, M. Bachman, R. Chang, G. P. Li and N. L. Allbritton, *Anal. Chem.*, 2003, **75**, 3688–3696.
63 M. Khine, A. Lau, C. Lonescu-Zanetti, J. Seo and L. P. Lee, *Lab Chip*, 2005, **5**, 38–43.
64 N. R. Munce, J. Li, P. R. Herman and L. Lilge, *Anal. Chem.*, 2004, **76**, 4983–4988.
65 D. Di Carlo, C. Ionescu-Zanetti, Y. Zhang, P. Hung and L. P. Lee, *Lab Chip*, 2005, **5**, 171–178.
66 J. T. Nevill, R. Cooper, M. Dueck, D. N. Breslauer and L. P. Lee, *Lab Chip*, 2007, **7**, 1689–1695.
67 K.-Y. Lu, A. M. Wo, Y.-J. Lo and K.-C. Chen, *Biosens. Bioelectron.*, 2006, **22**, 568–574.
68 J. Wen, L. A. Legendre, J. M. Bienvenue and J. P. Landers, *Anal. Chem.*, 2008, **80**, 6472–6479.
69 H. Tian, A. F. R. .Huhmer and J. P. Landers, *Anal. Biochem.*, 2000, **283**, 175–191.
70 M. C. Breadmore, K. A. Wolfe, I. G. Arcibal, W. K. Leung, D. Dickson, B. C. Giordano, M. E. Power, J. P. Ferrance, S. H. Feldman, P. M. Norris and J. P. Landers, *Anal. Chem.*, 2003, **75**, 1880–1886.
71 K. A. Wolfe, M. C. Breadmore, J. P. Ferance, M. E. Power, J. F. Conroy, P. M. Norris and J. P. Landers, *Electrophoresis*, 2002, **23**, 727–733.
72 Q. Wu, J. M. Bienvenue, B. J. Hassan, Y. C. Kwok, B. C. Giordano, P. M. Norris, J. P. Landers and J. P. Ferrance, *Anal. Chem.*, 2006, **78**, 5704–5710.
73 J. Wen, C. Guillo, J. P. Ferrance and J. P. Landers, *Anal. Chem.*, 2006, **78**, 1673–1681.
74 J. Wen, C. Guillo, J. P. Ferrance and J. P. Landers, *Anal. Chem.*, 2007, **79**, 6135–6142.
75 L. A. Christel, K. Petersen, W. McMillan and M. A. Northrup, *J. Biomech. Eng.*, 1999, **121**, 22–27.
76 N. C. Cady, S. Stelick and C. A. Batt, *Biosens. Bioelectron.*, 2003, **19**, 59–66.
77 N. C. Cady, S. Stelick, M. V. Kunnavakkam and C. A. Batt, *Sens. Actuators, B*, 2005, **107**, 332–341.
78 X. Chen, D. Cui, C. Liu, H. Li and J. Chen, *Anal. Chim. Acta*, 2007, **584**, 237–243.
79 H. M. Ji, V. Samper, Y. Chen, W. C. Hui, H. J. Lye, F. B. Mustafa, A. C. Lee, L. Cong, C. K. Heng and T. M. Lim, *Sens. Actuators A: Physical*, 2007, **139**, 139–144.
80 T. Poeckh, S. Lopez, A. O. Fuller, M. J. Solomon and R. G. Larson, *Anal. Biochem.*, 2008, **373**, 253–262.
81 J. W. Hong, V. Studer, G. Hang, W. F. Anderson and S. R. Quake, *Nat. Biotechnol.*, 2004, **22**, 435–439.
82 M. Mahalanabis, H. Al-Muayad, M. D. Kulinski, D. Altman and C. M. Klapperich, *Lab Chip*, 2009, DOI: 10.1039/b905065p.
83 J. Kim, M. Johnson, P. Hill, R. Sonkul, J. Kim and B. K. Gale, in *5th Conf. Microtechnol. Med. Biol. (MMB)*, Quebec, Canada, 2009.
84 C. J. Easley, J. M. Karlinsey, J. M. Bienvenue, L. A. Legendre, M. G. Roper, S. H. Feldman, M. A. Hughes, E. L. Hewlett, T. J. Merkel, J. P. Ferrance and J. P. Landers, *Proc. Natl. Acad. Sci. U. S. A.*, 2006, **103**, 19272–19277.
85 T. Nakagawa, R. Hashimoto, K. Maruyama, T. Tanaka, H. Takeyama and T. Matsunaga, *Biotechnol. Bioeng.*, 2006, **94**, 864–868.
86 W. Cao, C. J. Easley, J. P. Ferrance and J. P. Landers, *Anal. Chem.*, 2006, **78**, 7222–7228.
87 M. A. Witek, M. L. Hupert, D. S.-W. Park, K. Fears, M. C. Murphy and S. A. Soper, *Anal. Chem.*, 2008, **80**, 3483–3491.
88 M. G. Elgort, M. G. Herrmann, M. Erali, J. D. Durtschi, K. V. Voelkerding and R. E. Smith, *Clin. Chem.*, 2004, **50**, 1817–1819.
89 J. Kim, K. V. Voelkerding and B. K. Gale, in *3rd IEEE-EMBS Spec. Conf. MMB*, Oahu, 2005, pp. 5–7.
90 J. Kim and B. K. Gale, *Lab Chip*, 2008, **8**, 1516–1523.
91 J. Kim, K. V. Voelkerding and B. K. Gale, *J. Micromech. Microeng.*, 2006, **16**, 33–39.
92 T. L. Hawkins, T. O'Connor-Morin, A. Roy and C. Santillan, *Nucleic Acids Res.*, 1994, **22**, 4543–4544.
93 H. H. Kessler, G. Mühlbauer, E. Stelzl, E. Daghofer, B. I. Santner and E. Marth, *Clin. Chem.*, 2001, **47**, 1124–1126.
94 J. Akutsu, Y. Tojo, O. Segawa, K. Obata, M. Okochi, H. Tajima and M. Yohda, *Biotechnol. Bioeng.*, 2004, **86**, 667–671.
95 T. Nakagawa, R. Hashimoto, K. Maruyama, T. Tanaka, H. Takeyama and T. Matsunaga, *Biotechnol. Bioeng.*, 2006, **94**, 864–868.
96 Q. Ramadan, V. Samper, D. Poenar and C. Yu, *Biomed. Microdevices*, 2006, **8**, 151–158.
97 K.-Y. Lien, C.-J. Liu, P.-L. Kuo and G.-B. Lee, *Anal. Chem.*, 2009, **81**, 4502–4509.
98 S. W. Yeung and I. M. Hsing, *Biosens. Bioelectron.*, 2006, **21**, 989–997.
99 G. Jiang and D. J. Harrison, *Analyst*, 2000, **125**, 2176–2179.
100 N. V. Zaytseva, V. N. Goral, R. A. Montagna and A. J. Baeumner, *Lab Chip*, 2005, **5**, 805–811.
101 N. V. Zaytseva, R. A. Montagna and A. J. Baeumner, *Anal. Chem.*, 2005, **77**, 7520–7527.
102 B. C. Satterfield, S. Stern, M. R. Caplan, K. W. Hukari and J. A. West, *Anal. Chem.*, 2007, **79**, 6230–6235.
103 D. Irimia, M. Mindrinos, A. Russom, W. Xiao, J. Wilhelmy, S. Wang, J. D. Heath, N. Kurn, R. G. Tompkins, R. W. Davis and M. Toner, *Integr. Biol.*, 2009, **1**, 99–107.
104 M. Kokoris, M. Nabavi, C. Lancaster, J. Clemmens, P. Maloney, J. Capadanno, J. Gerdes and C. F. Battrell, *Methods*, 2005, **37**, 114–119.

This journal is © The Royal Society of Chemistry 2009

APPENDIX B

PROTOCOLS FOR EXTRACTION OF NUCLEIC ACID USING LABVIEW CONTROLLED INSTRUMENT

Stepwise Control Sequences Used to Perform Nucleic Acid Extraction

Table B.1 Protocol steps for basic extraction of DNA

Step	Description	Solenoid					Time (ms)	Hexcode
1	TE buffer pretreatment of filter	4					003000	80:00:00
2		4	19				006000	80:00:40
3		19	10	11	12		003000	00:E0:40
4		10	11	12	21		030000	00:E0:01
5		21	14				003000	00:02:01
6		14					005000	00:02:00
7	Load buffer pretreatment	1					003000	10:00:00
8		1	16				006000	10:08:00
9		16	10	12			003000	00:A8:00
10		10	12	21			030000	00:A0:01
11		21	14				003000	00:02:01
12		14					005000	00:02:00
13	Sample mixing with load buffer	4					003000	80:00:00
14		4	15				006000	80:04:00
15		15	1				003000	10:04:00
16		15	1	16			007000	10:0C:00
17		15	16	11	7	8	003000	0C:4C:00
18	Mixing	16	22	11	7	8	005000	0C:48:02
19		22	11	7	8		007000	0C:40:02
20		22	7	8			003000	0C:00:02
21		7	8	16			008000	0C:08:00
22		7	8	22			008000	0C:00:02
23		7	8	16			008000	0C:08:00
24		7	8	22			015000	0C:00:02
25	Pass through filter	22	9	8	12		003000	08:90:02
26		9	8	12	21		060000	08:90:01
27	Out to waste	21	14				003000	00:02:01
28		14					010000	00:02:00
29	Wash	2					003000	20:00:00
30		2	16				006000	20:08:00
31		16	10	12			003000	00:A8:00
32		10	12	21			030000	00:A0:01
33	out to waste	21	14				003000	00:02:01
34		14					010000	00:02:00
35	Dry	5	12	14			060000	01:82:00
36	Elution	4					003000	80:00:00
37		4	19				008000	80:00:40
38		19	10	11	6		003000	02:60:40
39		10	11	6	20		030000	02:60:80
40		20	11	12			003000	00:C0:80
41		11	12				015000	00:C0:00
42							003000	00:00:00

Table B.2 Protocol steps for basic extraction of RNA

Step	Description	Solenoid					Time (ms)	Hexcode
1	Mix 50uL of sample with 100uL of BPR (becomes Mix 1)	3					002000	40:00:00
2	draw sample into CH3	3	17				005000	40:00:10
3		17	6	7			002000	06:00:10
4	move to CH4	6	7	15			008000	06:04:00
5		3	15				002000	40:04:00
6		3	17	15			005000	40:04:10
7		17	6	7	15		002000	06:04:10
8		6	7	15			006000	06:04:00
9	Introduce and mix 350uL of B-ME-RLT to MIX 2 (now Mix 3)	15	1				003000	10:04:00
10	draw RLT	15	1	16			010000	10:0C:00
11	prepare to move Lysed sample to CH5	15	16	11	7	8	003000	0C:4C:00
12	Move mixtures to CH5, prepare to move to CH6	11	16	7	8	22	010000	0C:48:02
13		16	7	8	22		003000	0C:08:02
14	move all mixtures to CH6	7	8	22			010000	0C:00:02
15	move to CH5	7	8	16			003000	0C:08:00
16	move all mixtures to CH6	7	8	22			003000	0C:00:02
17	move to CH5	7	8	16			003000	0C:08:00
18	move all mixtures to CH6	7	8	22			003000	0C:00:02
19	move to CH5	7	8	16			003000	0C:08:00
20	move all mixtures to CH6	7	8	22			015000	0C:00:02
21	Introduce and mix 250uL of Ethanol to MIX 3 (now Mix 4)	22	4				002000	80:00:02
22	Draw EtOH to CH4	22	4	15			006000	80:04:02
23		22	15	11			002000	00:44:02
24	send to CH5	22	16	11			007000	00:48:02
25		22	16	7	8		002000	0C:08:02
26	move to CH6	22	7	8			006000	0C:00:02
27	move to CH5	16	7	8			003000	0C:08:00
28	Move to CH6	22	7	8			003000	0C:00:02
29	FWD	7	8	16			003000	0C:08:00
30	BCKWD	7	8	22			003000	0C:00:02
31	FWD	7	8	16			003000	0C:08:00
32	BCKWD	7	8	22			010000	0C:00:02
33	Pass MIX 4 through the silica filter (prepare)	22	9	8	12		001000	08:90:02
34	Pass MIX 4 through the silica filter (prepare)	22	9	8	12		002000	08:90:02
35	FWD	21	9	8	12		020000	08:90:01
36	BCKWD	22	9	8	12		020000	08:90:02
37	FWD	21	9	8	12		045000	08:90:01
38	Send waste to waste bottle…..Ready….	21	14				003000	00:02:01
39	Go!	14					020000	00:02:00
40	drain to waste	14	5	12			008000	01:82:00
41		14	12				003000	00:82:00
42		14					001000	00:02:00
43	Make sure everything is empty (open valves)	8	9	12			003000	08:90:00
44	Open ch 7	8	9	12	21		010000	08:90:01

Table B.2 continued

Step	Description	Solenoid					Time (ms)	Hexcode
45	Send waste to waste bottle…..Ready….	21	14				003000	00:02:01
46	Go!	14					008000	00:02:00
47	drain to waste	14	5	12			008000	01:82:00
48		14	12				003000	00:82:00
49		14					001000	00:02:00
50	Introduce 350uL of rpe buffer and pass thru silica filter	3					003000	40:00:00
51	draw rpe	3	16				010000	40:08:00
52	prepare to move thru filter	16	10	12			002000	00:A8:00
53	GO!	21	10	12			025000	00:A0:01
54	Send waste to waste bottle	21	14				003000	00:02:01
55		14					010000	00:02:00
56	drain to waste	14	5	12			008000	01:82:00
57		14	12				003000	00:82:00
58		14					001000	00:02:00
59	Introduce 350uL of Rpe buffer and pass thru silica filter	3					003000	40:00:00
60	draw Rpe	3	16				010000	40:08:00
61	prepare to move thru filter	16	10	12			003000	00:A8:00
62	GO!	21	10	12			025000	00:A0:01
63	Send waste to waste bottle	21	14				003000	00:02:01
64		14					010000	00:02:00
65	drain to waste	14	5	12			060000	01:82:00
66		14	12				003000	00:82:00
67		14					001000	00:02:00
68	Elution Step	4					3000	80:00:00
69		4	19				8000	80:00:40
70		19	10	11	6		3000	02:60:40
71		10	11	6	20		3000	02:60:80
72		19	10	11	6		3000	02:60:40
73		10	11	6	20		3000	02:60:80
74		19	10	11	6		3000	02:60:40
75		10	11	6	20		3000	02:60:80
76		19	10	11	6		3000	02:60:40
77		10	11	6	20		3000	02:60:80
78		19	10	11	6		3000	02:60:40
79		10	11	6	20		3000	02:60:80
80		19	10	11	6		3000	02:60:40
81		10	11	6	20		6000	02:60:80
82		20	10	11	6	12	4000	02:E0:80
83	output	20	11	12			3000	00:C0:80
84		11	12				6000	00:C0:00
85	end						3000	00:00:00

Table B.3 Protocol steps for extraction of RNA from viral samples

Step	Description	Solenoid					Time (ms)	Hexcode
1	Mix 50uL of sample with 100uL of BPR (becomes Mix 1)	3	6	7			003000	00:00:00
2	draw sample into CH3	3	6	7	15	17	008000	46:00:00
3		17	6	7	15		003000	46:04:10
4	move to CH4	6	7	15			008000	06:04:10
5		3	15				003000	06:04:00
6		3	17	15			005000	40:04:00
7		17	6	7	15		003000	40:04:10
8		6	7	15			009000	06:04:10
9	Introduce and mix 350uL of B-ME-RLT to MIX 2 (now Mix 3)	15	1				003000	06:04:00
10	draw RLT	15	1	16			010000	10:04:00
11	prepare to move Lysed sample to CH5	15	16	11	7	8	003000	10:0C:00
12	Move mixtures to CH5, prepare to move to CH6	11	16	7	8	22	010000	0C:4C:00
13		16	7	8	22		003000	0C:48:02
14	move all mixtures to CH6	7	8	22			010000	0C:08:02
15	move to CH5	7	8	16			003000	0C:00:02
16	move all mixtures to CH6	7	8	22			003000	0C:08:00
17	move to CH5	7	8	16			003000	0C:00:02
18	move all mixtures to CH6	7	8	22			003000	0C:08:00
19	move to CH5	7	8	16			003000	0C:00:02
20	move all mixtures to CH6	7	8	22			020000	0C:08:00
21	Introduce and mix 250uL of Ethanol to MIX 3 (now Mix 4)	22	4				003000	0C:00:02
22	Draw EtOH to CH4	22	4	15			010000	80:00:02
23		22	15	11			003000	80:04:02
24	send to CH5	22	16	11			010000	00:44:02
25		22	16	7	8		003000	00:48:02
26	move to CH6	22	7	8			006000	0C:08:02
27	move to CH5	16	7	8			006000	0C:00:02
28	Move to CH6	22	7	8			006000	0C:08:00
29	FWD	7	8	16			006000	0C:00:02
30	BCKWD	7	8	22			006000	0C:08:00
31	FWD	7	8	16			006000	0C:00:02
32	BCKWD	7	8	22			020000	0C:08:00
33	Pass MIX 4 through the silica filter (prepare)	22	9	8	12		001000	0C:00:02
34	Pass MIX 4 through the silica filter (prepare)	22	9	8	12		003000	08:90:02
35	FWD	21	9	8	12		030000	08:90:02
36	BCKWD	22	9	8	12		030000	08:90:01
37	FWD	21	9	8	12		060000	08:90:02
38	Send waste to waste bottle…..Ready….	21	14				003000	08:90:01
39	Go!	14					030000	00:02:01
40	drain to waste	14	5	12			008000	00:02:00
41		14	12				003000	01:82:00
42		14					001000	00:82:00

Table B.3 continued

Step	Description	Solenoid					Time (ms)	Hexcode
43	Make sure everything is empty (open valves)	8	9	12			003000	00:02:00
44	Open ch 7	8	9	12	21		025000	08:90:00
45	Send waste to waste bottle…..Ready….	21	14				003000	08:90:01
46	Go!	14					015000	00:02:01
47	drain to waste	14	5	12			008000	00:02:00
48		14	12				003000	01:82:00
49		14					001000	00:82:00
50	Introduce 350uL of RW1 buffer and pass thru silica filter	2					003000	00:02:00
51	draw RW1	2	16				010000	20:00:00
52	prepare to move thru filter	16	10	12			003000	20:08:00
53	GO!	21	10	12			010000	00:A8:00
54		16	10	12			010000	00:A0:01
55		21	10	12			010000	00:A8:00
56		16	10	12			010000	00:A0:01
57		21	10	12			040000	00:A8:00
58	Send waste to waste bottle	21	14				003000	00:A0:01
59		14					025000	00:02:01
60	drain to waste	14	5	12			008000	00:02:00
61		14	12				003000	01:82:00
62		14					001000	00:82:00
63	Introduce 350uL of RW1 buffer and pass thru silica filter	2					003000	00:02:00
64	draw RW1	2	16				010000	20:00:00
65	prepare to move thru filter	16	10	12			003000	20:08:00
66	GO!	21	10	12			040000	00:A8:00
67	Send waste to waste bottle	21	14				003000	00:A0:01
68		14					010000	00:02:01
69	drain to waste	14	5	12			008000	00:02:00
70		14	12				003000	01:82:00
71		14					001000	00:82:00
72	Introduce 350uL of rpe buffer and pass thru silica filter	3					003000	00:02:00
73	draw rpe	3	16				010000	40:00:00
74	prepare to move thru filter	16	10	12			003000	40:08:00
75	GO!	21	10	12			010000	00:A8:00
76		16	10	12			010000	00:A0:01
77		21	10	12			010000	00:A8:00
78		16	10	12			010000	00:A0:01
79		21	10	12			040000	00:A8:00
80	Send waste to waste bottle	21	14				003000	00:A0:01
81		14					010000	00:02:01
82	drain to waste	14	5	12			008000	00:02:00
83		14	12				003000	01:82:00
84		14					001000	00:82:00
85	Introduce 350uL of Rpe buffer and pass thru silica filter	3					003000	00:02:00

Table B.3 continued

Step	Description	Solenoid					Time (ms)	Hexcode
86	draw Rpe	3	16				010000	40:00:00
87	prepare to move thru filter	16	10	12			003000	40:08:00
88	GO!	21	10	12			010000	00:A8:00
89		16	10	12			010000	00:A0:01
90		21	10	12			010000	00:A8:00
91		16	10	12			010000	00:A0:01
92		21	10	12			040000	00:A8:00
93	Send waste to waste bottle	21	14				003000	00:A0:01
94		14					010000	00:02:01
95	drain to waste	14	5	12			008000	00:02:00
96		14	12				003000	01:82:00
97		14					001000	00:82:00
98	Introduce 350uL of Rpe buffer and pass thru silica filter	3					003000	00:02:00
99	draw Rpe	3	16				010000	40:00:00
100	prepare to move thru filter	16	10	12			003000	40:08:00
101	GO!	21	10	12			40000	00:A8:00
102	Send waste to waste bottle	21	14				3000	00:A0:01
103		14					10000	00:02:01
104	Long drying time (in current MF protocol its step #40)	5	12	21	14		120000	00:02:00
105		14	12	21			3000	01:82:01
106		14					6000	00:82:01
107	Elution Step	4					3000	00:02:00
108		4	19				8000	80:00:00
109		19	10	11	6		3000	80:00:40
110		10	11	6	20		5000	02:60:40
111		19	10	11	6		5000	02:60:80
112		10	11	6	20		5000	02:60:40
113		19	10	11	6		5000	02:60:80
114		10	11	6	20		5000	02:60:40
115		19	10	11	6		5000	02:60:80
116		10	11	6	20		5000	02:60:40
117		19	10	11	6		5000	02:60:80
118		10	11	6	20		5000	02:60:40
119		19	10	11	6		5000	02:60:80
120		10	11	6	20		5000	02:60:40
121		20	10	11	6	12	6000	02:60:80
122	output	20	11	12			3000	02:E0:80
123		11	12				10000	00:C0:80
124	end						3000	00:C0:00
125							0	00:00:00

Table B.4 Steps for extracting RNA from bacteria samples.

Step	Description	Solenoid					Time (ms)	Hexcode
1	Open Valve for Port I5	**3**					3000	40:00:00
2	draw 50 ul sample into CH3	**3**	**17**				10000	40:00:10
3		**17**	**6**	**7**			3000	06:00:10
4	move to CH4	**6**	**7**	**15**			10000	06:04:00
5	Open valve for port I4	**15**	**2**				3000	20:04:00
6	draw 50 ul BPR to ch3	**15**	**2**	**17**			5000	20:04:10
7	move BPR to CH4	**15**	**17**	**6**	**7**		10000	06:04:10
8		**15**	**6**	**7**			3000	06:04:00
9	Open valve for port I4	**15**	**2**				3000	20:04:00
10	draw 50 ul BPR to ch3	**15**	**2**	**17**			5000	20:04:10
11	move to CH4	**15**	**17**	**6**	**7**		10000	06:04:10
12		**15**	**6**	**7**			3000	06:04:00
13	Incubate Mixture for 5min at room temp (20-25C)	**15**					300000	00:04:00
14	Open valve for port I3	**15**	**1**				3000	10:04:00
15	Draw in 50 ul Lysozyme to ch3	**15**	**1**	**17**			3000	10:04:10
16	move to CH4	**15**	**17**	**6**	**7**		6000	06:04:10
17		**15**	**6**	**7**			3000	06:04:00
18	Open valve for port I3	**15**	**1**				3000	10:04:00
19	Draw in 50 ul Lysozyme to ch3	**15**	**1**	**17**			3000	10:04:10
20	move to CH4	**15**	**17**	**6**	**7**		6000	06:04:10
21		**15**	**6**	**7**			3000	06:04:00
22	Incubate Mix 2 for 10min at **ROOM TEMP (20-25C)**	**15**					600000	00:04:00
23	Open valve for port I8	**15**	**1**				3000	10:04:00
24	draw 350 ul RLT	**15**	**1**	**16**			10000	10:0C:00
25	prepare to move Lysed sample to CH5	**15**	**16**	**11**	**7**	**8**	3000	0C:4C:00
26	Move mixtures to CH5, prepare to move to CH6	**11**	**16**	**7**	**8**	**22**	10000	0C:48:02
27		**16**	**7**	**8**	**22**		3000	0C:08:02
28	move all mixtures to CH6	**7**	**8**	**22**			10000	0C:00:02
29	move to CH5	**7**	**8**	**16**			3000	0C:08:00
30	move all mixtures to CH6	**7**	**8**	**22**			20000	0C:00:02
31	Open valve for port I7	**22**	**4**				3000	80:00:02
32	Draw 250 ul EtOH to CH4	**22**	**4**	**15**			10000	80:04:02
33		**22**	**15**	**11**			3000	00:44:02
34	send to CH5	**22**	**16**	**11**			10000	00:48:02
35		**22**	**16**	**7**	**8**		3000	0C:08:02
36	move to CH6	**22**	**7**	**8**			6000	0C:00:02
37	move to CH5	**16**	**7**	**8**			6000	0C:08:00
38	Move to CH6	**22**	**7**	**8**			20000	0C:00:02
39	Pass MIX 4 through the silica filter (prepare)	**22**	**9**	**8**	**12**		3000	08:90:02
40	FWD	**21**	**9**	**8**	**12**		30000	08:90:01
41	BCKWD	**22**	**9**	**8**	**12**		30000	08:90:02
42	FWD	**21**	**9**	**8**	**12**		60000	08:90:01
43	Send waste to waste bottle…..Ready….	**21**	**14**				3000	00:02:01

Table B.4 continued

Step	Description	Solenoid					Time (ms)	Hexcode
44	Go!	**14**					30000	00:02:00
45	Make sure everything is empty (open valves)	**8**	**9**	**12**			3000	08:90:00
46	Open ch 7	**8**	**9**	**12**	**21**		25000	08:90:01
47	Send waste to waste bottle…..Ready….	**21**	**14**				3000	00:02:01
48	Go!	**14**					15000	00:02:00
49	Open valve for I9	**2**					3000	20:00:00
50	draw 350 ul RW1	**2**	**16**				10000	20:08:00
51	prepare to move thru filter	**16**	**10**	**12**			3000	00:A8:00
52	GO!	**21**	**10**	**12**			40000	00:A0:01
53	Send waste to waste bottle	**21**	**14**				3000	00:02:01
54		**14**					25000	00:02:00
55	Open Valve for I1	**4**					3000	80:00:00
56	Draw water….	**4**	**19**				5000	80:00:40
57	prepare to send to CH5	**19**	**10**	**11**			3000	00:60:40
58	send to CH5	**10**	**11**	**16**			10000	00:68:00
59		**7**	**8**	**16**			3000	0C:08:00
60	send to CH6	**7**	**8**	**22**			10000	0C:00:02
61		**22**	**13**				3000	00:01:02
62	send to CH7	**13**	**21**				10000	00:01:01
63		**21**	**14**				3000	00:02:01
64	send to waste	**14**					15000	00:02:00
65	Repeat RW1 well rinse	**4**					3000	80:00:00
66	Draw water….	**4**	**19**				5000	80:00:40
67		**19**	**10**	**11**			3000	00:60:40
68	send to CH5	**10**	**11**	**16**			10000	00:68:00
69		**7**	**8**	**16**			3000	0C:08:00
70	send to CH6	**7**	**8**	**22**			10000	0C:00:02
71		**22**	**13**				3000	00:01:02
72	send to CH7	**13**	**21**				20000	00:01:01
73		**21**	**14**				3000	00:02:01
74	send to waste	**14**					40000	00:02:00
75	Open valve for port I2	**1**					3000	10:00:00
76	draw DNAse into ch2	**1**		**18**			10000	10:00:20
77		**18**	**3**				3000	40:00:20
78	Draw RDD to CH5	**18**	**3**	**16**			10000	40:08:20
79	DNAse moves to CH5	**18**	**16**	**9**	**10**		3000	00:38:20
80		**16**	**9**	**10**			10000	00:38:00
81		**16**	**10**	**12**			3000	00:A8:00
82	move to filter	**10**	**12**	**21**			40000	00:A0:01
83		**21**	**14**				3000	00:02:01
84	junk to waste	**14**					20000	00:02:00
85	Incubate DNAse 1 on silica filter for **5min** 20-25C	**0**					300000	00:00:00
86	Open valve for port I2	**1**					3000	10:00:00
87	draw DNAse ONLY	**1**		**18**			10000	10:00:20

Table B.4 continued

Step	Description	Solenoid					Time (ms)	Hexcode
88		**18**	**3**				3000	40:00:20
89	draw RDD ONLY	**18**	**3**	**16**			10000	40:08:20
90	DNAse moves to CH5	**18**	**16**	**9**	**10**		3000	00:38:20
91		**16**	**9**	**10**			10000	00:38:00
92		**16**	**10**	**12**			3000	00:A8:00
93	move to filter	**10**	**12**	**21**			45000	00:A0:01
94		**21**	**14**				3000	00:02:01
95	junk to waste	**14**					20000	00:02:00
96	Incubate DNAse 1 on silica filter for 5**min** 20-25C	**0**					300000	00:00:00
97	Open valve to port I9	**2**					3000	20:00:00
98	draw RW1	**2**	**16**				10000	20:08:00
99		**16**	**10**	**12**			3000	00:A8:00
100	send to filter	**21**	**10**	**12**			40000	00:A0:01
101	Send waste to waste bottle	**21**	**14**				3000	00:02:01
102		**14**					15000	00:02:00
103	Open valve for port I6	**4**					3000	80:00:00
104	draw RPE	**4**	**17**				10000	80:00:10
105		**17**	**6**	**7**			3000	06:00:10
106	move to CH4	**6**	**7**	**15**			10000	06:04:00
107	Draw EtOH to CH4	**4**	**15**				10000	80:04:00
108		**15**					3000	00:04:00
109		**15**	**11**				3000	00:44:00
110	send to CH 5	**11**	**16**				8000	00:48:00
111		**16**	**10**	**12**			3000	00:A8:00
112	send through filter	**10**	**12**	**21**			25000	00:A0:01
113		**21**	**14**				3000	00:02:01
114	send to waste	**14**					15000	00:02:00
115	Suck in **50uL of RPE** buffer and 200uL of ethanol and mix	**4**					3000	80:00:00
116	draw RPE	**4**	**17**				10000	80:00:10
117		**17**	**6**	**7**			3000	06:00:10
118	move to CH4	**6**	**7**	**15**			10000	06:04:00
119	Draw EtOH to CH4	**4**	**15**				10000	80:04:00
120		**15**					3000	00:04:00
121		**15**	**11**				3000	00:44:00
122	send to CH 5	**11**	**16**				8000	00:48:00
123		**16**	**10**	**12**			3000	00:A8:00
124	send through filter	**10**	**12**	**21**			25000	00:A0:01
125		**21**	**14**				3000	00:02:01
126	send to waste	**14**					15000	00:02:00
127	Suck in **50uL of RPE** buffer and 200uL of ethanol and mix	**4**					3000	80:00:00
128	draw RPE	**4**	**17**				10000	80:00:10
129		**17**	**6**	**7**			3000	06:00:10
130	move to CH4	**6**	**7**	**15**			10000	06:04:00
131	Draw EtOH to CH4	**4**	**15**				10000	80:04:00

Table B.4 continued

Step	Description	Solenoid					Time (ms)	Hexcode
132		**15**					3000	00:04:00
133		**15**	**11**				3000	00:44:00
134	send to CH 5	**11**	**16**				8000	00:48:00
135		**16**	**10**	**12**			3000	00:A8:00
136	send through filter	**10**	**12**	**21**			25000	00:A0:01
137		**21**	**14**				3000	00:02:01
138	send to waste	**14**					15000	00:02:00
139	Suck in **50uL of RPE** buffer and 200uL of ethanol and mix	**4**					3000	80:00:00
140	draw RPE	**4**	**17**				10000	80:00:10
141		**17**	**6**	**7**			3000	06:00:10
142	move to CH4	**6**	**7**	**15**			10000	06:04:00
143	Draw EtOH to CH4	**4**	**15**				10000	80:04:00
144		**15**					3000	00:04:00
145		**15**	**11**				3000	00:44:00
146	send to CH 5	**11**	**16**				8000	00:48:00
147		**16**	**10**	**12**			3000	00:A8:00
148	send through filter	**10**	**12**	**21**			25000	00:A0:01
149		**21**	**14**				3000	00:02:01
150	send to waste	**14**					15000	00:02:00
151	Long drying time (in current MF protocol its step #40)	**5**	**12**	**21**	**14**		300000	01:82:01
152		**12**	**21**	**14**			3000	00:82:01
153		**21**	**14**				3000	00:02:01
154		**14**					3000	00:02:00
155		**0**					3000	00:00:00
156	open valve for port I1	**4**					3000	80:00:00
157	Draw in 150 ul H20	**4**	**19**				10000	80:00:40
158	open valves	**19**	**10**	**11**	**6**		3000	02:60:40
159	pass through filter	**10**	**11**	**6**	**20**		15000	02:60:80
160		**20**					3000	00:00:80

Table B.5 Protocol steps for extracting DNA from blood samples

Step	Description	Solenoid					Time (ms)	Hexcode
1	proteinase solution in	4					002000	80:00:00
2		4	17				010000	80:00:10
3		17	7	6			002000	06:00:10
4		7	8	15			010000	0C:04:00
5	100 ul sample in	15	3				002000	40:04:00
6		15	3	17			004000	40:04:10
7		15	17	6	7		002000	06:04:10
8		15	6	7			004000	06:04:00
9		15	3				002000	40:04:00
10		15	3	17			004000	40:04:10
11		15	17	6	7		002000	06:04:10
12		15	6	7			004000	06:04:00
13	50 ul AL buffer in	15	2				002000	20:04:00
14		15	2	17			010000	20:04:10
15		15	17	6	7		002000	06:04:10
16		15	6	7			010000	06:04:00
17	Mix	17	6	7			003000	06:00:10
18		15	6	7			003000	06:04:00
19		17	6	7			003000	06:00:10
20		15	6	7			003000	06:04:00
21		17	6	7			003000	06:00:10
22		15	6	7			003000	06:04:00
23	incubate for 10 minutes	15					600000	00:04:00
24	input 100 ul of etoh	15	1				002000	10:04:00
25		15	1	17			004000	10:04:10
26		15	17	6	7		002000	06:04:10
27		15	6	7			004000	06:04:00
28		15	1				002000	10:04:00
29		15	1	17			004000	10:04:10
30		15	17	6	7	11	002000	06:44:10
31		15	6	7	16	11	004000	06:4C:00
32		6	7	11	16		004000	06:48:00
33		16	11				002000	00:48:00
34	Mix	15	11				003000	00:44:00
35		16	11				003000	00:48:00
36		15	11				003000	00:44:00
37		16	11				003000	00:48:00
38	Pass through filter	16	13	12			002000	00:89:00
39		13	12	21			040000	00:81:01
40		21	14				002000	00:02:01
41		14					002000	00:02:00
42		14	5	12			004000	01:82:00
43		14					008000	00:02:00
44	wash with AW1	1					002000	10:00:00
45		1	16				015000	10:08:00

Table B.5 continued

Step	Description	Solenoid					Time (ms)	Hexcode
46		16	13	12			002000	00:89:00
47		12	13	21			040000	00:81:01
48		21	14				002000	00:02:01
49		14					010000	00:02:00
50	wash with AW2	2					002000	20:00:00
51		2	16				015000	20:08:00
52		16	13	12			002000	00:89:00
53		12	13	21			040000	00:81:01
54		21	14				002000	00:02:01
55		14					010000	00:02:00
56	Dry	5	12	14			120000	01:82:00
57	elution	4					002000	80:00:00
58		4	19				004000	80:00:40
59		19	10	11	6		002000	02:60:40
60		10	11	6	20		010000	02:60:80
61		20	11	6	10	12	001000	02:E0:80
62		20	11	12			002000	00:C0:80
63		11	12				003000	00:C0:00
64							001000	00:00:00

APPENDIX C

MATLAB CODE FOR 1D STEADY STATE AND 1D TRANSIENT SIMULATIONS FOR INTERNAL TEMPERATURES OF MULTILAYER POLYCARBONATE OSCILLATORY FLOW PCR CHIP

```
%% 1D trasient simulation of temperature in multi-layer thin chip
clear
it1=0;
for tbot2=[0.000127]%0.00024,0.000376,0.000501]
    clear T Tinitial Ts a1 alpha chamberx cs ks r rhos
thicknesses times ts u uold x;
    it1=it1+1;
    tmax = 1; % end time
ti=.01; % time interval to sample answer for plotting "every ti
seconds"
Tinf=20+273; % Ambient Air Temperature
Tgoal=273+60; % temperature you want the fluid to reach
h0=.0628*(Tgoal-273)+9.2062+10; % Set convection coefficient
q0=18*(Tgoal-273)-571.21 %heat flux from 3d simulation w/m^2
fluidtemp=273+95; % Set temperature of fluid to be pumped into
channel
tins1=0.000127; % Thickness of insulating layer on top of chip
tinsw1=0.000126; % Thicnkess of top water layer
ttop=.000127; % Thicnkess of top chip layer
tmid=.000127; % Thicnkess of middle chip layer *sample*
tbot=.000127; % Thicnkess of bottom chip layer
tbotw=.000127; % thickness of bottom water layer
tbot2=0.000127; % thickness of bottom insulating layer
tins2=0.0003; % Thicnkess of layer between chip and heater
%heater between these two layers
tins3=0; % Thicnkess of layer under heater
points=25; % number of points per layer (assuming no layer is
zero)

thicknesses=[tins1,tinsw1,ttop,tmid,tbot,tbotw,tbot2,tins2,tins3]
;
% alternative number of points per layer
if min(thicknesses)>0
    si=min(thicknesses)/points; % space increment calculate
else
    si=.00002;  % manually set alternative space increment
end

x=[0:si:sum(thicknesses)];  % x vector distance through chip

% Thermal conductivity of materials database
kpdms=.16;
ksilicond=.21;
kh20=.58;
kpolyc=.2;
```

```
kalum=250;

% Density of materials database
rpdms=965;
rsilicond=965;
rh20=1000;
rpolyc=1220;
ralum=2700;

% Heat capacity of materials database
cpdms=120;
csilicond=120;
ch20=4181; %4181
cpolyc=1200;
calum=910;

%Assign properties to layers
kins1=kpolyc; rins1=rpolyc; cins1=cpolyc;
kinsw1=kh20;   rinsw1=rh20;   cinsw1=ch20;
ktop=kpolyc; rtop=rpolyc; ctop=cpolyc;
kmid=kh20;   rmid=rh20;   cmid=ch20;
kbot=kpolyc; rbot=rpolyc; cbot=cpolyc;
kbotw=kh20;   rbotw=rh20;   cbotw=ch20;
kbot2=kpolyc; rbot2=rpolyc; cbot2=cpolyc;
kins2=kalum; rins2=ralum; cins2=calum;
kins3=kpdms; rins3=rpdms; cins3=cpdms;

% Create vectors of the properties associated with the entire
geometry
ks=ones(1,length(x));
ks(find(x<tins3))=kins3;
ks(find(x>=tins3 & x<tins3+tins2))=kins2;
ks(find(x>=tins3+tins2 & x<tins3+tins2+tbot2))=kbot2;
ks(find(x>=tins3+tins2+tbot2 & x<tins3+tins2+tbot2+tbotw))=kbotw;
ks(find(x>=tins3+tins2+tbot2+tbotw &
x<tins3+tins2+tbot2+tbotw+tbot))=kbot;
ks(find(x>=tins3+tins2+tbot2+tbotw+tbot &
x<tins3+tins2+tbot2+tbotw+tbot+tmid))=kmid;
ks(find(x>=tins3+tins2+tbot2+tbotw+tbot+tmid &
x<tins3+tins2+tbot2+tbotw+tbot+tmid+ttop))=ktop;
ks(find(x>=tins3+tins2+tbot2+tbotw+tbot+tmid+ttop &
x<tins3+tins2+tbot2+tbotw+tbot+tmid+ttop+tinsw1))=kinsw1;
ks(find(x>=tins3+tins2+tbot2+tbotw+tbot+tmid+ttop+tinsw1 &
x<tins3+tins2+tbot2+tbotw+tbot+tmid+ttop+tinsw1+tins1))=kins1;
%ks(find(x>=tins3+tins2+tbot+tmid+ttop))=kins1;
```

```
rhos=ones(1,length(x));
rhos(find(x<tins3))=rins3;
rhos(find(x>=tins3 & x<tins3+tins2))=rins2;
rhos(find(x>=tins3+tins2 & x<tins3+tins2+tbot2))=rbot2;
rhos(find(x>=tins3+tins2+tbot2 &
x<tins3+tins2+tbot2+tbotw))=rbotw;
rhos(find(x>=tins3+tins2+tbot2+tbotw &
x<tins3+tins2+tbot2+tbotw+tbot))=rbot;
rhos(find(x>=tins3+tins2+tbot2+tbotw+tbot &
x<tins3+tins2+tbot2+tbotw+tbot+tmid))=rmid;
rhos(find(x>=tins3+tins2+tbot2+tbotw+tbot+tmid &
x<tins3+tins2+tbot2+tbotw+tbot+tmid+ttop))=rtop;
rhos(find(x>=tins3+tins2+tbot2+tbotw+tbot+tmid+ttop &
x<tins3+tins2+tbot2+tbotw+tbot+tmid+ttop+tinsw1))=rinsw1;
rhos(find(x>=tins3+tins2+tbot2+tbotw+tbot+tmid+ttop+tinsw1 &
x<tins3+tins2+tbot2+tbotw+tbot+tmid+ttop+tinsw1+tins1))=rins1;

cs=ones(1,length(x));
cs(find(x<tins3))=cins3;
cs(find(x>=tins3 & x<tins3+tins2))=cins2;
cs(find(x>=tins3+tins2 & x<tins3+tins2+tbot2))=cbot2;
cs(find(x>=tins3+tins2+tbot2 & x<tins3+tins2+tbot2+tbotw))=cbotw;
cs(find(x>=tins3+tins2+tbot2+tbotw &
x<tins3+tins2+tbot2+tbotw+tbot))=cbot;
cs(find(x>=tins3+tins2+tbot2+tbotw+tbot &
x<tins3+tins2+tbot2+tbotw+tbot+tmid))=cmid;
cs(find(x>=tins3+tins2+tbot2+tbotw+tbot+tmid &
x<tins3+tins2+tbot2+tbotw+tbot+tmid+ttop))=ctop;
cs(find(x>=tins3+tins2+tbot2+tbotw+tbot+tmid+ttop &
x<tins3+tins2+tbot2+tbotw+tbot+tmid+ttop+tinsw1))=cinsw1;
cs(find(x>=tins3+tins2+tbot2+tbotw+tbot+tmid+ttop+tinsw1 &
x<tins3+tins2+tbot2+tbotw+tbot+tmid+ttop+tinsw1+tins1))=cins1;


% plot(ks)
n1=0;
Th=Tgoal;
err=1;
tcorr=.1;
% while err>0.001
% n1=n1+1;
% Th=Th+tcorr;
% % U=1/(ttop/ktop+tmid/kmid+tbot/kbot+tins2/kins2); %
calculating
```

```
% % the thermal resistance to find q across the entire chip
% %Ttop=(h0*Tinf+Th*U)/(h0+U); % find temperature on boundary
with ambient
% q=q0; % calculate heat flux
%
% % use q to find the temperature at each interface
% Tins2=-q*tins2/kins2+Th;
% Tbot2=-q*tbot2/kbot2+Tins2;
% Tbotw=-q*tbotw/kbotw+Tbot2;
% Tbot=-q*tbot/kbot+Tbotw;
% Tmid=-q*tmid/kmid+Tbot;
% Ttop=-q*ttop/ktop+Tmid;
% Tinsw1=-q*tinsw1/kinsw1+Ttop;
% Tins1=-q*tins1/kins1+Tinsw1;
%
% % fluid chamber is the area of interest, find the average
temperature of
% % the fluid in the chamber
% Tchamber(n1)=(Tmid+Tbot)/2;
% err=abs(Tgoal-Tchamber(n1));
% tcorr=Tgoal-Tchamber(n1);
% end

q=q0; % calculate heat flux

% use q to find the temperature at each interface
Tins2=-q*tins2/kins2+Th;
Tbot2=-q*tbot2/kbot2+Tins2;
Tbotw=-q*tbotw/kbotw+Tbot2;
Tbot=-q*tbot/kbot+Tbotw;
Tmid=-q*tmid/kmid+Tbot;
Ttop=-q*ttop/ktop+Tmid;
Tinsw1=-q*tinsw1/kinsw1+Ttop;
Tins1=-q*tins1/kins1+Tinsw1;

% fluid chamber is the area of interest, find the average
temperature of
% the fluid in the chamber
n1=1;
Tchamber(n1)=(Tmid+Tbot)/2;



%%% locate the section of the x-vector associated with the fluid
chamber
```

```
chamberx=find(x>tins3+tins2+tbot2+tbotw+tbot &
x<=tins3+tins2+tbot2+tbotw+tbot+tmid);

%Plot the calculated temperature profile in the chip
ts=[0,tins2,tins2+tbot2,tins2+tbot2+tbotw,tins2+tbot2+tbotw+tbot,
tins2+tbot2+...
    tbotw+tbot+tmid,tins2+tbot2+tbotw+tbot+tmid+ttop,tins2+tbot2+
tbotw+tbot+tmid+ttop+tinsw1,...
    tins2+tbot2+tbotw+tbot+tmid+ttop+tinsw1+tins1];

Ts=[Th,Tins2,Tbot2,Tbotw,Tbot,Tmid,Ttop,Tinsw1,Tins1];
plot(ts,Ts)
disp(['heatertemp temp: ',num2str(Th-273)])
disp(['chamber temp: ',num2str(Tchamber-273), ' +/- ',
num2str(Tchamber-Tmid)])
disp(['surface temp: ',num2str(Ttop-273)])
% %%
% Calculate Biot number to determine if lumped capacitance method
can be
% used
% Rcond=(tins1/kins1+ttop/ktop+tmid/kmid+tbot/kbot+tins2/kins2);
% Rconv=1/h0;
% Bi=Rcond/Rconv

% %% transient
% --- Define constants and initial condition


L = max(x); % length of domain in x direction
alpha=ks./(rhos.*cs);

nx = length(x); % number of nodes in x direction
dx = L/(nx-1);
nt = ceil(max(alpha)*tmax/(.5*dx.^2)); % number of time steps


dt = tmax/(nt);
% rhos=1000*ones(1,length(x));
% cs=1200*ones(1,length(x));

% alpha=ones(1,length(x))*kh20./(rh20.*ch20);
% r=.25*ones(1,length(x))
r = alpha.*dt./dx.^2;
plot(r)
% %% set initial temperature to what was calculated above
```

```
Tinitial=ones(1,length(x));
Tinitial(1)=Th;
for k=2:length(x)
    if Tinitial(k-1)>=Tins2;
        Tinitial(k)=Tinitial(k-1)-(Th-Tins2)/(tins2/dx);
    elseif Tinitial(k-1)>=Tbot2;
        Tinitial(k)=Tinitial(k-1)-(Tins2-Tbot2)/(tbot2/dx);
        elseif Tinitial(k-1)>=Tbotw;
        Tinitial(k)=Tinitial(k-1)-(Tbot2-Tbotw)/(tbotw/dx);
        elseif Tinitial(k-1)>=Tbot;
        Tinitial(k)=Tinitial(k-1)-(Tbotw-Tbot)/(tbot/dx);
    elseif Tinitial(k-1)>=Tmid;
        Tinitial(k)=Tinitial(k-1)-(Tbot-Tmid)/(tmid/dx);
    elseif Tinitial(k-1)>=Ttop;
        Tinitial(k)=Tinitial(k-1)-(Tmid-Ttop)/(ttop/dx);
    elseif Tinitial(k-1)>=Tinsw1;
        Tinitial(k)=Tinitial(k-1)-(Ttop-Tinsw1)/(tinsw1/dx);
    else Tinitial(k-1)>=Tins1;
        Tinitial(k)=Tinitial(k-1)-(Tinsw1-Tins1)/(tins1/dx);


    end

end
plot(x,Tinitial)
% %%
% --- Loop over time steps
t = 0;
% u = Th*ones(1,length(x));% initial condition
% u(1)=Th;
% u(length(u))=Tinf;
u=Tinitial; % initial condition as solved by 1D steady state

u(chamberx)=fluidtemp;
chambertemp(1)=mean(u(chamberx))
times(1)=0;
T(1,:)=u;

dtdx2=dt/dx^2;
figure (2)
a1=(alpha(2:nx-1)*dtdx2./(ks(2:nx-1)*4).*(ks(3:nx)-ks(1:nx-2)));
plot(a1)
% %%
figure(3)
tic;
```

```
% subplot(2,2,1)
for m=1:nt
    uold = u; % prepare for next step
    t = t + dt;

    for j=2:nx-1
            %u(j) = r(j-1)*uold(j-1) + r2(j)*uold(j) +
r(j)*uold(j+1);
            u(j)=dtdx2*alpha(j)*(uold(j-1)-
2*uold(j)+uold(j+1))+uold(j)+...
                alpha(j)*dtdx2/(ks(j)*2)*(ks(j+1)-
ks(j))*(uold(j+1)-uold(j));


    end

    u(end)=(ks(end)/(h0*dx)*uold(nx-
1)+Tinf)/(1+ks(end)/(h0*dx));  %convective boundary condition
    % vectorized
%     u(2:nx-1)=dtdx2.*alpha(2:nx-1).*(uold(1:nx-2)-2*uold(2:nx-
1)+uold(3:nx))+uold(2:nx-1)+...
%         alpha(2:nx-1).*dtdx2./(ks(2:nx-1)*4).*(ks(3:nx)-
ks(1:nx-2)).*(uold(3:nx)-uold(1:nx-2));
%
%     u(end)=(ks(end)/(h0*dx)*uold(nx-
1)+Tinf)/(1+ks(end)/(h0*dx));  %convective boundary condition


    if mod(t,ti)<mod(t-dt,ti)
        index1=round(t/ti)+1
        chambertemp(it1,index1)=mean(u(chamberx));

        times(index1)=t;
        T(index1,:)=u;
        plot(x,u-273)
        title('1-D Transient Temperature, Multiple Layers')
        xlabel('Distance (m)')
        ylabel('Temperature (K)')
        axis([0, L, 50, 100])
        text(0,60,['Time: ', num2str(t)]) % display time on graph
        text(0,65,['Fluid temp: ', num2str(chambertemp(index1)-
273)]) % display time on graph
        M(round(t/ti))=getframe(gcf);
        disp(['Current time: ',num2str(t), '.   End time: ',
```

```
num2str(tmax)])

        %pause(.01)
        if abs(mean(u(chamberx))-Tchamber)<.1
            break % break when the fluid reaches the desired
temperature
        end
    end
 %modtest(m)=mod(t,ti);
end
toc
subplot(2,2,2)
surf(x,times,T-273)
subplot(2,2,3)
plot(times,chambertemp-273)
subplot(2,2,4)
plot(x,u)

end
%%
filename=['chambertemp_',num2str(fluidtemp),'_',num2str(Th),'_',n
um2str(tmax)]
movie(gcf,M,1,10);
%%
movie2avi(M,'60_97_3sec.avi','COMPRESSION','None')
%%
filename1=['chambertemp_',num2str(fluidtemp),'_',num2str(Th),'.da
t']
save(filename,'chambertemp', '-ascii')
load filename
%%
```